ABSTRACT

Title of Document: GRAPHENE OXIDE MEMBRANES FOR WATER PURIFICATION

Meng Hu, Ph.D., 2015

Directed By: Associate Professor Baoxia Mi, Department of Civil and Environmental Engineering

Graphene oxide (GO) is a two-dimensional material with a single layer carbon lattice, which is decorated with oxygenated functional groups on the basal plane as well as on the edges. Due to its unique properties, GO has attracted many applications including electronics, energy, sensors, optics, etc. Recently, it has been demonstrated that the graphene surface of GO presents long slip lengths of water, thus allowing for an unimpeded water flow. It was anticipated that the ultrafast water transport would be translated into membrane separations, in order to address one of the major challenges for membrane technology—low performance. It was also expected that GO might provide solutions to other obstacles facing membrane technology, such as membrane fouling. These two overarching themes, the technical limitations for membrane technology and the potential of GO to overcome those restrictions, inspired the current study.

The main objective of this dissertation was to develop highly efficient membranes for water purification based on GO. Also investigated were the transport mechanisms for the designed GO membranes, the potential of GO to mitigate membrane fouling, and the feasibility of GO membrane regeneration. Major achievements of the study include: (1) the development of high performance GO membranes for nanofiltration and forward osmosis by two facile and sustainable methods, (2) the elucidation of transport mechanisms to guide better GO membrane design, (3) the application of GO for fouling mitigation in pressure retarded osmosis processes, and (4) the validation for regenerable GO membranes. Collectively, not only do the findings provide the first experimental verification for the ultrafast water transport in GO membranes, they also suggest that the GO membrane could be a promising prototype of next generation membranes with high performance, low fouling propensity, and full regenerability. The work has already begun to show its profound impact in the membrane field, as seen in the publications it has prompted.

GRAPHENE OXIDE MEMBRANES FOR WATER PURIFICATION

By

Meng Hu

Dissertation submitted to the Faculty of the Graduate School of the
University of Maryland, College Park, in partial fulfillment
of the requirements for the degree of
Doctor of Philosophy
2015

Advisory Committee:
Associate Professor Baoxia Mi, Chair
Professor Allen P. Davis
Professor Sheryl H. Ehrman
Dr. Christopher M. Stafford
Professor Alba Torrents

Dedication

To

Grandpa and Diaodiao

Acknowledgements

First and foremost, I would like to thank my advisor, Professor Baoxia Mi, for introducing me to the field of graphene oxide. I am also grateful for her advice and support during the doctoral study. It is under Professor Mi's tutelage and guidance that I have matured as a researcher.

I would also like to thank Professors Allen P. Davis, Sheryl H. Ehrman, Alba Torrents, and Dr. Christopher M. Stafford for serving on the dissertation committee and for their comments and support.

Thanks also go to current and former members in Professor Mi's lab at the University of Maryland: Yan Kang, Yoontaek Oh, Sunxiang Zheng, Limei Jin, Yaolin Liu, Qian Yang, Haiyin Yu, and Yong Gao for their help on the research. I want to also thank Dr. Wen-An Chiou and the staff at the NanoCenter, and Dr. Karen Gaskell and the staff at the Surface Analysis Center.

This work was financially supported by the National Science Foundation (NSF) under Grant Nos. CBET-1158601, CBET-1351430, and CBET-1154572. I was also supported by the Ann G. Wylie Dissertation Fellowship from the University of Maryland. These supports are gratefully acknowledged.

My journey would not have been possible without the continuous support from my family back in China and in the US, to whom I am always grateful.

Table of Contents

List of Tables

List of Figures

Chapter 1: Introduction

1.1 Research Motivation

Membrane technology has been playing an increasingly important role in addressing the global water crisis [1, 2]. Membrane processes, such as nanofiltration (NF), reverse osmosis (RO), and forward osmosis (FO), have demonstrated their advantages in reliably removing traditional and emerging water contaminants over conventional treatment technologies [3-5]. Research and development in the past few decades have led to continual membrane performance improvement and marked cost reduction [1, 2]. All the advancements contribute to the wider adoption of membrane technology in water utilities.

At the center of the above-mentioned membrane processes is a semi-permeable membrane that allows the passage of water yet rejects water pollutants. The market of such semi-permeable membranes has been dominated by thin-film composite (TFC) polyamide (PA) membranes due to their salient advantages such as good separation capability and wide pH tolerance [1, 6, 7]. A TFC PA membrane generally consists of a thin (approx. 100 nm) selective PA layer formed via interfacial polymerization, a highly porous support for the PA layer, and finally a non-woven fabric to provide the mechanical strength [1, 6, 7]. In comparison to its predecessor, the anisotropic cellulose acetate membrane, the PA membrane exhibits much higher water permeability and wider pH compatibility [6, 7].

Although originally developed for RO/NF applications, the PA membranes have been successfully extended to the surging FO process [8]. Rather than working against the natural osmotic difference, FO utilizes it to drive water from the feed to the draw, which is then purified to obtain clean water. As FO eliminates the need of additional

hydraulic pressure as the driving force, it is considered a sustainable technology to augment water sources [1].

Despite the advancement and advantages, the TFC membrane also faces critical technical limitations regarding , for example, chlorine resistance [9, 10], fouling resistance [11, 12], and energy efficiency [13, 14]. It is also a challenge to make TFC membranes with thinner, more hydrophilic, and more porous support layers, which are crucial for high-performance FO membranes [15]. Besides, tuning membrane functionality during the synthesis of TFC membranes often becomes a formidable task. This is because the interfacial polymerization procedure for making TFC membranes has stringent requirements on the selection of chemicals, solvents, support layer, and reaction conditions. Therefore, new membrane materials and synthesis methods are highly desirable to significantly lessen the above problems while the water separation performance of the new membrane is at least comparable to, if not better than, that of the existing membranes.

The recently emerging graphene-based nanomaterials, graphene oxide (GO) in particular, have exhibited many interesting properties, which may be exploited to synthesize high performance membranes that avoid the aforementioned problems. As a single layer carbon sheet bearing carboxyl, hydroxyl, and epoxide functional groups, GO offers an extraordinary potential for making functional membrane materials with high chemical stability, strong hydrophilicity, and excellent antifouling properties [16, 17]. Most importantly, molecular simulations have demonstrated ultra-high flux, orders of magnitude higher than that of current TFC membranes, could be achieved through either the nanopores on the GO sheet or the capillary channels between GO planar surfaces [18,

19]. However, great technical hurdles need to be overcome before realizing the intriguing potential of GO in making next generation membranes. For instance, it is still impractical and extremely challenging to prepare a large area of monolayer graphene and generate high-density nanopores with controllable, relatively uniform sizes [17, 20]. Membranes prepared via GO solution filtration are not directly suitable for water purification, since stacked GO nanosheets disperse in water due to their strong hydrophilicity [17].

1.2 Research Objectives

The proposed research attempts to realize the potential of GO as a highly effective membrane material. This is achieved by systematically characterizing GO nanosheets, identifying membrane synthesis method, assessing GO membrane properties, and applying GO membranes for fouling control. It is anticipated that not only will the employment of GO bring advanced membrane performance, but also lead to a green membrane synthesis method. Specific research objectives are

- To systematically understand the properties of GO and construct high performance GO membranes
- To understand transport mechanisms for the GO membrane
- To unveil fouling mechanisms of the GO membrane
- To assess the regenerability of the GO membrane

1.3 Dissertation Organization

This Ph.D. dissertation comprises eight chapters including this introduction. The following briefly summarizes the remaining seven chapters.

- Chapter 2: A literature review is performed on the challenges facing membrane technology in terms of membrane materials and synthesis method, and on graphene oxide (GO) and particularly its potential as a new membrane material.
- Chapter 3: This chapter introduces a method of synthesizing GO membranes for NF via chemical cross-linking. By employing a cross-linker, GO nanosheets were covalently bonded to form a selective layer. The GO membranes showed promising performance and properties in comparison to commercial NF membranes.
- Chapter 4: FO membranes were developed by taking advantage of the charge property of GO. GO were sequentially deposited onto a substrate along with a cationic polyelectrolyte, poly(allylamine hydrochloride) (PAH), via electrostatic interactions. The layer-by-layer method provides a simple alternative to synthesizing high performance FO membranes.
- Chapter 5: Basic transport mechanisms are elucidated for the GO membranes.
- Chapter 6: This chapter investigates fouling mechanisms of GO membranes in FO and pressure retarded osmosis (PRO) modes. Compared to conventional FO membranes made via interfacial polymerization, the GO membranes showed significantly lower fouling propensity in PRO mode owing to the additional GO layers adjacent to the membrane support. The GO membranes also exhibited higher flux recovery upon cross-flow rinsing.
- Chapter 7: Regeneration of GO membranes was studied by investigating how to effectively remove the GO layers and to re-construct the GO layers onsite
- Chapter 8: This chapter summarizes major findings from the present research endeavor, and identifies future research topics.

Chapter 2: Literature Review

2.1 Challenges for Membrane Technology

Nanofiltration (NF), reverse osmosis (RO), and the recently resurgent forward osmosis (FO) membrane processes are among the most effective strategies to achieve high removal of both traditional and emerging contaminants from water [3-5]. All these processes require the use of semipermeable membranes, the market of which has been dominated for decades by thin-film composite (TFC) polyamide membranes due to their salient advantages such as good separation capability and wide pH tolerance. Despite decades of research and development, TFC membranes still face important technical limitations [2]. First and foremost is the issue of energy efficiency for the TFC membranes in membrane processes. Numerous cost analyses on membrane operations point out that considerable amount of energy is used for hydraulic pressure to maintain designed water flux and overcome concentration polarization [13, 14, 21, 22]. Thus development of highly permeable membranes has been proposed to reduce energy consumption [23-25]. Although the performance of TFC membranes have been improving steadily evidenced by the power consumption reduction over the past few decades, significant enhancement is necessary before reaching the theoretical minimum energy requirement for membrane separations [1]. Membrane fouling is another challenge that can impact membrane permeability negatively and thus decrease process efficiency [26-29]. It may even lead to premature replacements of membrane modules [30, 31], which adds to the overall operational cost. One intrinsic defect of the TFC membranes is the susceptibility of the polyamide network to chlorine degradation [10, 32], which is usually applied to control biofouling. Active chlorine species attack the

polyamide layer by N-chlorination of the amide N-H bond and subsequent ring-chlorination, which eventually damages the integrity of the selective layer and results in the failure of the TFC membrane [32-35].

In light of the above discussion, it is imperative to develop highly permeable membranes that present strong fouling and chlorine resistance. Towards this goal, this dissertation turns to graphene oxide, a novel two-dimensional material that may enable high performance next generation membranes for water purification.

2.2 Graphene Oxide

Although existed for a century and a half, graphene oxide (GO) has only started to amass enormous attention since the discovery of graphene [36, 37]. As a derivative of graphene, GO contains a range of oxygenated functional groups decorated at the peripheral and either side of the carbon lattice. Because of its ability to be mass produced via chemical oxidation followed by mechanical exfoliation, GO is frequently considered a precursor to graphene and other graphene-based materials, such as reduced GO [38]. Yet GO is also endowed with many exciting properties that may see potential applications in electronics [39], energy [40], sensors [41], optics [42], environmental remediation [43], separations [44, 45], etc.. This section reviews the properties and application of GO pertaining to its potential in developing high-performance next-generation membranes.

2.2.1 Synthesis

The general procedures of GO synthesis include oxidation of graphite flakes and mechanical exfoliation of the resulted graphitic oxide. The first preparation of GO dispersion dated back to 1860 when Brodie oxidized graphite in the presence of

potassium chlorate ($KClO_3$) and fuming nitric acid (HNO_3) [37]. The method was later modified by Staudenmaier [46], as $KClO_3$ was added in multiple aliquots in a single reaction batch. In 1958, Hummers and Offeman [47] introduced another oxidation approach based on a mixture of concentrated sulfuric acid (H_2SO_4) and potassium permanganate ($KMnO_4$). These three routes provide the basis for the synthesis of GO, although other methods with variations/modifications have been reported [48-50]. It should be noted that GO prepared with different methods may have varying properties [17]. Nevertheless, mass producible GO from cheap graphite flakes may have the potential to be a cost-effective membrane material.

2.2.2 Properties

As briefly mentioned above, GO exhibits many exciting properties for various applications. Of particular interest, for the sake of this dissertation, are those that are highly desirable to make high performance membranes for water purification.

Structural properties. While the exact chemical composition of GO is under debate, it is agreed upon that GO is a single-atom-thick sp^2 hybridized carbon lattice with oxygenated functional groups at the edges and on the basal planes. The early understanding of GO structure derived from experimental attempts using various techniques including nuclear magnetic resonance (NMR), chemical reactivity analysis, infrared spectroscopy (IR), Raman spectroscopy, thermogravimetric analysis (TGA), x-ray photoelectron spectroscopy (XPS), etc. A number of theoretical models have been proposed to better understand the macro-/microscopic structure of GO. These models have been thoroughly reviewed in Dreyer et al. [17]. Briefly, early models generally consisted of regular lattices with discrete repeating units and functional groups. For

example, the Hofmann model composed of graphite basal planes and epoxide groups, giving a stoichiometric ratio of C:O 2:1 [51]. Later efforts adopted a nonstoichiometric model due to the amorphous nature of GO. Most notably, the Lerf and Klinowski model delineates two regions on GO, one aromatic region with unoxidized benzene rings and the other with aliphatic six-membered rings, based on their NMR results [52]. Although these early studies outlined the basic GO structural information, detailed structure at atomic scale remained largely unknown. Such knowledge was only possible recently with the aid of aberration-correction high-resolution transmission electron microscopy (TEM). Boasting a resolution down to 1-Å, TEM is able to resolve every carbon atom in the field of view and provides a closer look at the atomic structure of GO. Using this tool, a refined picture is available for GO structure—GO sheets largely maintain the highly crystalline carbon lattice (graphite region) as in graphene [53, 54]; occasional defect areas or holes (normally under 5 nm^2) appear which are dominated by clustered five- and seven-membered rings [53, 55, 56]; oxidized regions form a continuous network of predominant epoxide and hydroxyl groups on the basal planes [56, 57]; carbonyl and carboxyl groups, despite their low density, are likely to appear along the edges of defects and GO sheets [56, 57].

These fascinating structural properties shed light on the potential of GO for developing efficient membranes. As in carbon nanotubes (CNTs), the graphitic regions of GO function as frictionless flow paths for water, leading to orders of magnitude of water flow enhancement due to incredibly long slip lengths [44, 58-60]. The slip length improvement is attributed to the formation of ordered hydrogen bonding in the nano-confined flow regime (i.e., between GO sheets) and weak interactions between

hydrophilic water and hydrophobic graphitic areas. The promising feature alone inspired many endeavors (including this dissertation) to pursue high flux membranes for water separations [45, 61]. Moreover, the functional groups of GO offer the capability of facile membrane synthesis and fine-tuning of membrane properties such as hydrophilicity, charge, functionality, etc.

Mechanical properties. Excellent mechanical strength is also necessary for prolonged membrane operation [62, 63]. Monolayer graphene may be the strongest material ever tested with the Young's modulus of 1.0 TPa and the fracture strength of 130 GPa, as Lee et al. found from their nanoindentation experiments using atomic force microscopy (AFM) with a diamond-coated tip [64]. Using similar tools, Gomez-Navarro et al. reported a Young's modulus of 0.25 TPa for a chemically reduced free-standing GO monolayer, which was also flexible within its elastic regime [65]. The difference in Young's modulus was contributed to the structural defects after oxidation, as evidenced in molecular simulations by Paci et al. [66]. The study also pointed out that the fracture strength of GO (63 GPa) was also lower than that of graphene at 116 GPa due to the oxidation of graphene [66]. The Young's modulus of a monolayer GO was also lower than that of pristine graphene, which was reported to be 0.21 GPa, due to the same reason [67]. Physically stacked GO films had Young's moduli an order of magnitude lower than that of a single (and double) layer GO [16, 65], because of competing bending and shear forces. Note that the fracture strength of the polyamide thin film (~200 nm), typical selective layer for RO, NF, and FO membranes, was estimated to be ~40 MPa [62, 63]. The extremely high fracture strength of GO suggests that GO membranes can be mechanically robust. Theoretical evidence has recently show that porous graphene

membranes can withstand pressures exceeding 57 MPa, roughly ten times that of typical pressures for seawater RO [68].

Antimicrobial properties. The antimicrobial properties of graphene-based materials are credited to their sharp aspect ratios, oxidative stress, charge transfer, and extraction of lipids from cell membranes [69-71]. Using transmission electron microscopy (TEM) studies, Hu et al. observed that GO nanosheets could be internalized and cause mild concentration-dependent cytotoxicity, and that the cellular structure of *E. coli* was largely compromised when in contact with GO [69]. This loss of cell integrity was postulated to be the result of either physical destruction or oxidation stress as found for carbon nanotubes (CNT) [69, 72]. By examining the efflux of cytoplasmic materials from the bacteria to the solution, Akhavan and Ghaderi confirmed that direct contact between bacteria and sharp edges of GO induced damage to the cell and the outflow of cytoplasmic materials [70]. It was further verified by the drastically higher RNA release from *S. aureus* (Gram-positive, no outer membrane) than that from *E. coli* (Gram-negative, with outer membrane) [70]. Interestingly, reduced GO displayed higher cytotoxicity due to partial elimination of surface charges and functional groups that in turn enabled enhanced charge transfer [69, 70]. Liu et al. compared antibacterial activity among graphite, graphite oxide, GO, and reduced GO, and proved the existence of oxidative stress, which was reactive oxygen species (ROS) independent as indicated by the oxidation of *in vitro* glutathione by GO and other graphene-based materials [71]. Based on the findings, they proceeded to propose a three-step antimicrobial mechanism similar to that for CNTs: initial deposition of bacteria on graphene-based materials, high

aspect ratio induced membrane stress, and the ROS-independent oxidation of cellular components [71, 73].

The direct proof for membrane stress exerted by GO came from molecular simulations performed by Tu et al., in which cell membrane damage was found to commence with dispersion interactions between GO sheets and lipid bilayers, followed by GO trapping/cutting into lipid membranes and concluded with vigorous extraction of phospholipid molecules from both inner and outer cell membranes onto GO sheets due to strong van der Waals and hydrophobic interactions [74]. These mechanisms explain the TEM observations from the authors and previous reports [70, 74].

Another computational-imaging study detailed the GO internalization to be initiated by membrane piercing by GO sheet asperities [75]. Recently, a force spectroscopy study suggests that the physical interactions between GO and *E. coli* are predominantly repulsive, highlighting the relative importance of other non-contact mechanisms such as membrane stress [76]. While far more work needs to be done both experimentally and theoretically to fully elucidate the antimicrobial mechanisms, it cannot be denied that the promising property is appealing to control biofouling of membranes, as will be discussed later.

2.2.3 Theoretical Investigation on Graphene Oxide Membranes

The concept of graphene-based water separation membranes was first examined by molecular simulations and other theoretical tools [77-80]. Generally, graphene sheets are impermeable [81], and thus pores ranging from sub-nanometer to nanometer size were designed on the graphene sheets, and passivated with functionalities. Molecular transport was then simulated through such nanoporous graphene membranes. Results suggest that

while pore size and chemical functionalization may determine the selectivity of the porous graphene, ultrafast transport can be achieved which is orders of magnitude higher than the conventional counterparts. Using first principles density functional theory calculations, Jiang et al. demonstrated that at 2.5 Å for the hydrogen passivated pore, extremely high permeance and selectivity of H_2 were simultaneously attainable at levels 10^5 and 10^{20} that of hydrogen separating silica membranes, respectively [77]. The promising outcome was ascribed to both the ultimate thinness and favorable diffusion barrier the graphene sheet presents [77]. Water transport was also modeled through the imaginable pores [78, 82]. Suk and Aluru compared the water flux through pores in graphene ranging from 0.75 to 2.75 nm to that through carbon nanotubes (CNTs) of similar tube diameters, and found lower flux at smaller sizes due to the frequent breaking of hydrogen bonding in water and defect-like water dipole orientation in the single-file flow regime, but higher flux at larger sizes as graphene pores showed decreased energy barrier at the entrance for the more bulk-like flow [78]. Suk and Aluru extended their simulation efforts to understand water transport mechanisms in the nanopores, which reveal that as the pore diameter increases, water viscosity and slip length for water confined in the pore decrease, and the water transport mechanisms switch from collective diffusion (i.e., diffusion by a chemical potential gradient) to frictional flow [82]. Other simulation investigations echoed similar conclusions [83]. These promising results regarding ultrafast water permeation inspired further simulation studies on the ion separation performance of the nanoporous graphene membranes.

Selective ion passage through graphene pores was first demonstrated by Sint et al. [79, 80, 84]. In their report, pores with a diameter of ~5 Å were passivated with either

hydrogen (positively charged) or fluorine−nitrogen (negatively charged), which block the passage of their co-ions (cations for H passivation and anions for F-N passivation, respectively). Both types of pores also show preferential rejection against certain solvated ions, e.g., no passage of fluoride ions through H-terminated pores [84]. Later Grossman's group explored the potential of nanopores for desalination specifically [79, 80]. In their first attempt, desalination was simulated through pores passivated with hydrogen atoms and hydroxyl groups with areal size from 1.5 to 62 $Å^2$ [79]. It was found that while rejection of NaCl understandably depends on the pore diameter, chemical functional groups may also play a role. The existence of hydroxyl groups leads to a two-time water flux increase due to their hydrophilicity, but it may also contribute to lower rejections due to their replacement of water molecules in ion hydration shells, which lowers the energy barrier for ion passage. Another interesting finding is that salt rejection decreases with elevated pressure for a given pore size, the opposite trend observed in conventional reverse osmosis (RO) processes. This is because the large effective volume of ions in solution respond more sensitively to the pressure increase than do water molecules. The study concludes with their optimal performance of up to two orders of magnitude higher water flux yet at similar or better rejection of NaCl, in comparison to that of currently available RO membranes [79]. Konatham et al. considered pores with size from 7.5 to 14.5 Å on graphene for desalination [85]. Similar steric effect on salt rejection was reported, where pores at 7.5 Å diameter show efficient ion exclusion but at 10.5 Å and 14.5 Å do not exert any resistance against ion transport. After functionalizing the pores with chemical groups (-OH, -COOH, and $–NH_2$), higher energy barrier against co-ions after their ionization occurred due to the steric effect and electrostatic repulsion. Yet

screening effects significantly lower the energy barriers for the ion transport at the pore entrance, and cause reduced ion rejection at higher concentrations.

Simulations of anomalous transport through stacked graphene/GO sheets also reveal some very interesting, albeit mixed, findings [44, 86]: (1) the hexagonal graphene lattice serves as an initial pattern for water molecules to form ordered and hexagonally symmetrical mono-, bi-, and tri-layered ice structures between graphene/GO sheets; (2) for ice mono- (interlayer spacing of about 6 Å) and tri-layers (interlayer spacing of about 11.38−11.46 Å), it is energetically favorable for water molecules to move along the carbon lattice than penetrate through hydrophilic pores newly created, explaining the impenetrable characteristic for graphene layers; (3) for ice bi-layers (interlayer spacing of 8.43−8.59 Å), however, hydrophilic functional groups (e.g., -OH) on the pores or the edges of the carbon sheets decrease the interlayer interactions between ice and interrupt the ice bilayer structure that allow water molecules to traverse to the neighboring void to form new ice bi-layers, which highlight the reason for the passage of water in GO films; and (4) a capillary-like pressure, in the scale of 1000 bars, enables low friction flow of monolayer water in the capillaries formed by the unoxidized regions in GO sheets.

2.2.4 Experimental Achievements on Graphene Oxide Membranes

Experimental explorations have begun recently to realize the immense potential in GO membranes. One type of such membranes involve creating pores on graphene/GO basal planes as in the simulation studies [20, 87-91]. For this very purpose, various techniques have been used including ultraviolet-induced oxidative etching [20], transmission electron microscope (TEM) cutting [87], chemical vapor deposition (CVD) with intrinsic defects [88, 89], focused ion beam (FIB) [90], oxygen plasma etching [91], etc. Although

these “tiny” nanoporous membranes, with the largest reported to be 25 mm^2 by CVD in [89], have been experimentally used for water/gas separation, protein translocation, and other applications [20, 87-91], large-scale employment of these porous membranes is technically restricted due to the limitations of the pore forming processes [45, 79].

Another type of GO membranes are obtained in the form of stacked GO sheets by simply filtering or spray-/spin-coating GO suspensions. As a proof of concept study for water separation membranes, Nair et al. demonstrated that micrometer thick GO laminates allow unimpeded permeation of water yet block other liquids, vapors, and gases, including helium [44]. As discussed above, their simulations attributed the anomalous water transport to the capillaries formed between graphene sheets, which provide a capillary-like pressure to maintain wetting on the external GO surface and low-friction flow pathways for monolayer water. This evaporation-limiting transport excludes the passage of other molecules due to reversible narrowing of the capillaries so that water cannot fill in low humidity, and/or to the clogging in the functional groups/spacers region by water molecules [44]. The high capillary-like pressure also act on ions that fit in the formed nanocapillary, making GO films precise molecular sieves with a sharp diameter cutoff at 9 Å [92]. For solutes of hydrated radii greater than 4.5 Å, no permeation occur through the GO laminates, yet smaller species, disregarding the charge, travel through the film at a similar rate that is three orders of magnitude higher than diffusion. Han et al. later conducted more detailed experiments to showcase the potential of the stacked graphene sheets for nanofiltration (NF) [93]. They used reduced GO to make the ultrathin laminates (22–53 nm thick, controlled by GO loading) via filtration, and found the flux to double that of GO films made in the same manner due to the disappearance of the

functional groups. Pure water flux reached ~22 $Lm^{-2}h^{-1}bar^{-1}$, and such high flux cannot be explained by parallel plate Hagen–Poiseuille equation. Rather, it could be well explained by the slip flow theory that suggests enhanced water flux with water flow velocity on the graphene surface. Although moderate rejections (20-60%) were achieved against ion salts, the reduced GO membranes showed near complete retention (> 99%) of organic dyes in dead end filtration mode due to both size exclusion and Donnan exclusion.

In order to precisely tune the interlayer spacing between layered graphene sheets, a number of approaches have been reported to cater to different applications of stacked GO films. Notably, these are physical or chemical intercalation and corrugation modulation by hydrothermal treatment. As an alternative tool to atomic force microscopy (AFM), Qiu et al. proposed water flux and rejection measurement as an indirect indicator to the degree of the graphene sheet corrugation after hydrothermal treatment of the GO films [94]. As the treatment temperature increased from 90 °C to 150 °C, water flux and pore size (by size exclusion experiments) increased monotonically, implying greater degree of corrugation to the sheets. Another method involves the expansion of the GO layers by inserting chemicals, creating chemical bonds, and performing volume-expansion reactions in the interlayers. For example, the interlayer distance was modified by stuffing alkylamines with different molecular weights [95] , copper hydroxide nanostrands [96], and multi-walled CNTs [97], and by selectively crosslinking GO with diboronic acid [98]. Because of the relatively small amplitude (~50 nm) and the likelihood of residues, a modified intercalating method was developed based on the temperature-dependent decomposition reaction of ammonium nitrate [99]. The decomposition of 1 mol of ammonium nitrate yields 1 mol of ammonia gas and nitric

acid at 140 °C, 3 mol of gases (N_2O and H_2O) at 200 °C, and 3.5 mol of gases (N_2, O_2, and H_2O) at 400 °C, respectively. Due to the mass/volume of the gases produced, the interlayer spacing can be tuned in the range of 123%-20000% for different separation applications. Although research on the physically stacked GO membranes yielded promising results in lab-scale dead-end filtration, these laminates are unlikely to find practical applications for water purification due to the hydrophilicity of GO and/or the shear stress induced by cross-flow conditions [45].

Thus the literature has seen a third category of GO membranes, which were designed with chemically bonded GO sheets as the selective layer. As the very first attempt (Chapter 3 in this dissertation) to achieve the potential of GO in making high performance membranes for water purification, our group innovatively exploited the functionality of oxygenated groups in GO and chemically cross-linked the GO sheets in a layer-by-layer fashion on a polysulfone support for a highly efficient NF membrane [45]. The cross-linker, 1,3,5-benzenetricarbonyl trichloride (TMC), not only inter-connected GO nanosheets with the necessary stability to overcome their inherent dispensability in water environment, but also separate the GO sheets to provide nanochannels for ultrafast water flow. The cross-linking also fine-tuned the charge and functionality of the GO membrane. Although the GO membrane in the present development stage had a relatively low rejection (6–46%) of monovalent and divalent salts, it exhibited a moderate rejection (46–66%) of Methylene blue and a high rejection (93–95%) of Rhodamine-WT. The rejection performance of the GO membrane was mainly determined by the spacing (estimated to be 1 nm) between GO layers and the charges on GO nanosheets. At similar rejection levels, the GO membrane exhibited a 4–10 fold flux (80 and 276 LMH/MPa)

over that of most commercial NF membranes. Our group later proposed an aqueous solution based synthesis method for a new forward osmosis (FO) membrane (Chapter 4 in this dissertation), benefiting from the charge properties of GO [61]. Water permeability of the GO membrane was found to be about one order of magnitude higher than that of a commercial FO membrane. The GO membrane also presented impeded transport towards neutral solutes due to the swelling-prone nature of electrostatically formed GO layers. These early investigations have sparked great efforts in developing stable GO membranes [100, 101] and membrane modification with GO [102-105], in order to realize the potential of GO in the membrane field. For example, diamine monomers were applied to cross-link filtered GO nanosheets, producing composite membranes with decreased interlayer distance and excellent pervaporation performance [100]. GO was assembled onto poly(ethylene imine) (PEI) treated hollow fiber membranes via electrostatic interactions, and the resulted membranes showed higher flux and mechanical strength and shortened the overall synthesis duration [101].

Lastly, GO has also been used to modify membrane properties for enhanced performance. A simple method is to blend GO sheets in the membrane matrix, making the so-called composite membranes. For instance, GO was incorporated into polysulfone membranes for improved hydrophilicity and salt rejection [102], and for fouling control [103]. Alternatively, one can graft GO onto membrane surface to better capitalize on the favorable properties of GO. Choi et al. sequentially assembled pristine GO (negatively charged) and aminated-GO (positively charged) onto polyamide (PA) RO membranes to protect the PA layer from chlorine attach [104]. Due to the unique water flow on graphene surface, the addition of GO did not impose extra resistance towards water

transport. Instead, the GO coating increased membrane hydrophilicity, lowered protein fouling propensity due to reduced surface roughness, and retarded chlorine diffusion and thus shielded the vulnerable PA from chlorine-induced degradation. Using 1-ethyl-3-[3-(dimethylamino)propyl]carbodiimide (EDC) and N-hydroxysuccinimide (NHS) chemistry, Perreault et al. coupled GO onto PA surface for enhanced biofouling resistance, and found that 1 h direct contact with the modified PA membrane led to ~65% *E Coli* inactivation whereas the control PA membrane had no such effect [105]. Their electron micrographs show that the exceptional anti-microbial property was mainly ascribed to physical cell damage induced by GO, and did not arrive at the expense of sacrificing membrane transport properties [105]. Mixture of GO and 1,3-Phenylene diamine (MPD) for interfacial polymerization also resulted in NF membranes with GO in the PA network [106, 107]. Again the PA membrane with GO showed higher permeability and better fouling performance due to the unique properties of GO. Similar studies have been reported by many others [108, 109], signifying the marked improvement brought by just GO modification.

2.3 Layer-by-Layer Assembly

Layer-by-layer (LbL) assembly is a relatively new and facile method of modifying surface properties and/or surface coating [110]. From the very perspective of creating thin separation coatings, the method has been used to develop membranes for pervaporation [111-113], nanofiltration (NF) [114-118], RO [114, 119], and lately FO [115, 120-122]. It consists of iterative soaking of a substrate (of any shape or surface morphology) in a polycation solution and a polyanion solution. Each iteration adds a

layer of the polycation/polyanion on the surface due to one or more of the following mechanisms: electrostatic interactions, hydrophobic interactions, hydrogen-bonding, dispersion forces, etc. [123]. Compared to the popular method of interfacial polymerization for RO membrane synthesis, the LbL assembly is more cost effective and environmentally friendly as all fabrication work can be completed in aqueous solutions. It is thus argued that LbL assembly may be a viable green alternative to interfacial polymerization for making high performance FO membranes [120, 122].

GO is typically negatively charged due to the ionization of carboxylic groups in water [124, 125], therefore it can be potentially used as a polyanion in an LbL assembly process. Indeed, GO thin films have been constructed electrostatically with cationic polyelectrolytes, such as poly(diallyldimethylammonium chloride) (PDDAMAC) and poly(allylamine hydrochloride) (PAH), as a precursor for conducting films [126, 127]. Using PDDAMAC as polycation, Kotov et al. built ultra-thin films comprising partially exfoliated GO platelets (2-3 GO sheets) in each GO layer [126]. The thickness of each layer was monitored to grow linearly, and was estimated to be 16 Å for PDDAMAC layer and 22 Å for GO layer [126]. This finding led to the study of LbL assembly of single-sheet GO films with PAH. Similarly, linearity was also observed for the thickness of successive layers [127]. It was also found that the film thickness was dependent upon the pH of the polyelectrolyte solutions, and thin films could be adsorbed on substrates regardless of their roughness [127].

Chapter 3: Enabling Graphene Oxide Nanosheets as Water Separation Membranes

3.1 Abstract

This chapter reports a novel procedure to synthesize a new type of water separation membrane using graphene oxide (GO) nanosheets such that water can flow through the nanochannels between GO layers while unwanted solutes are rejected by size exclusion and charge effects. The GO membrane was made via layer-by-layer deposition of GO nanosheets, which were cross-linked by 1,3,5-benzenetricarbonyl trichloride, on a polysulfone support. The cross-links provided the stacked GO nanosheets with the necessary stability to overcome their inherent dispensability in water environment and also fine-tuned the charges, functionality, and spacing of the GO nanosheets. We then tested the membranes synthesized with different numbers of GO layers to demonstrate their interesting water separation performance. It was found that the GO membrane flux ranged between 80 and 276 LMH/MPa, roughly 4-10 times higher than that of most commercial nanofiltration membranes. Although the GO membrane in the present development stage had a relatively low rejection (6-46%) of monovalent and divalent ions, it exhibited a moderate rejection (46-66%) of Methylene blue and a high rejection (93-95%) of Rhodamine-WT. The chapter is concluded by emphasizing that the facile synthesis of a GO membrane exploiting the ideal properties of inexpensive GO materials offers a myriad of opportunities to modify its physicochemical properties, potentially making the GO membrane a next-generation, cost-effective, and sustainable alternative to the long-existing thin-film composite polyamide membranes for water separation applications.

3.2 Introduction

Dwindling water resources and increasing water consumption have forced us to consider new advanced water treatment technologies that can provide a safe water supply in a more energy efficient, environmentally sustainable way [2, 128]. Nanofiltration (NF), reverse osmosis (RO), and the recently resurgent forward osmosis (FO) membrane processes are among the most effective strategies to achieve high removal of both traditional and emerging contaminants from water [3-5]. All these processes require the use of semipermeable membranes, the market of which has been dominated for decades by thin-film composite (TFC) polyamide membranes due to their salient advantages such as good separation capability and wide pH tolerance.

Despite their advantages, TFC membranes face important technical limitations regarding, for example, chlorine resistance [10, 32], fouling resistance [12, 26, 28, 129], and energy efficiency [13, 14]. It is also a challenge to make TFC membranes with thinner, more hydrophilic, and more porous support layers, which are crucial for high-performance FO membranes [15]. Besides, tuning membrane functionality during the synthesis of TFC membranes often becomes a formidable task. This is because the interfacial polymerization procedure for making TFC membranes has stringent requirements on the selection of chemicals, solvents, support layer, and reaction conditions. Therefore, new membrane materials and synthesis methods are highly desirable to significantly lessen the above problems while the water separation performance of the new membrane is at least comparable to, if not better than, that of the existing membranes.

The recently emerging graphene-based nanomaterials have exhibited many interesting properties such as adsorption of metal and organic dyes, antimicrobial capability, and photocatalytic degradation of organic molecules [71, 130-134]. In particular, graphene oxide (GO) nanosheets – oxygenated graphene sheets bearing carboxyl, hydroxyl, and epoxide functional groups – offer an extraordinary potential for making functional nanocomposite materials with high chemical stability, strong hydrophilicity, and excellent antifouling properties [16, 17, 135], all of which could be promisingly exploited in water treatment processes. So far, most water-related applications of GO have focused on its adsorptive and photocatalytic properties[130-132].

The concept of using graphene-based nanomaterials to make water separation membranes was first examined by molecular simulations [18, 79]. Nanopores were simulated on the surface of super-high strength graphene monolayers to allow water to permeate through them while selectively rejecting other substances. It was demonstrated that, by controlling pore sizes and functional groups on the nanopores, one could make a monolayer graphene membrane potentially useful for desalination, with a water permeability of several magnitudes higher than that of current RO membranes. Recently an experimental study on porous graphene membranes was reported, where ultraviolet-induced oxidative etching was used to generate nanopores on graphene sheets and the membrane selectivity for gas separation was tested [20]. Despite these simulation and experimental efforts, there exist at present significant technical difficulties in creating such membranes for real-world water separation applications. For instance, it is still impractical to prepare a large area of monolayer graphene [17]. It is also extremely

challenging to generate high-density nanopores with controllable, relatively uniform sizes on the graphene sheet [20].

Using an alternative strategy, we may fabricate a water separation membrane with stacked GO nanosheets. This is because the GO nanosheet is single-atom-thick with lateral dimensions as high as tens of micrometers, making it highly stackable [17]. The two-dimensional channels between the stacked GO nanosheets may allow water to pass through while rejecting unwanted solutes, a mechanism similar to that of the pores in traditional membrane structures. Molecular simulations have predicted that water has a very large slip length (i.e., low friction) on graphene surfaces, resulting in an extremely high rate of water flow in planar graphene nanochannels [136-142]. This property promises high water flux in stacked GO nanosheets. In addition, GO nanosheets can be mass-produced via chemical oxidization and ultrasonic exfoliation of graphite [143-146], thereby significantly lowering the material manufacturing cost and facilitating scale-up of the membrane synthesis process. Furthermore, the functional groups (particularly carboxyl groups) on GO nanosheets provide convenient sites for further functionalization to enhance properties such as charges and specific interactions with water contaminants [147-152]. With these exceptional properties, GO becomes an ideal material for potentially making high-performance membranes for water separation.

Experimental evidence has demonstrated that stacked GO nanosheets made by a simple solution filtration method exhibited excellent mechanical strength in dry conditions [20], and could be used as a gas/vapor separation membrane [153]. A superfast permeation of water vapor through such a GO membrane was observed and credited to a nearly frictionless flow of monolayered water through the planar capillaries

formed by the closely stacked GO nanosheets [153]. This exciting water vapor transport phenomenon has inspired us to explore the feasibility of innovatively using the stacked GO nanosheets as a membrane to filtrate water in liquid phase.

It should be emphasized that the above water vapor/gas separation GO membrane in its present form is not directly suitable for water separation. This is because a GO membrane made via solution filtration is unstable in water, as GO nanosheets are extremely hydrophilic [17]. To resolve this problem, stable bonding must be created between GO nanosheets to prevent their dispersion in water. While our paper was under review, water purification by a membrane comprising unbonded GO nanosheets was reported [154]. Based on our lab experience, however, unbonded GO layers can be easily damaged even with a gentle finger touch or detached from the membrane support by water rinsing. Besides, even though some performance data can be collected through extremely careful handling of the membrane made with unbonded GO nanosheets, such a membrane does not survive the cross-flow testing conditions, which are typical in real-world membrane operations. These lab observations reinforce the need for sufficient bonding of GO nanosheets in order to make the GO membrane viable for use in water separation.

Many fundamental questions arise when GO nanosheets are considered a candidate material for making water separation membranes. For example, water transport through the nanochannels of stacked GO nanosheets in aqueous solution has not been experimentally characterized. Thus, whether high water permeability can be achieved with a GO membrane is yet to be answered. It is also unclear whether the nanochannels within a GO membrane can provide enough barriers for the removal of targeted water

contaminants (e.g., salts, organic molecules, and inorganics). Indeed, it is critical to properly engineer the nano-structure of stacked GO nanosheets so that desirable water separation performance can be achieved. So far, successful synthesis of a membrane using bonded GO nanosheets and with stable water separation performance has not been reported in the literature.

As a first attempt to answer the above identified questions, a novel procedure is presented in this paper to make a new type of water separation membrane using stacked GO nanosheets. We deposited GO nanosheets via a layer-by-layer (LbL) approach on a polydopamine-coated polysulfone support and then cross-linked them by 1,3,5-benzenetricarbonyl trichloride (TMC). Next, we characterized the physicochemical properties of GO nanosheets and also the resulting GO membrane by various techniques. In addition, quartz crystal microbalance with dissipation (QCM-D) was used to validate the LbL approach used in the GO membrane synthesis. Finally we tested and compared water flux and rejection performance of GO membranes containing different numbers of deposited GO layers.

3.3 Materials and Methods

3.3.1 GO Preparation

We prepared GO from graphite using the modified Hummers method [143, 145]. First, flake graphite was oxidized in a mixture of $KMnO_4$, H_2SO_4, and $NaNO_3$ (Sigma-Aldrich, St. Louis, MO); the resulting pasty solution was then diluted and sifted through a polyester nonwoven fabric filter (PET, grade 3249, Ahlstrom, Helsinki, Finland) by vacuum filtration. The GO solids retained by the fabric filter were suspended in deionized

(DI) water and centrifuged at 8000 g-force using a Sorvall RC 6+ (Thermo Scientific, Marietta, OH). The GO solids remaining at the bottom of the centrifuge tube went through at least three cycles of re-suspension in DI water and then centrifugation to completely wash out chemical residuals. The washed GO suspension was subsequently ultrasonicated (S-4000, Misonix, Farmingdale, NY) to exfoliate GO particles into GO nanosheets. As the last step, the sonicated solution was centrifuged at 8000 g-force to remove any un-exfoliated graphite residues, resulting in a pure GO nanosheet suspension.

3.3.2 GO Membrane Synthesis

The overall membrane synthesis procedure is illustrated in Figure 3.1(a). First, we used a porous polysulfone membrane (Sepro Membranes, Inc, Oceanside, CA) as the base support and dip-coated it in dopamine solution, which was composed of 2 g/L dopamine (Sigma-Aldrich, St. Louis, MO) and 10 mM Tris buffer (Sigma-Aldrich, St. Louis, MO) at pH 8.5. Dopamine polymerized to form polydopamine on the polysulfone support. Then, the polydopamine-coated support was dried in oven at 65 °C and subsequently soaked in 0.15 wt.% of TMC solution that was dissolved in Isopar for 10 min. Both TMC and Isopar were purchased from Sigma-Aldrich (St. Louis, MO). The support was then rinsed with Isopar to remove excessive TMC and subsequently soaked in GO solution (2.8 wt.%, dissolved in Isopar), which had been sonicated to break up any GO aggregates possibly formed due to their high hydrophilicity, for 10 min to attach the first layer of GO nanosheets onto the membrane support. Next, the membrane was rinsed in Isopar to remove excessive GOs and then alternately dipped into TMC and GO solutions for a prescribed number of cycles to create the desired number of additional layers of TMC

and GO. Finally, the synthesized GO membrane was boiled in a 95 °C water bath for 2 h to completely remove any residual Isopar.

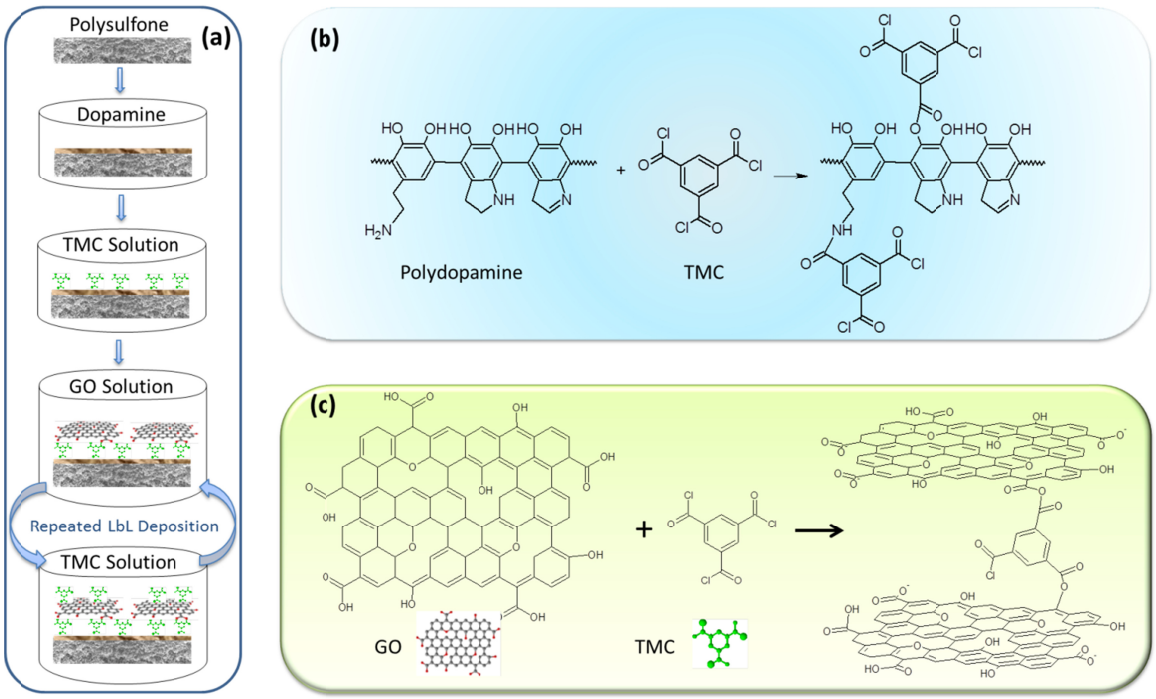

Figure 3.1 Schematic illustration of (a) a step-by-step procedure to synthesize the GO membrane, (b) the mechanism of reactions between polydopamine and TMC, and (c) the mechanism of reactions between GO and TMC.

3.3.3 Characterization Techniques for GO Nanosheets and GO Membranes

The properties of GO nanosheets and GO membranes were characterized by Raman spectroscopy (LabRam ARAMIS, HORIBA Scientific, Edison, NJ), atomic force microscopy (AFM) (Multimode, Digital Instruments, Plainview, NY), x-ray photoelectron spectroscopy (XPS) (Kratos AXIS 165, Kratos Analytical, UK), Fourier transform infrared (FTIR) spectroscopy (Nicolet 6700, Thermo Scientific, Marietta, OH), scanning electron microscopy (SEM) (SU-70, Hitachi High Technologies America, Gaithersburg, MD), and zeta-potential analyzer (Zetasizer Nano ZS90, Malvern

Instruments, UK). For the AFM imaging of GO nanosheets, a few drops of diluted GO suspension were deposited on a smooth glass, which was then dried before being loaded onto AFM. All membrane samples were dried in oven at 65 °C prior to characterization.

3.3.4 QCM-D Experiments

The QCM-D experiments were performed with a Q-sense E4 system (Q-sense, Sweden) to characterize the rate of polydopamine/GO/TMC deposition during GO membrane synthesis. A Q-sense open module 401 (Q-sense, Sweden) with a gold sensor was used in the measurement. This open module enabled the pipetting of solution directly to the sensor surface and the monitoring of polymer growth and LbL deposition on the sensor without any concern of flow channel contamination. The coating protocol for the QCM-D experiments, including the coating sequence, duration of dipping, and coating solution composition, was kept the same as that used for the synthesis of GO membranes. The sensor vibration frequency and dissipation were recorded at 7 overtones during the coating process. A viscoelastic model from the Q-Tools software (Q-sense, Sweden) was used to analyze the frequency and dissipation data for the calculation of the amount of mass (ng/cm^2) deposited on the sensor surface.

3.3.5 Membrane Flux and Rejection Tests

We investigated water flux and rejection performance of the GO membrane using a dead end membrane filtration system. This system consists of a feed tank pressurized with a nitrogen cylinder, a stirred cell (Amicon 8050) from Millipore (Billerica, MA), and a digital balance (Denver Instruments, Denver, CO) to monitor the permeate water flux, which can be automatically recorded by a PC using data acquisition software. DI water was used to test the pure water flux of the membrane. Before the flux test, the membrane

coupon was installed in the stirred cell and stabilized overnight under a trans-membrane pressure of 50 psi (0.34 MPa). A polydopamine-coated polysulfone membrane (i.e., the membrane without TMC yet) was chosen as a control, because TMC was used to cross-link GO nanosheets and thus it was considered part of the GO layers of the synthesized membrane.

To characterize membrane rejection performance, we tested the GO membrane with the following feed solutions in the listed order, one at a time: NaCl (20 mM), Na_2SO_4 (10 mM), Methylene blue (MB) (7.5 mg/L), and Rodamine-WT (R-WT, 7.5 mg/L). All chemicals were obtained from Sigma-Aldrich (St. Louis, MO), and no pH was adjusted in the prepared solution. Note that MB is a positively charged cation with a molecular weight of 284 Daltons, and R-WT is a negatively charged anion with a molecular weight of 487 Daltons. In each rejection test, the experiment was stabilized under 50 psi (0.34 MPa) for 2 h to eliminate the adsorption effect of GO, before the feed and permeate samples were collected for concentration analysis. The concentrations of NaCl and Na_2SO_4 were measured by a conductivity meter (Accumet Excel XL30, Thermo Scientific, Marietta, OH). The concentrations of MB and R-WT were analyzed using a UV-VIS spectrophotometer (UV160U, Shimadzu Scientific Instruments, Columbia, MD) at a wavelength of 590 and 355 nm, respectively. The membrane was rinsed with DI water for at least 2 h between testing with different solutions.[155]

3.4 Results and Discussion

3.4.1 Physicochemical Properties of GO Nanosheets

We used several characterization techniques to understand the unique physicochemical properties (e.g., shape, functionality) of GO nanosheets, as these properties could greatly affect the subsequent GO membrane synthesis and eventually the membrane performance. The GO suspension prepared by the modified Hummers method had a yellowish/light brown color, indicating that the carbon lattice structure was distorted by the added oxygenated functional groups, since pure graphene or graphite is black. The fabricated GO nanosheets were very hydrophilic and remained suspended in water for several months without a sign of aggregation or deposition. The Raman spectrum (Figure 3.2(a)) shows a G peak at ~1590 cm^{-1}, which signifies the sp^2 hybridization of graphitic carbon, and a D peak at ~1350 cm^{-1}, which confirms carbon lattice distortion. The FTIR spectrum (Figure 3.2(b)) indicates the presence of un-oxidized sp^2 C=C bonds in the carbon lattice (1630 cm^{-1}), oxygen-containing functional groups of C-O vibrations (1047cm^{-1}) and C=O stretching vibration (1724 cm^{-1}). The XPS data (Figure 2(c)) show that about 60% of carbon was not oxidized, 32% had C-O bond (representing hydroxyl and epoxide groups), and 7% had COOH bond. The zeta potential measurement (Figure 3.2(d)) reveals that the GO nanosheets were negatively charged over a wide pH range. It is seen from the AFM image (Figure 3.2(e)) that the lateral sizes of GO nanosheets vary between 100 and 5000 nm. The depth profiles (Figure 3.2(f)) obtained by analyzing the AFM image demonstrate that the heights of GO nanosheets are in the range of 1-2 nm, indicating the GO nanosheets contained either single or double layers of carbon lattice.

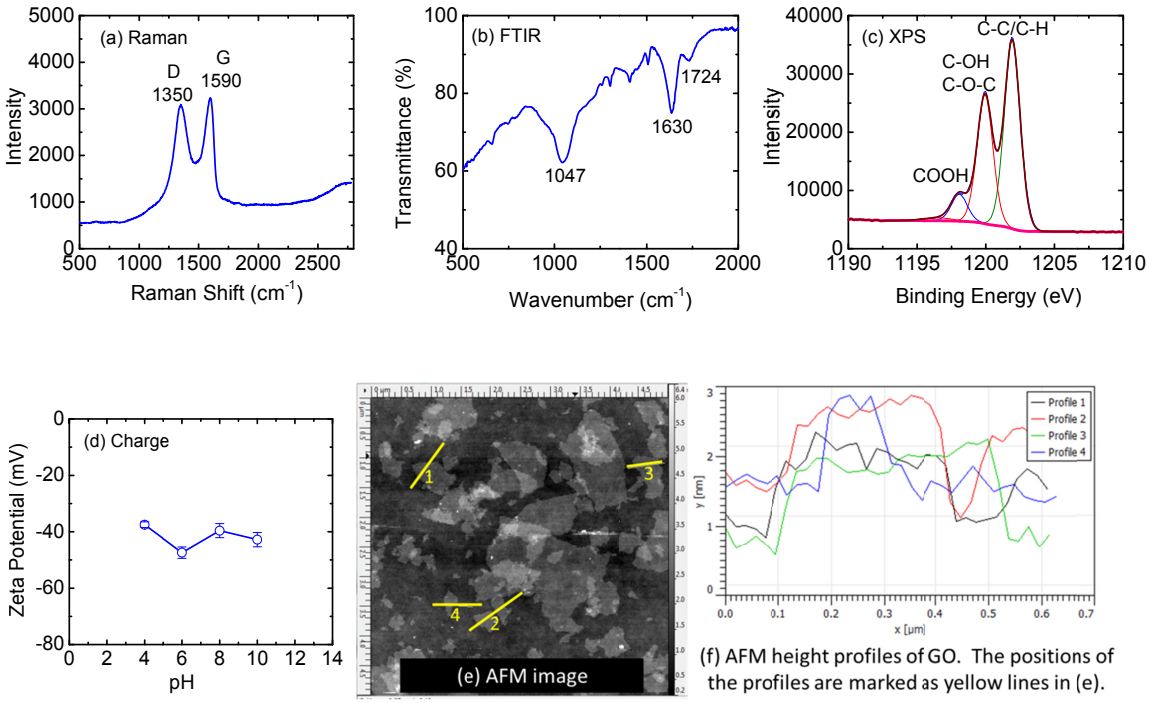

Figure 3.2 Characterization of GO nanosheets.

3.4.2 QCM-D Validation of the Membrane Synthesis Procedure

QCM-D experiments were performed to examine the effectiveness of the procedure for making the GO membrane. The kinetics of polydopamine coating was analyzed with a clean sensor. As shown in Figure 3.3(a), the clean sensor was first tested in DI water for 0.2 h to calibrate the initial reading to 0 ng/cm^2. Then, DI water was replaced by a freshly prepared dopamine solution. Since turbulence was generated by the pipetting of solution in and out of the open module, the noisy data between 0.2 and 0.6 h were rejected in the data analysis. The stabilized data between 0.6 and 1.2 h reveals a continuous increase in the mass on the sensor surface. This trend suggests that, under studied conditions, a layer of polydopamine was effectively coated on the polysulfone support and that the layer thickness increased linearly with time during the first hour or so. Specifically, after being soaked in the dopamine solution for around 1 h, the sensor surface was coated with a total

of ~1200 ng/cm^2 polydopamine. Therefore, by appropriately varying the coating time, we may be able to accurately control the deposition of polydopamine and hence to obtain the desired polydopamine coverage and coating thickness on the membrane support.

After polydopamine coating, the LbL deposition of TMC and GO on the polydopamine-coated sensor was also analyzed by QCM-D experiments. To be consistent with the LbL membrane coating protocol, the polydopamine-coated sensor was taken out of the open module to let dry in oven before being put back to the QCM-D system for the LbL deposition study. As shown in Figure 3.3(b) for the case of 8 GO layers, the dried polydopamine-coated sensor was first tested in pure Isopar for 0.2 h to calibrate the initial reading to 0 ng/cm^2. Then the sensor was alternately soaked in TMC and GO solutions while the change in mass on the sensor was monitored continuously. Each cycle of TMC and GO soaking took around 0.5 h and one additional GO layer was created on the sensor surface, with TMC working as a cross-linker between GO layers. Figure 3.3(b) reveals that the sensor mass increases continuously with the increasing number of GO layers, even though significant fluctuation of data caused by the in-and-out solution pipetting induced turbulence is observed. After the deposition of 8 GO layers, a total of ~1500 ng/cm^2 TMC-crosslinked GO was coated on the polydopamine surface. Although unknown experimentally, the density of GO layer may be estimated considering that typical graphene has a density of 2.2 g/cm^3 and the spacing between GO nanosheets is generally twice that between graphene nanosheets [17]. In this way a density of 1.1 g/L (i.e., half the graphene density) was obtained for the cross-linked GO layer. Based on this density, the thickness of the GO membrane (excluding the polysulfone support) with 8 cross-linked GO layers was estimated to be 14 nm by the Q-tools software.

The increase of membrane thickness observed in QCM-D measurement suggests that the LbL procedure is effective for coating GO onto a polydopamine surface. The membrane with deposited GO layers was experimentally proven to be stable despite Isopar rinsing between deposition steps, even under the turbulence created by the pipetting of solutions in and out of the open module. This stability indicates that TMC is capable of functioning as an effective cross-linker between polydopamine and the GO nanosheets closest to the membrane support as well as between neighboring GO nanosheets, thereby enabling the stacked GO nanosheets as a membrane that is indeed viable in water environment.

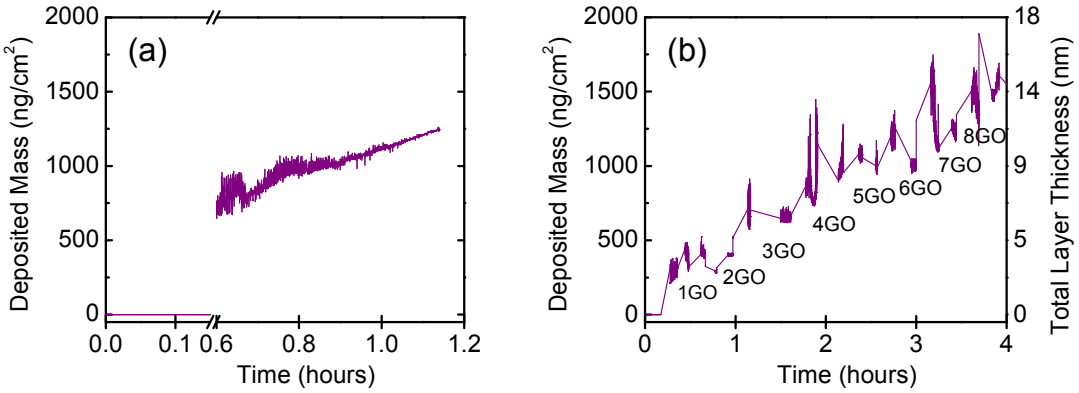

Figure 3.3 QCM-D characterization of deposition rates for (a) the polydopamine coating and (b) the LbL synthesis of TMC/GO layers. The polydopamine coating test started with a clean gold sensor in DI water to calibrate the initial reading to 0 ng/cm2, and then the DI was replaced by an aqueous solution containing 2 g/L dopamine and 10 mM Tris buffer at pH 8.5. The LbL deposition test started with an oven-dried, polydopamine-coated sensor in Isopar to calibrate the initial reading to 0 ng/cm2, and then the sensor was alternately exposed to 0.15 wt.% TMC and 2.8 wt.% GO solutions, both of which were dissolved in Isopar. Each cycle of TMC/GO coating lasted around 0.5 h, followed by Isopar rinsing.

3.4.3 GO Membrane Synthesis

Synthesis of the GO membrane took three major steps. The first step was to create active functional sites on the membrane support so that the first GO layer can be strongly bonded to these sites to ensure membrane stability. To this end, we first coated the polysulfone support with polydopamine, a proven effective coating material for polymeric membranes [156]. Then, the polydopamine-coated support was submerged in TMC solution, which contained three active acyl chloride groups. As shown in Figure 3.1(b), the acyl chloride groups in TMC reacted with the hydroxyl or amine groups in polydopamine to form ester or amide bonds. As a result, free acyl chloride groups were created on the polydopamine-coated membrane surface.

In the second step, the first GO layer was attached to the polydopamine-TMC-treated membrane support. Because the exposure of GO to TMC anchored free acyl chloride groups on the support surface, when the polydopamine-TMC-treated support was subsequently soaked in GO solution, the free acyl chloride groups reacted with the carboxyl or hydroxyl groups in GO to form anhydride or ester bonds, as schematically illustrated in Figure 3.1(c). Ester bonds were likely the dominant cross-linking bonds in the GO membrane, because anhydride bonds might hydrolyze when the GO membrane was exposed to an aqueous environment. Therefore, the first GO layer could be firmly attached to the support by chemical bonds, with TMC working as the cross-linker between polydopamine and GO. Note that without polydopamine coating, the GO layer could not have been effectively attached to the polysulfone support.

As the last step, the LbL deposition of TMC and GO was repeated by alternately soaking the membrane in TMC and GO solutions. During each deposition process, TMC

reacted with GO to chemically bond the newly deposited TMC/GO layer onto the membrane surface. The reaction mechanism was the same as that illustrated in Figure 1(c). Each cycle of alternate soaking created additional layers of TMC and GO, again with TMC functioning as a cross-linker now between neighboring GO layers. The total number of repeated deposition cycles determined the number of GO layers in the final membrane product, with the last deposited layer always being GO.

3.4.4 GO Membrane Characterization

SEM was used to examine the surface morphology of the polysulfone, polydopamine-coated polysulfone, and GO membranes, respectively. Pores with 10-30 nm in diameter are observed in Figure 3.4(a) on the relatively smooth surface of the pure polysulfone membrane. Polydopamine coating slightly reduced the pore sizes because it was deposited on the pore walls as well as on the surface of the support. At this stage, the pores were still visible and some bumps were created on the membrane surface (Figure 3.4(b)). After the coating of GO layers, however, the membrane surface morphology was significantly changed, where pores became invisible and the surface was composed of scale-like structures. Figure 3.4(c) shows the image for a representative 7-layered GO membrane. We examined GO membranes made with different numbers (i.e., 5-50) of GO layers but did not observe any significant changes in surface morphology. The surface of the TMC-crosslinked GO membrane was relatively hydrophilic with an average water contact angle of around 60°, which was higher than that of a non-crosslinked GO membrane (around 20°). This difference suggests that TMC as a cross-linker decreases the hydrophilicity of the GO membrane.

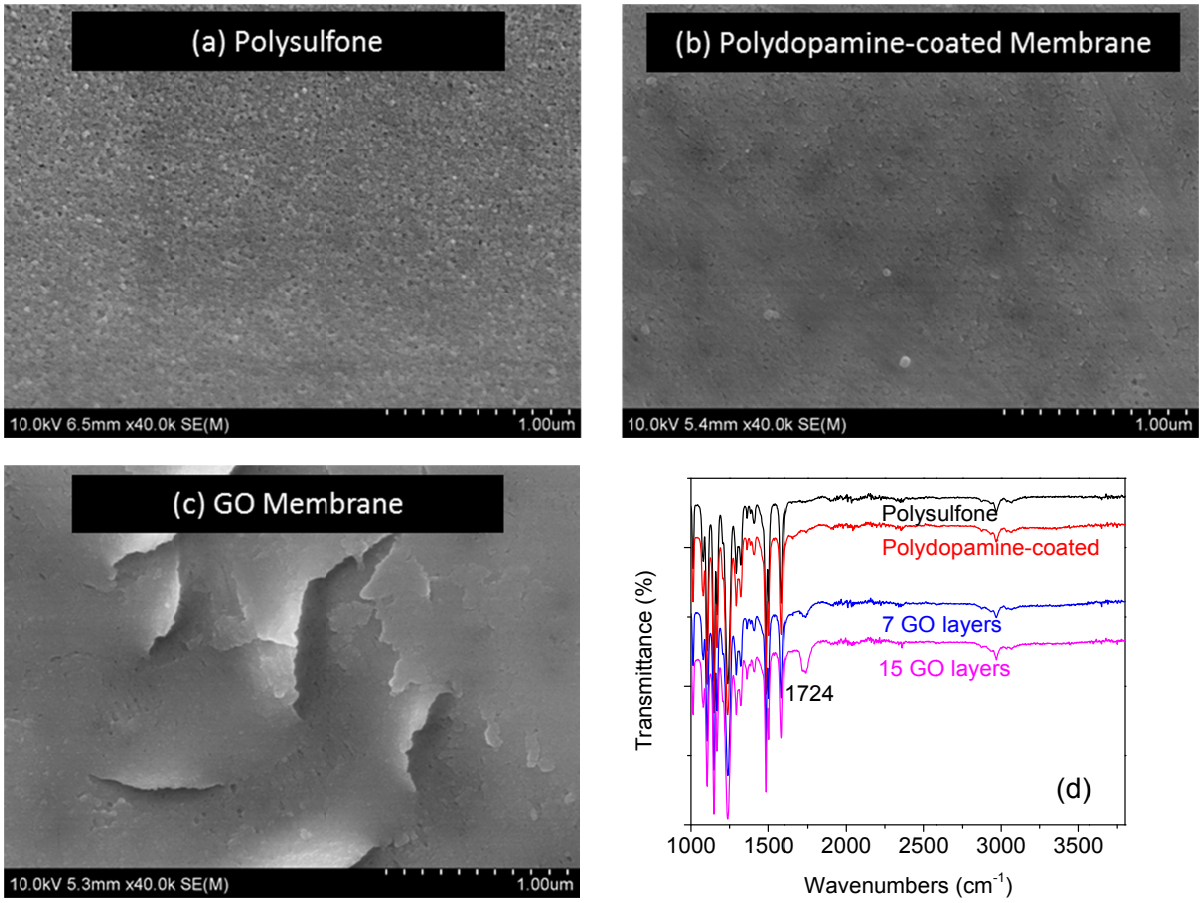

Figure 3.4 SEM characterization of (a) the polysulfone membrane support, (b) the polydopamine-coated membrane support, and (c) the 7-layered GO membrane (Note that GO membranes with other different numbers of GO layers had a similar surface morphology), and (d) FTIR spectra of two representative GO membranes, compared side-by-side with those of the polysulfone support and polydopamine-coated support.

FTIR was used to characterize membrane functional groups. As shown in Figure 3.4(d), polysulfone and polydopamine-coated membranes lead to very similar FTIR spectra. The FTIR spectra of the GO membranes, however, reveal a differentiating peak at 1724 cm^{-1}, which is absent from the spectra of the polysulfone and polydopamine-coated membranes. This peak represents the stretching vibration of C=O bonds, which

are present in carboxyl, anhydrides, and ester groups. The anhydride and ester groups could result from the reactions between TMC and polydopamine or between TMC and GO. The carboxyl groups were either present in GO or possibly formed by the hydration of anhydride bonds or unreacted acyl chloride groups in TMC. It is observed in Figure 3.4(d) that the strength of the peak at 1724 cm^{-1} increases with the increasing number of GO layers, again confirming the successful LbL deposition of GO and TMC during the synthesis of GO membranes.

3.4.5 GO Membrane Performance

Water flux of the synthesized GO membranes was tested under a trans-membrane pressure of 50 psi (0.34 MPa). As shown in Figure 3.5(a), water flux of the polydopamine-coated membrane (i.e., the one without any GO layers yet) is 1340 ± 40 l/m^2-h-MPa (LMH/MPa), which decreases to 80 – 276 LMH/MPa after the membrane were coated with 5 – 50 layers of GO. It is interesting to observe that water flux does not decrease monotonically as the number of GO layers increases. In other words, under the studied conditions, there seems no obvious correlation between water flux and the number of GO layers. This observation possibly suggests that the water resistance of GO coating does not linearly depend on the thickness of a GO membrane. We suspect that the phenomena can be partially attributed to the unique water transport properties of the GO nanochannels. Note that the flux behavior in GO nanochannels is similar to that in CNT membranes, where water permeability is not significantly affected by the membrane thickness [79]. In order to fully explain the flux behavior, however, we need to have a complete understanding of the size, shape, functionality of the GO flow channels. We are

currently making an effort to characterize the GO channel properties and elucidate the water transport mechanisms in these channels.

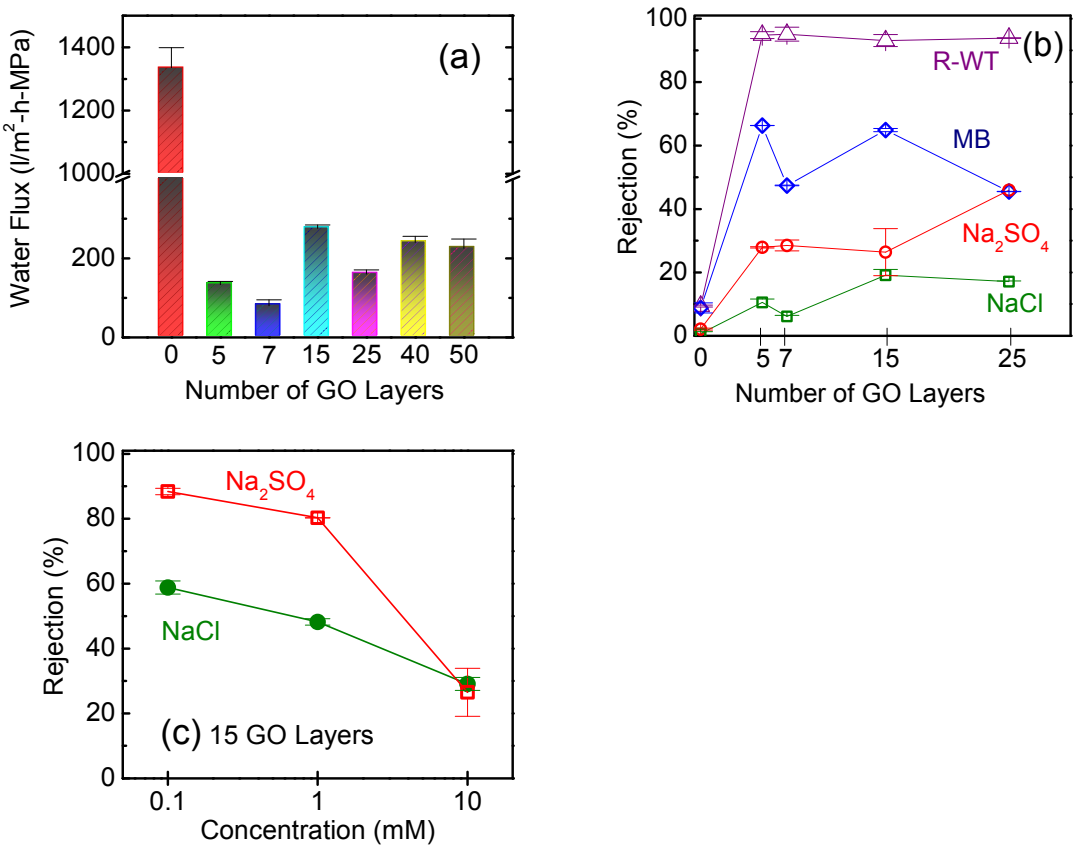

Figure 3.5 GO membrane performance: (a) water flux with different numbers of GO layers, (b) rejection of salts and organic dyes with different numbers of GO layers, and (c) effect of salt concentration on the rejection by the 15-layered GO membrane. The data at 0 layer are those of the polydopamine-coated membrane. All flux and rejection tests were performed under 50 psi (0.34 MPa). The rejection tests in (b) were performed with 20 mM NaCl, 10 mM Na_2SO_4, 7.5 mg/L MB, and 7.5 mg/L R-WT solutions, respectively.

The separation performance of the synthesized GO membrane was examined using NaCl as a representative monovalent salt, Na_2SO_4 as a representative divalent salt, and two organic dyes (MB and R-WT). As seen in Figure 5(b), the polydopamine-coated

membrane as a control had almost no rejection of the ions and less than 10% rejection of the dyes. Note that the polysulfone support itself had no rejection of either ions or dyes. After GO coating, the rates of rejection of NaCl and Na_2SO_4 increased to 6 – 19% and 26 – 46%, respectively, depending on the specific number of GO layers deposited. The GO coating also significantly improved the rejection of organic dyes: the rates of rejection of MB and R-WT were in a range of 46 – 66% and 93 – 95%, respectively. The higher rate for R-WT rejection can be attributed to two factors. First, R-WT has a higher molecular weight than MB, resulting in higher rejection by the size exclusion effect. Second, GO membranes were negatively charged due to the presence of carboxyl groups, thereby enhancing the rejection of negatively charged R-WT instead of the positively charged MB.

In general, we believe that the spacing between GO layers and the charges on GO nanosheets are two dominant factors determining the rejection performance of the GO membrane. The spacing between GO layers sandwiched by TMC molecules (0.7 nm) is estimated to be around 1 nm. The rejection rates for salts and dyes observed in our study are at a reasonable level for membranes with pores of 1 nm in size. For instance, the salt rejection of our GO membrane is comparable to that of a CNT membrane with sub-2-nm sized pores.[157] Currently we are exploring effective, accurate approaches to spacing characterization in order to fully understand the underlying rejection mechanism.

It cannot be stressed more that, in order to correctly assess the water separation performance of a GO membrane, the adsorption effect of GO nanosheets must be excluded during a rejection test. GO is known as a very strong adsorbent for many organic substances, including most organic dyes (e.g., MB) [131]. In our rejection tests

with MB and R-WT, we observed that concentration of these dyes in the permeate water collected at the beginning of the experiments was below the detection limit of 1 μg/L; after around 0.5 h of continuous filtration, however, the dye concentration began to stabilize at a higher level. This observation suggested that the initial high rejection was attributed not to the defining mechanisms (i.e., size exclusion and charge effects) of a water separation membrane but to GO's inherent adsorption capacity, which was typically reached within 1 h. Unfortunately, some researchers might not have eliminated the adsorption effect of GO when investigating the water separation performance of a GO membrane, leading to incorrect conclusions. For example, in a most recent study on unbonded GO membranes, only the initial 5-10 ml of permeate was collected in the rejection test and the resulting ~100% rejection was unconvincingly attributed to the separation capability of the membrane [154]. In our study, we have intentionally excluded GO's adsorption effect by stabilizing each rejection experiment for at least 2 h prior to the collection of permeate and feed samples for rejection analysis.

In order to understand how the charge effects influence the water separation performance of the GO membrane, we studied the rejection of NaCl and Na_2SO_4 at different solution concentrations. As shown in Figure 3.5(c), the rejection decreases significantly as ionic strength (i.e., solution concentration) increases. Specifically, the Na_2SO_4 rejection drops from around 88% at 0.1 mM to nearly 26% at 10 mM, while the NaCl rejection falls from around 59% at 0.1 mM to around 29% at 10 mM. This observation indicates that charge effects greatly contribute to the separation mechanisms of the GO membrane. Note that the Debye lengths for 0.1 mM NaCl, 0.1 mM Na_2SO_4, 10 mM NaCl, and 10 mM Na_2SO_4 are 31 nm, 18 nm, 3.1 nm, and 1.8 nm, respectively. In

general, as the Debye length decreases, the electrostatic repulsion between ions and the charged membrane decreases due to the suppressed electrostatic double layers, thereby causing the rejection rate to drop.

3.4.6 Promise and Future of the GO Membrane

We have demonstrated that selective and permeable GO membranes can be synthesized via a simple LbL coating approach. The GO membrane has exhibited a number of fascinating advantages over existing membranes. First, it uses graphite as an inexpensive raw material, significantly lowering the membrane fabrication cost. Second, the synthesis procedure for both GO nanosheets and GO membrane are simple and scalable, providing technical readiness for scaling up the membrane production. In the present stage, the synthesized GO membrane has very high rejection of an organic dye with a molecular weight of around 500 Daltons. Water flux of the GO membrane is about 4-10 times higher than that of most currently commercially available NF membranes.

Further adjusting of GO properties and the membrane synthesis protocol will hopefully improve water flux and ion rejection. Potential improvement strategies include engineering the spacing between GO layers by incorporating different-sized cross-linkers, modifying membrane charges by functionalizing GO with different functional groups, and optimizing membrane thickness by varying the number of GO layers. Indeed, the facile synthesis of economical GO membranes with enhanced performance promisingly qualifies this new type of membrane as a next-generation, cost-effective, and sustainable alternative to the long-existing thin-film composite polyamide membranes for water separation applications.

3.5 Conclusions

A novel procedure was reported to synthesize a new type of water separation membrane using graphene oxide (GO) nanosheets. The GO membrane was made via layer-by-layer deposition of GO nanosheets, which were cross-linked by 1,3,5-benzenetricarbonyl trichloride, on a polydopamine-coated polysulfone support. The cross-linking not only provided the stacked GO nanosheets with the necessary stability to overcome their inherent dispensability in water environment but also fine-tuned the charges, functionality, and spacing of the GO nanosheets. The GO membrane flux ranged between 80 and 276 LMH/MPa, roughly 4–10 times higher than that of most commercial nanofiltration membranes. Although the GO membrane in the present development stage had a relatively low rejection (6–46%) of monovalent and divalent salts, it exhibited a moderate rejection (46–66%) of Methylene blue and a high rejection (93–95%) of Rhodamine-WT. The promising separation performance was attributed to that water can flow through the nanochannels between GO layers while unwanted solutes are rejected by size exclusion and charge effects. The facile synthesis of a GO membrane exploiting the ideal properties of inexpensive GO materials offers a myriad of opportunities to modify its physicochemical properties, potentially making the GO membrane a next-generation, cost-effective, and sustainable alternative to the long-existing thin-film composite polyamide membranes for water separation applications.

Chapter 4: Layer-by-layer Assembly of Graphene Oxide Membranes via Electrostatic Interaction

4.1 Abstract

We fabricated a novel type of water purification membrane by layer-by-layer assembling negatively charged graphene oxide (GO) nanosheets on a porous poly(acrylonitrile) support and interconnecting them with positively charged poly(allylamine hydrochloride) (PAH) via electrostatic interaction. A series of characterization techniques were used to confirm the successful assembly of multiple GO-PAH bilayers, quantify their composition and thickness, and understand the structure of the GO membrane. Quartz crystal microbalance-dissipation (QCM-D) results showed that each GO-PAH bilayer in the membrane is around 16.5 nm thick and dominated by GO (mass of GO is 2-5 times higher than that of PAH), indicating multiple layers of GO nanosheets exist in each bilayer. This is most likely because the mass-to-charge ratio of GO is much higher than that of PAH. Transport of water and selected solutes in the GO membrane was investigated in a pressurized system and also in a forward osmosis (FO) and pressure retarded osmosis (PRO) system. Water permeability of the GO membrane was found to be about one order of magnitude higher than that of a commercial FO membrane. The GO membrane exhibited a much lower solute flux for sucrose (as a representative uncharged species) than for ionic species, although the hydrated radius of the ions is comparable to that of sucrose. This is most likely because the GO-PAH bilayers swell in ionic solutions. In solutions of low ionic strength, the GO membrane retained a tight structure and exhibited low high rejection to sucrose (~99%), indicating a MWCO of around 342 or an equivalent pore size of around 1 nm. Therefore, at the present stage, the

GO membrane can be well suited for applications such as FO-based emergency water purification using sugary draw solutions and water treatment not requiring high ionic strength.

4.2 Introduction

As a sheet of carbon atoms arranged in a honeycomb lattice and decorated with oxygenated functional groups (i.e., carboxyl, hydroxyl, epoxy groups), graphene oxide (GO) can be mass-produced by oxidizing and exfoliating graphite [17] and has great potential as building blocks for the fabrication of inexpensive yet high-performance water purification membranes [16, 44, 45, 79, 158]. Compared with traditional membrane materials such as polyamide, this two-dimensional (2D) material promisingly offers a number of significant benefits in facilitating the fabrication process and improving the physicochemical properties of membranes. In particular, the unique 2D structure of GO makes it ideal for creating a new class of membrane by stacking GO nanosheets via a layer-by-layer (LbL) assembly technique, which is relatively cost-effective and environmentally friendly because all fabrication steps can be performed in aqueous solutions while traditional membrane synthesis procedures (e.g., interfacial polymerization) often involve complex chemical reactions and use organic solvents.

Unlike traditional membranes that separate unwanted substances from feed water as water passes through the pores within the membrane active layer, a GO membrane relies on the nano-sized interlayer spaces to filtrate water as it zigzags within the layered GO film deposited on a support substrate. The long slip length caused by the capillary effect makes it possible for water to flow nearly without any friction [44, 159], a very

desired material property for making high-flux membranes. Recently it has been experimentally shown that a GO membrane can outperform commercial nanofiltration (NF) membranes in terms of water flux (an order of magnitude higher) while demonstrating at least the same level of solute rejection [45]. Besides, it is worth emphasizing that stacking of 2D nanosheets offers a unique opportunity to very flexibly optimize various membrane properties during, as opposed to after, membrane fabrication. For example, membrane selectivity can be tuned by manipulating the spacing between GO nanosheets, membrane antifouling properties can be enhanced by adjusting the functional groups and charges on GO nanosheets, and membrane regenerability can be realized via reversible binding interactions between GO nanosheets.

Membrane integrity must be ensured in order for a GO membrane to be practically useful for water-solute separation. So far, most layered GO membranes have been fabricated via a simple solution-filtration process [44, 154, 160] and hence are highly susceptible to dispersion in an aqueous environment due to the extreme hydrophilicity of GO nanosheets. To resolve this issue, neighboring GO layers need be bonded firmly to each other and so does the outermost layer to the support substrate. There exist different bonding strategies for making a stable GO membrane [161]. One strategy is to establish covalent bonding between GO layers by using appropriate cross-linkers such as trimesoyl chloride (TMC) [45]. Another promising strategy is to bond stacked GO nanosheets through electrostatic interaction. Because GO nanosheets are negatively charged due to the ionization of carboxylate groups in water [124, 125], they can act as polyanions and electrostatically bind to positively charged polyelectrolytes such as poly(allylamine hydrochloride) (PAH) [126, 127]. Note that although the binding

forces between assembled polyelectrolyte layers are mainly contributed by electrostatic interaction, hydrophobic interaction and hydrogen bonding may also be involved but to a lesser extent [123]. Compared with covalent bonding, electrostatic bonding may lead to GO membrane fabrication that advantageously features simpler reaction, more flexible control of chemistry, less usage of organic solvent, and reduction of by-products. In fact, the LbL technique has proven very useful for assembling oppositely charged polyelectrolytes to form thin films or coatings for membranes used in pervaporation [112, 113], NF [114, 116-118, 162], solvent resistant NF [163] reverse osmosis [114, 119], and forward osmosis (FO) [120, 122, 162, 164, 165]. An added benefit is that an electrostatically bonded GO membrane is potentially regenerable, that is, existing GO layers on the membrane can be released by varying solution chemistry to, for example, extremely high pH and/or surfactant concentrations, thereby enabling the deposition of fresh GO layers to regain membrane functionality.

In the present study, we explored the potential use of layered GO membrane in FO and pressure retarded osmosis (PRO) processes. As an energy-inexpensive alternative to the conventional pressure-driven membrane processes, the FO/PRO membrane technology has experienced an accelerated development over the past decade [166-169]. In contrast to other types of water purification membranes, FO/PRO membranes must have a relatively thin, hydrophilic support in order to reduce internal concentration polarization (ICP), which is caused by the hindered solute transport within the support layer and can significantly reduce membrane flux and aggravate membrane fouling. To date, the existing commercial FO/PRO membranes can be categorized into cellulose-based membranes and thin-film composite (TFC) membranes. Synthesized via phase

separation, cellulose-based membranes have excellent antifouling properties but exhibit relatively low water flux and high salt passage and only work within a narrow pH range [12, 170, 171]. In comparison, TFC membranes show excellent salt rejection at the cost of low pure water flux due to ICP effects caused by the thick, dense membrane support [170, 172]. Therefore, development of high-performance FO/PRO membranes has been a major task in the journey of achieving the full benefit of such a sustainable technology [168, 170].

Herein we propose to electrostatically bond layered GO nanosheets to form a stable GO membrane and test its suitability for FO/PRO processes. Briefly speaking, the LbL technique was employed to assemble oppositely charged GO and PAH layers on both sides of a charged support substrate in order to minimize internal concentration polarization. The GO membrane was then characterized using a series of techniques to confirm the successful assembly of multiple GO-PAH bilayers, quantify their composition and thickness, and understand the structure and charge properties of the GO membrane. Next, we tested the GO membrane in cross-flow pressurized and also in FO/PRO membrane systems in order to characterize the transport of water and solutes within the GO membrane, using a commercially available FO membrane as a baseline.

4.3 Materials and Methods

4.3.1 Membrane support preparation

The membrane support substrate was made of polyacrylonitrile (PAN) through phase inversion and partial hydrolysis. First, a PAN solution was prepared by dissolving 18 g PAN (Mw ≈ 150,000) and 2 g LiCl in 80 g *N,N*-dimethylformamide (DMF) (≥ 99.8%) at

60 °C. All the chemicals were obtained from Sigma-Aldrich (St. Louis, MO). After cooling to room temperature, the PAN solution was stored overnight in a vacuum desiccator. Next, the PAN solution was cast on a clean glass plate using an aluminum casting rod with a gate height of 125 μm. Then, the glass plate along with the cast PAN film was immediately soaked in a DI water bath for 10 min, during which phase inversion took place to form the PAN support, which finally underwent partial hydrolysis in 1.5 M NaOH for 1.5 h at 45 °C[113, 122] and was thoroughly rinsed with DI water.

4.3.2 GO membrane fabrication

The GO membrane was synthesized via the LbL assembly of GO and PAH on the hydrolyzed PAN (hPAN) support substrate. The GO solution (1 g/L, pH 4) was prepared in our lab using the modified Hummers method [48, 143], with the detailed procedure described in a previous study [45]. The PAH solution was prepared by dissolving 1 g/L PAH in DI water and the pH was adjusted from 4.6 to 4 using HCl and NaOH solutions. To fabricate the layered GO membrane, a typical assembly cycle involved soaking the hPAN support in the PAH solution for 30 min and then in the GO solution for another 30 min, thereby adding one GO-PAH bilayer onto each side of the hPAN support. Repeating a prescribed number of such soaking cycles led to a GO membrane with a desired number of GO-PAH bilayers on each side of the hPAN support. The GO membrane was thoroughly rinsed with DI water between successive soaking treatments.

4.3.3 Characterization of membrane properties.

The hPAN membrane support with or without assembled GO-PAH bilayers was characterized by Fourier transform infrared (FTIR) spectroscopy (Nicolet 6700, Thermo Scientific, Marietta, OH) and scanning electron microscopy (SEM) (SU-70, Hitachi High

Technologies America, Gaithersburg, MD). Their elemental compositions were analyzed using X-ray photoelectron spectroscopy (XPS) (Kratos AXIS 165, Kratos Analytical, Spring Valley, NY).

4.3.4 Quantification of LbL assembly

Quartz crystal microbalance with dissipation (QCM-D) (E-4, Biolin Scientific, Linthicum Heights, MD) was used to monitor the process of assembling GO-PAH bilayers on an hPAN film. A QCM-D gold sensor (14 mm in diameter) was coated with a PAN film, hydrolyzed in 1.5 M NaOH solution, and mounted in a QCM-D chamber. The sensor was successively exposed to PAH (1 g/L, pH 4) and GO (1 g/L, pH 4) solutions to mimic the LbL assembly of a GO membrane. The mass of GO or PAH deposited on a sensor was quantified by monitoring and then model-fitting the changes in frequency and dissipation, respectively, of the sensor against time using Q-Tool software (Biolin Scientific, Linthicum Heights, MD).

4.3.5 Quantification of charge properties

The charge properties of GO and PAH solutions (1 g/L each) were measured using a zeta-potential analyzer (Zetasizer Nano ZS90, Malvern Instruments, UK) at selected pHs. The solution pHs were adjusted by adding HCl and NaOH. No other ionic species were added to the solutions. QCM-D can effectively characterize the charge density of a thin film using, for example, CsCl as a probing species [173]. Therefore, we used QCM-D to measure the charge densities of the PAN and hPAN supports. To do so, a sensor coated with PAN or hPAN was stabilized in DI water and then in 1 mM CsCl solutions at pH 4, 7, and 10, respectively. Changes in frequency were used to calculate the charge densities

of the PAN and hPAN, based on the Sauerbrey equation hard-coded in the Q-Tool software (Biolin Scientific, Linthicum Heights, MD).

4.3.6 Membrane performance evaluation

The GO membrane performance was evaluated under hydraulic pressure as well as in FO and PRO modes. A commercial FO membrane (Hydration Technology Innovations or HTI, Albany, OR) was also evaluated as a comparison. A dead-end membrane system was used to test the pure water permeability of the hPAN membrane support with or without assembled GO-PAH bilayers. The membrane system consists of an Amicon cell 8010 (Millipore, Billerica, MA), a pressure vessel (Sterlitech, Kent, WA), and a digital balance (Denver Instruments, Denver, CO) that measures the permeate flow rate and sends data to a PC for recording. The pure water flux was measured under a transmembrane pressure of 50 psi (345 kPa).

The FO/PRO membrane system consists of a lab-made FO/PRO membrane cell, two magnetic pumps (Cole Parmer, Vernon Hills, IL), feed and draw solution tanks, a temperature-controlled water bath (Neslab, Newington, NH), a digital balance (Denver Instruments, Denver, CO), and a PC for data acquisition. To test water flux, a membrane coupon with an effective area of 20 cm^2 was mounted in the membrane cell between the feed and draw solution channels. The membrane was then tested in FO mode (with the membrane front side, i.e., the side of hPAN that had smaller pores, facing the feed solution) as well as in PRO mode (with the membrane front side facing the draw solution). We used DI water as the feed solution and three types of draw solutions: 1 M $MgCl_2$, 0.25 M trisodium citrate (TSC), and 1 M sucrose solutions. This is because 1 M $MgCl_2$ is often used as the draw solution in FO studies, 0.25 M TSC provides roughly the

same osmotic pressure as 1 M $MgCl_2$, and 1 M sucrose serves as neutral draw solution. The temperature of feed and draw solutions was controlled at 25 °C. The weight change of a draw solution was recorded every 5 min and used to calculate the pure water flux.

Solute flux was evaluated by monitoring the back diffusion of draw solutes through a membrane. To do so, we measured the time-varying draw solute concentration of the feed solution by using a conductivity meter (Accumet Excel XL30, Thermo Scientific, Marietta, OH) for $MgCl_2$ and TSC and a TOC analyzer (Shimadzu TOC-5000, Shimadzu Scientific Instruments, Columbia, MD) for sucrose. The solute flux is calculated as

$$J_s = \left[C(V_0 - J_w At) - C_0 V_0\right] / At \tag{4-1}$$

where J_s is the solute flux, C_0 and C are the initial and time-varying concentrations, respectively, of the feed solution, V_0 is the initial feed volume, A is the membrane surface area, and t is the time. The solute permeability test lasted 2 h during which measurement was taken every 30 min, and the average of all measurements is reported in the present study.

4.4 Results and Discussion

4.4.1 Preparation of membrane support

Due to the convenience in manipulating its structure and functional groups, PAN was selected to fabricate the membrane support via phase inversion [113]. Figure 4.1(a) shows the cross-section of the PAN support, which was relatively thin (~60 μm) and contained finger-like structures with low tortuosity. There were dense skin layers on both sides of the support, with one side (referred to as the front side, Figure 4.1(b)) even

denser and smoother than the other side (referred to as the back side, Figure 4.1(c)). Such dense skin layers are ideal for effectively forming a dense barrier layer with much less imperfection on each side of the support.

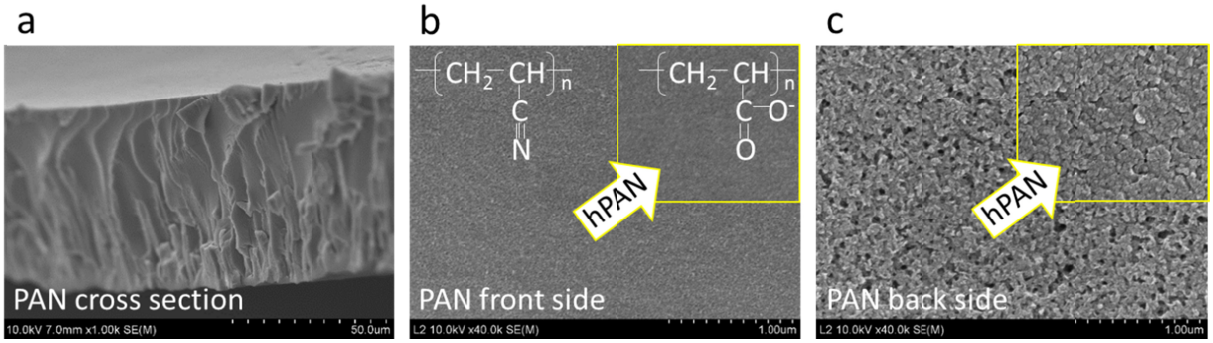

Figure 4.1 SEM images of the PAN membrane support: (a) cross section, (b) front side, and (c) back side. The boxed areas in (b) and (c) were the front and back sides of the partially hydrolyzed PAN (hPAN), respectively.

PAN was partially hydrolyzed to turn into hPAN such that a portion of nitrile functional groups (─C≡N) were converted to carboxylate functional groups (─COO^-),[113, 120, 122, 162] which were necessary for the membrane support to securely attach the first PAH layer. As revealed by the FTIR spectra in Figure 4.2(a), both PAN and hPAN spectra have a signature peak at 1450 cm^{-1} for nitrile, while partial hydrolysis led to a small new peak in the hPAN spectra at 1560 cm^{-1}, confirming the formation of carboxylate functional groups. The replacement of nitrile by carboxylate can also be verified by the decreased N/C ratio and the increased O/C ratio from XPS analysis (Figure 4.2(b)). In addition, the O/C ratio for the front side of hPAN is much higher than that for the back side, possibly because the degree of hydrolysis on the front side was larger than that on the back side due to the smaller pore sizes (demonstrated in Figure 4.1(b)) and thus larger exposed surface area on the front side. Also because the

penetration depth of XPS on the back side was higher due to the looser structure there (demonstrated in Figure 4.1(c)), the overall O/C ratio for the back side is lower. Note that the partial hydrolysis of PAN did not cause observable changes in the cross-sectional structure but slightly narrowed the surface pores of the membrane support, as shown in the boxed areas of Figure 4.1(b-c). The relatively small pore sizes and smooth surface made hPAN an ideal substrate for the LbL assembly.

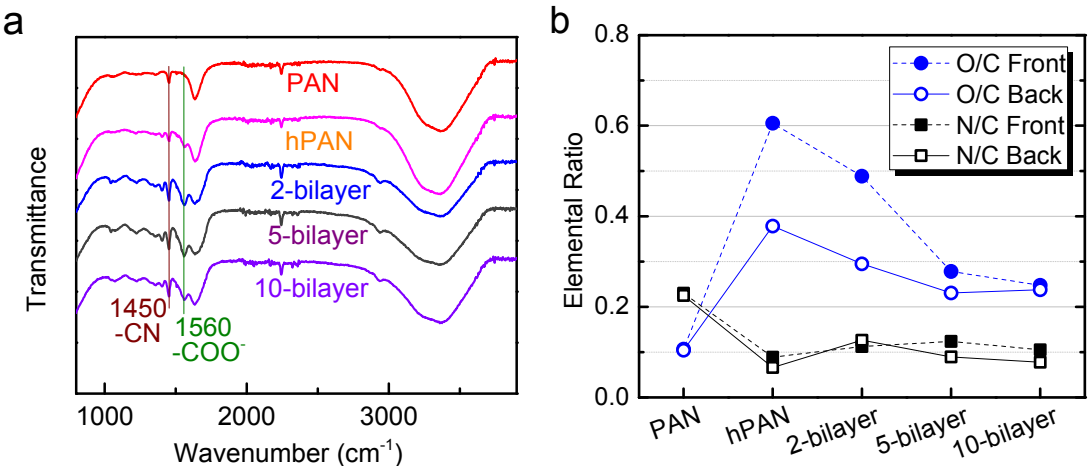

Figure 4.2 Characterization of (a) functional groups on the front side of membrane supports and GO membranes by FTIR spectrometer, and (b) elemental ratios of membrane supports and GO membranes by XPS analysis. The FTIR spectra of the membrane back side are similar to that of the front side.

4.4.2 Charge properties of membrane support, GO, and PAH

The charges of PAN and hPAN were probed by Cs^+ in QCM-D experiments. As demonstrated in Figure 4.3(a), the PAN support did not carry any detectable charge at the studied pH values. In contrast, the hPAN support contained significant negative charges at pHs 7 and 10 but relatively low charges at pH 4, confirming the successful conversion of nitrile to carboxylate functional groups, which have a pKa of ~4. Despite the low charge density at pH 4, as will be seen later, the first PAH layer was still successfully

assembled on the hPAN support, indicating that interactions (e.g., hydrophobic force, hydrogen bonding) besides electrostatic interaction also played a role in the deposition of the first PAH layer.

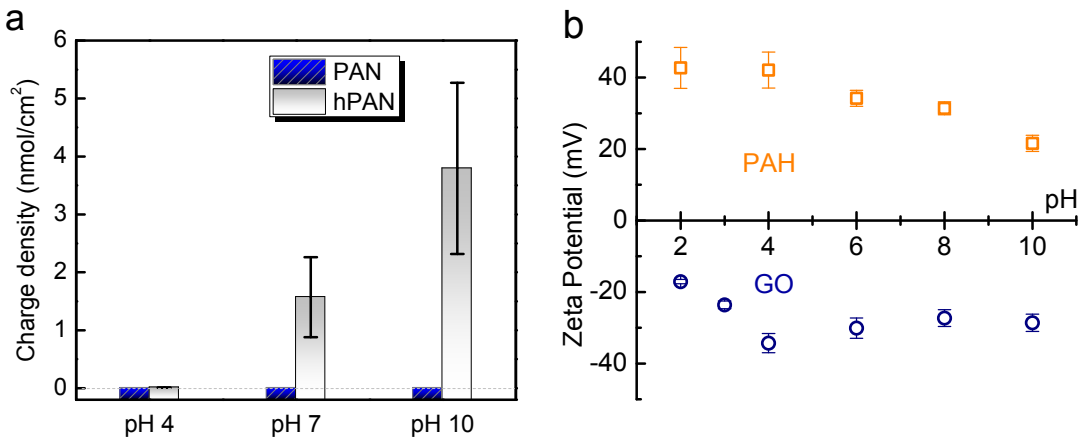

Figure 4.3 Characterization of (a) charge density of membrane supports by QCM-D, and (b) zeta potentials of GO and PAH at different pHs.

The charge properties of GO and PAH were analyzed using zeta potential measurement to evaluate the feasibility of the LbL assembly of GO-PAH bilayers via electrostatic interaction as the pH value varies. As shown in Figure 4.3(b), GO and PAH were able to remain positively and negatively charged, respectively, over a wide pH range of 2 to 10, thereby ensuring the stability of the electrostatically assembled GO-PAH bilayers and hence the GO membrane.

4.4.3 LbL assembly of GO membrane

The process of LbL assembly of a GO membrane is schematically illustrated in Figure 4.4. The hPAN support was first immersed in the PAH solution to attach positively charged PAH, and then in GO solution to deposit negatively charged GO on top of PAH, thus completing the assembly of the first GO-PAH bilayer on each side of the hPAN

support. Such a deposition cycle was repeated to assemble a desired number of GO-PAH bilayers. Note that the pHs of both PAH and GO solutions were kept at 4, close to the natural values of the as-prepared solutions. Therefore, significant amount of acid or base was not needed to adjust the solution pH and hence the solution ionic strength was kept to a minimum, thereby avoiding the formation of a loosely packed membrane structure due to the otherwise hydration of polyelectrolytes[174, 175] and also preventing GO nanosheets from aggregation due to the charge screening effect.[176]

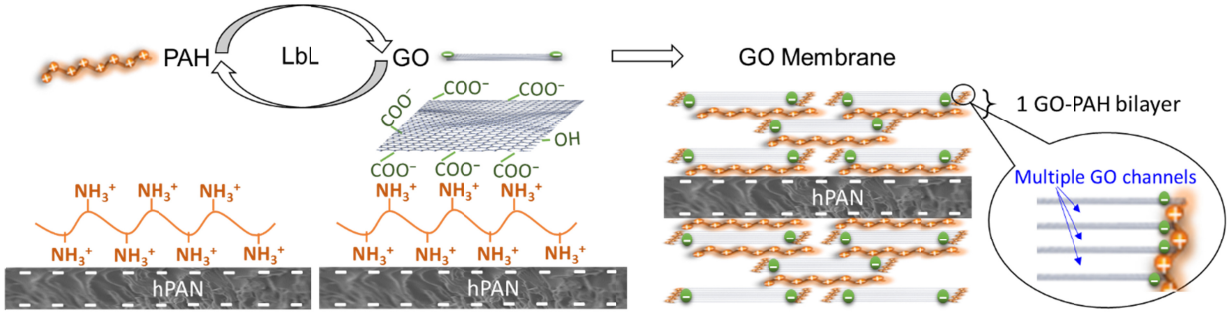

Figure 4.4 Schematic diagram of LbL assembly of a GO membrane by alternately soaking an hPAN support substrate in 1 g/L PAH (pH 4) solution and in 1 g/L GO solution (pH 4) to deposit a prescribed number of GO-PAH bilayers on both sides of hPAN.

4.4.4 Characterization of GO membrane

The SEM images in Figure 4.5 clearly show that the two sides of GO membranes were rougher than those of the original hPAN support (Figure 4.1(b-c)), respectively, indicating a successful assembly of multiple GO-PAH bilayers. Also note that there existed significant difference between the surface morphology of the two sides of the original hPAN support but such difference was reduced as the number of GO-PAH bilayers increased, indicating that a higher surface coverage by GO-PAH was achieved on both sides of the hPAN support.

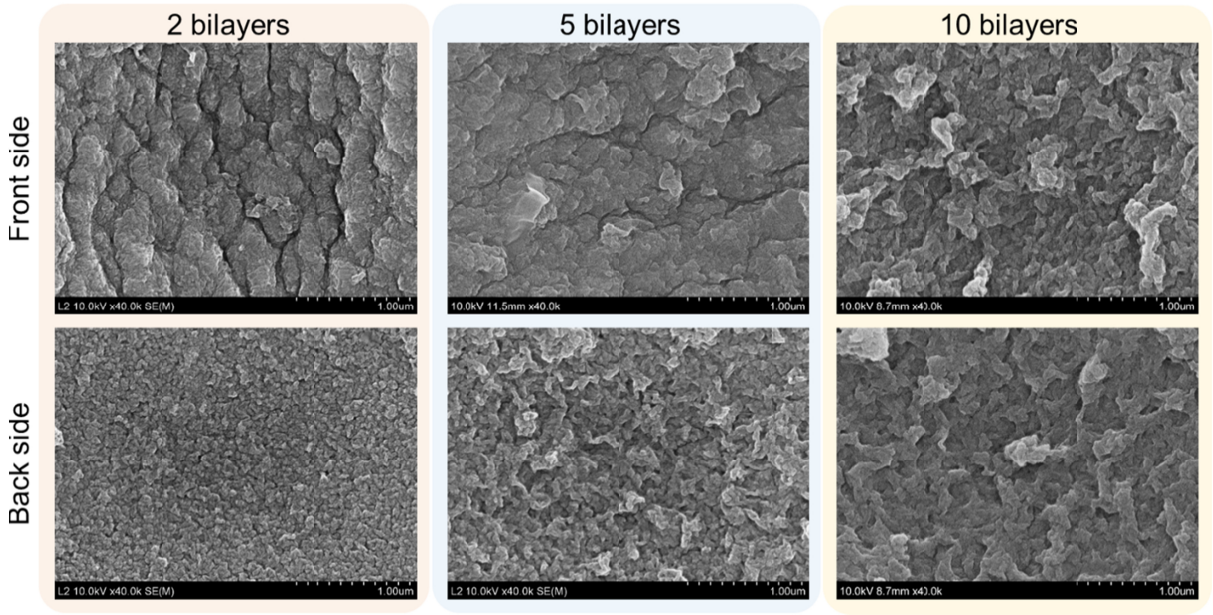

Figure 4.5 SEM images of the GO membranes made of different numbers of GO-PAH bilayers.

Additional evidence is available for the successful assembly of GO-PAH bilayers by the LbL procedure. For example, Figure 4.2(b) shows that the O/C ratio gradually decreases with the increasing number of GO-PAH bilayers, indicating that the GO-PAH layers contain less oxygen than the hPAN support. On the other hand, the N/C ratio remains almost constant, most likely because the nitrogen contents of the GO-PAH bilayers and the hPAN support are similar. Note that the O/C ratios for both front and back sides of the 10-bilayer GO membrane reached almost the same value of 0.24, indicating that the two surfaces attained the same level of coverage by GO-PAH. The FTIR spectra in Figure 4.2(a) also reveal that the intensity of the carboxylate groups at 1560 cm^{-1} increased as more GO-PAH bilayers were assembled.

4.4.5 Composition and thickness of GO membrane

QCM-D was employed to monitor the LbL assembly of GO-PAH bilayers so as to quantify the composition and thickness of the GO membrane. The raw frequency and dissipation data as well as the derived mass of PAH and GO are plotted in Figure 4.6. It is clearly shown that the masses of GO and PAH both increased steadily with the increasing number of bilayers, proving the successful assembly of multiple GO-PAH bilayers. Besides, the mass of GO was consistently greater (2 to 5 times) than that of PAH after any deposition cycle, most likely due to the combined effects of the higher charge density (and thus lower mass-to-charge ratio) of PAH and the larger lateral dimensions (and thus higher mass-to-charge ratio) of GO.

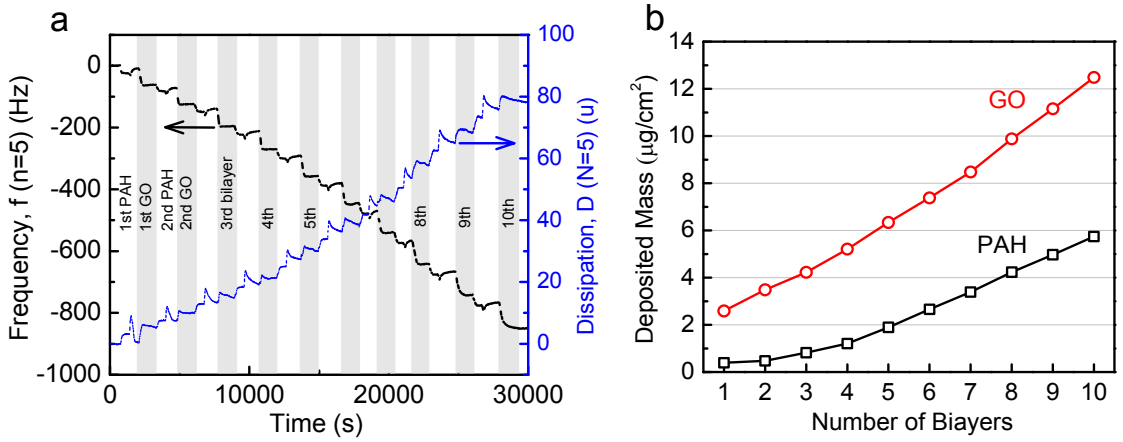

Figure 4.6 (a) Frequency and dissipation plot for the assembly of GO-PAH bilayers on an an hPAN-coated sensor that simulated the surface chemistry of an hPAN membrane support. (b) Cumulative masses of GO and PAH during the LbL assembly of a GO-PAH film on an hPAN-coated QCM-D sensor.

The quantified mass of GO and PAH enables us to estimate the total GO-PAH thickness of a GO membrane. For example, the 10-bilayer GO membrane had a total deposited mass of 18.2 μg/cm^2 on the hPAN-coated sensor (Figure 4.6(b)). Assuming a GO membrane density of 1.1 g/cm^3, it is estimated that the total GO-PAH thickness on

each side of the hPAN support is ~165 nm and hence a single GO-PAH bilayer is ~16.5 nm thick on average, much more than that (~1 nm) of a pure GO layer in previously reported GO membranes [44, 45], suggesting that multiple GO layers were deposited during each GO-PAH deposition cycle. As will be discussed later, the high rejection and low solute flux of sucrose (with a hydrated radius of 0.5 nm) for the GO membrane indicate that the GO channel size (i.e., the clear interlayer spacing, h) was ~1 nm, further supporting the existence of multiple GO layers within one GO-PAH bilayer. Since the thickness d_0 of a single GO nanosheet is ~0.3 nm[44], a typical GO layer in the present GO membrane should have an overall thickness of $d = h + d_0 = \sim 1.3$ nm, keeping in mind that PAH might be sandwiched as a spacer between GO nanosheets. Therefore, a total of 16.5/1.3≈13 GO layers may have existed in one GO-PAH bilayer. In fact, deposition of multiple GO layers during one assembly cycle is quite reasonable because, compared with PAH, GO has a low charge density and hence multiple GO layers were needed to compensate all charges on PAH. Furthermore, since most charges on GO are located along its edges [17], multiple GO nanosheets may have been electrostatically edge-connected to PAH, considering possible partial overlapping of these GO nanosheets as they were actually deposited at an angle other than perfectly flat. Accordingly, multiple GO layers were formed during a single deposition cycle. Figure 4.4 illustrates the structure of a GO membrane where multiple GO layers (and thus multiple inter-GO channels) exist in each GO-PAH bilayer.

4.4.6 Water flux of GO membrane

The water flux of the GO membrane was measured in a hydraulically pressurized membrane system. As shown in Figure 4.7(a), the water permeability (i.e., water flux

normalized by transmembrane pressure) of the GO membranes ranged from 2.1 to 5.8 l/m^2-h-atm (LMH/atm) and was much lower than that of the PAN (88.4 LMH/atm) and hPAN support (19.0 LMH/atm), indicating that the existence of GO-PAH bilayers led to significant hydraulic resistance and hence lowered the water flux.

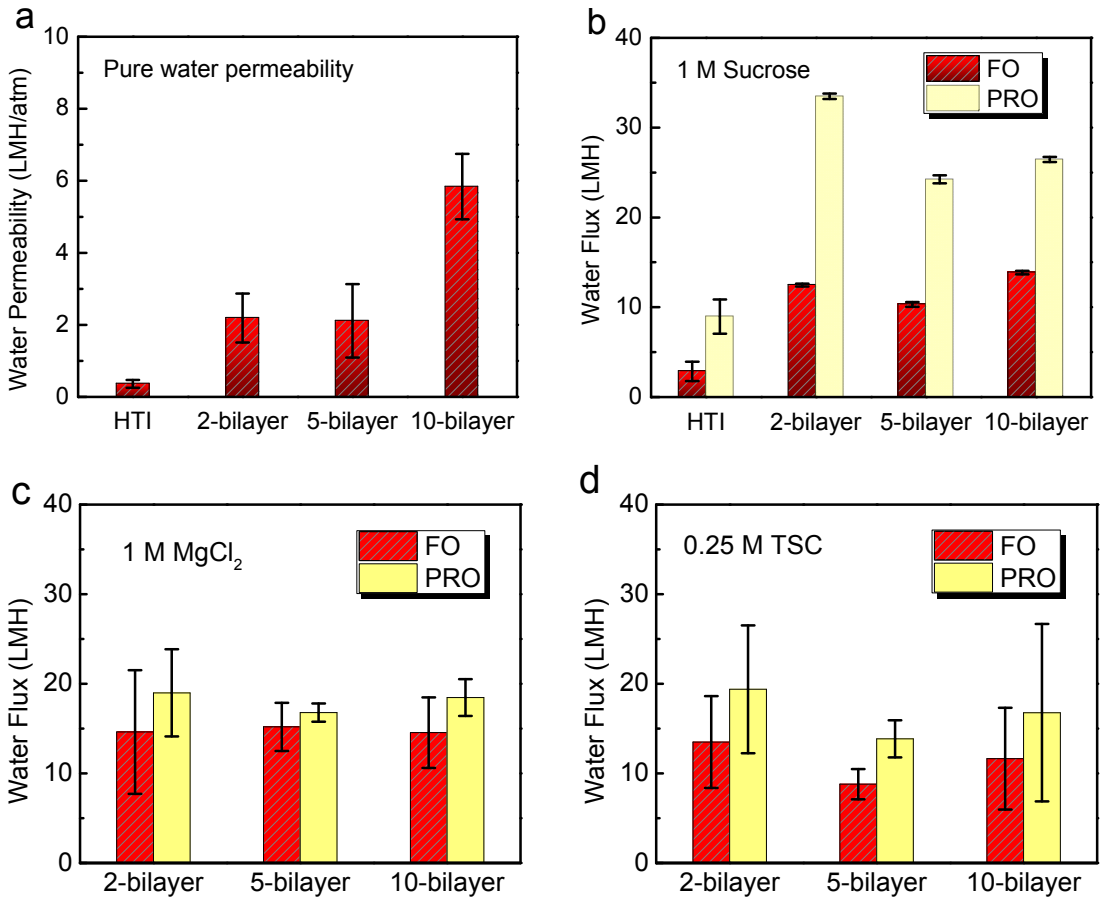

Figure 4.7 Water fluxes of GO membranes. (a) Pure water permeability under hydraulic pressure. Water flux in FO and PRO modes with (b) 1M sucrose, (c) 1 M $MgCl_2$, and (d) 0.25 M TSC as draw solutions, respectively.

At the current stage, the water permeability of the GO membrane is one order of magnitude higher than that (0.36 ± 0.11 LMH/atm) of the commercial HTI membrane [177], as compared in Figure 4.7(a). Note that the GO membrane permeability can be further improved by increasing GO porosity and decreasing its tortuosity, both of which

may be achieved by, for example, optimizing GO lateral dimension, creating vertically aligned GO nanosheets (i.e., generating straight-through GO channels), and/or varying deposition conditions.

We also tested the water flux of the GO membrane in FO and PRO modes using DI water as feed solution and using 1 M sucrose, 1 M $MgCl_2$, and 0.25 M TSC as draw solutions, respectively. Figure 4.7(b) shows that, when sucrose was used as draw solute, the GO membrane flux was about 3 to 4 times that of the HTI membrane in FO and PRO modes, respectively. Note that water flux of the GO membrane in PRO mode was more than twice that in FO mode, indicating the existence of significant ICP in FO mode. We hypothesize that the structural integrity and separation capability of the GO-PAH bilayers deposited on the back side of the hPAN support was less than that on the front side. This hypothesis is consistent with the observation in Figure 4.7 that as the number of GO-PAH bilayers increased, the flux difference between FO and PRO modes decreased in general.

It is observed in Figure 4.7(c-d) that water fluxes of a GO membrane in FO and PRO modes were very similar when using $MgCl_2$ and TSC as draw solutes, respectively, indicating that ICP would simultaneously exist or be absent in FO and PRO modes. In fact, previous studies have demonstrated that a polyelectrolyte film can significantly hydrate and thus expand its thickness under high ionic strength [178]. As a result, regardless of the direction that a GO membrane was placed in the test system (i.e., use of the membrane in FO vs. PRO mode), the GO-PAH bilayers in contact with the high-concentration draw solution would hydrate and lead to a loose structure, which allowed ions to transport and hence caused ICP in the membrane support.

4.4.7 Solute flux of GO membrane

To understand solute transport in the GO membrane, we measured the solute flux in FO as well as in PRO mode. As shown in Figure 4.8, the solute fluxes for sucrose, $MgCl_2$ and TSC, are in the range of 0.1±0.1, 3.3±1.2, and 0.7±0.6 mol/m^2/h, respectively. The results demonstrate that the solute fluxes for ionic species were much higher than those of uncharged species, even though these species sizes are similar (e.g., both sucrose and TSC have hydrated diameter of ~1 nm). The high solute fluxes (i.e., low rejection) for ionic species can be most likely attributed to the hydration effect of the GO-PAH film under high ionic strength [110, 174]. Since polyelectrolytes became more hydrated under a higher ionic strength condition, it leads to a larger inter-GO-layer spacing and thus looser and thicker film. Recent studies have shown that such dependency on ionic solution strength is applicable for both GO and PAH [176]. Therefore, the thickness and inter-GO-layer spacing of the active layer partly depended on the ionic strength of the solution to which the active layer was exposed. In comparison, sucrose, which is a neutral solute, could not exert such effect on the GO membrane. As a result, the GO membrane remained tight and thus had a low solute flux.

Comparison of the solute fluxes in FO and PRO modes showed different behavior for sucrose and ionic draw solutions ($MgCl_2$ and TSC). When sucrose is used as draw solution, the solute flux is higher in PRO mode than in FO mode. This is because the ICP effect in FO mode causes the dilution of draw solution in the membrane support, thus decreasing the amount of solute permeating through the GO membrane. When the ionic solutions are used as draw solution, however, the effects are more complicated because ICP effects are present in both FO and PRO modes due to the swelling/hydration of the

GO-PAH bilayers on the draw solution side. As a result, the solute flux is affected not only by ICP but also by the integrity of the GO-PAH bilayers on the front and back sides. Therefore, there is no obvious trend for the solute flux in FO and PRO modes. Overall, the solute flux behavior in FO and PRO modes is consistent with the water flux behavior and further confirms our hypothesis on the unique transport phenomena in the GO membranes.

It appears that the GO membrane at the current stage may not be directly applicable for high salinity applications. This is because without covalent cross-linking, the GO membrane would probably swell under high ionic strength and thus considerably lose its solute rejection capability. Nevertheless, the sucrose flux of the GO membrane was low enough to avoid significant back diffusion of draw solutes, even though it is still more than 7 times that of an HTI membrane (Figure 4.8(a)). For example, the 10-bilayer GO membrane exhibited around 99% rejection of sucrose (with a hydrated diameter of around 1 nm), indicating that the channel cutoff size (i.e., the inter-GO-layer spacing) of the GO membrane was close to ~1 nm or the molecular weight cut-off (MWCO) of the membrane is around 342. Therefore, the present GO membrane can be well suited for many important applications such as FO-based emergency water supply that uses sugary draw solutions as well as water purification and wastewater reuse that do not mandate high ionic strength conditions.

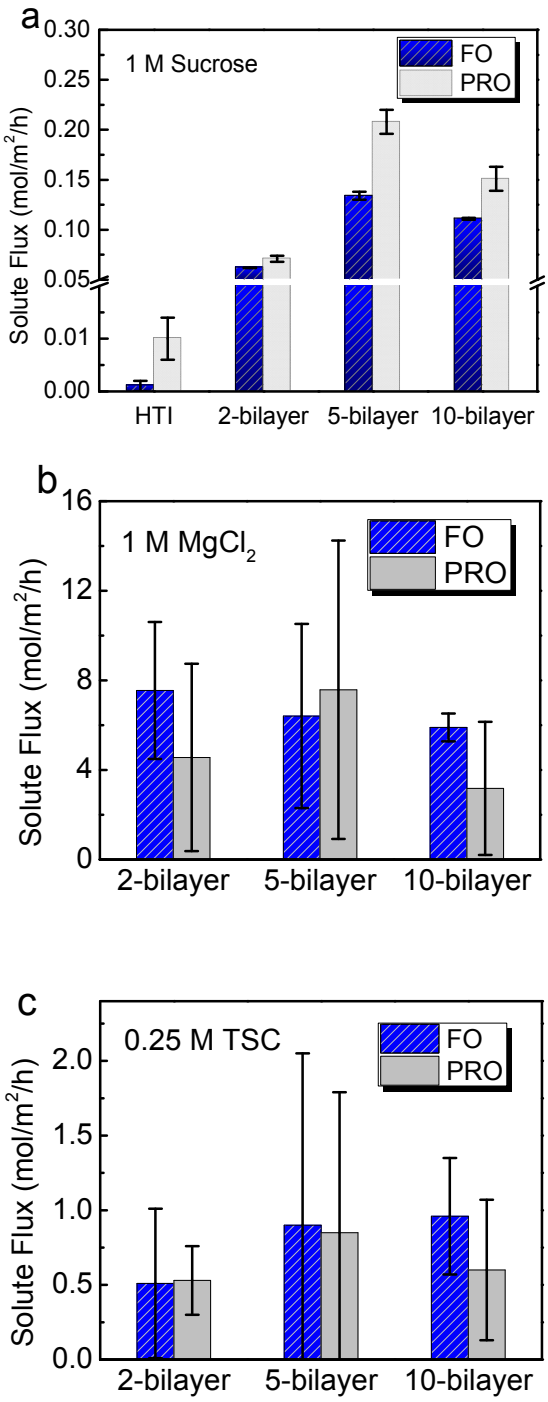

Figure 4.8 Solute fluxes of GO membranes using (a) 1 M sucrose, (b) 1 M $MgCl_2$, and (c) 0.25 M TSC as draw solutions, respectively.

4.4.8 Effect of bilayer number

Increasing water flux and decreasing solute flux are usually two competing objectives in designing a high-performance membrane: an increase in water flux is often accompanied by a decrease in membrane resistance and also an increase in solute flux. This statement, however, seems not applicable for the present GO membrane under certain conditions. For example, when 1 M sucrose was used as draw solution, the 2-bilayer GO membrane exhibited high water flux (Figure 4.7(b)) and low solute flux (Figure 4.8(a)) almost regardless of the specific operation mode (i.e., FO vs. PRO). Overall, there seems no conclusive correlation between the number of bilayers and the water/solute flux of a GO membrane. This interesting phenomenon could be attributed to the superfast water transport along the surface of GO nanosheets [44, 45]. Since an increase in the number of GO-PAH bilayers did not significantly increase the hydraulic resistance of a GO membrane, the membrane flux did not correlate well with the bilayer number. It also indicates that an effective GO membrane can be fabricated by merely having two bilayer deposition cycles.

4.5 Conclusions

The graphene oxide (GO) membrane made by the stacking of bonded GO nanosheets represents a radically new type of water purification membrane that holds great promise for high-performance, sustainable water treatment applications. In this paper we have demonstrated that a GO membrane can be successfully fabricated by layer-by-layer assembly of GO and PAH via electrostatic interaction. The QCM-D results showed that each GO-PAH bilayer is around 16.5 nm thick and the mass of GO in each bilayer is 2 to

5 times higher than that of PAH, most likely due to the higher mass-to-charge ratio of GO. Such composition indicates than each bilayer contains multiple layers of GO nanosheets. We have found that water permeability of the GO membrane is about one order of magnitude higher than that of a commercial FO membrane. At the current stage, the solute flux of sucrose as a representative uncharged species is much lower than that of ionic species ($MgCl_2$ and TSC), although the hydrated radius of TSC is comparable to that of sucrose. We hypothesize that this is because the hydration of the layered GO nanosheets in solutions of high ionic strength (i.e., $MgCl_2$ and TSC solutions) enlarges GO interlayer spacing. Therefore, in order to minimize the hydration effects in solutions of high ionic strength, future research is warranted to further stabilize the interlayer forces (e.g., by creating covalent bond). Nevertheless, the GO membrane retained a tight structure in low ionic strength and exhibited high rejection to sucrose (~99%), indicating a MWCO of around 342 or an equivalent pore size of around 1 nm.

Chapter 5: Transport Mechanisms in Graphene Oxide Membranes

5.1 Abstract

Graphene oxide (GO) has shown great promise in developing highly efficient membranes for water separation. Elucidation of the transport mechanisms is critical to better designing membranes to fully exploit the potential of GO. This chapter aims at understanding the transport phenomena for the GO membrane synthesized by the layer-by-layer assembly of GO and poly(allylamine hydrochloride) (PAH) via electrostatic interactions. It was found that water traveled through the GO membrane at a velocity of 4.8×10^{-4} m/s under a 1-atm transmembrane pressure, two orders of magnitude higher than the velocity (8.4×10^{-7} m/s) of water flowing between two hypothetical parallel plates. It implies that PAH most likely connected the GO nanosheets at the edges, which left the graphene surfaces largely intact for the ultrafast water transport. This is further supported with the significant impeding effect the GO membrane exerted on the solute transport either by the hydrophobic graphene surface or by the negatively charged path formed. The study provides for the first time experimental verification of the fast water transport through GO channels in an electrostatically assembled GO membrane, and may inspire the development of next generation membranes based on the highly adaptable GO.

5.2 Introduction

Graphene-based materials have attracted tremendous attention in various fields thanks to many of their exciting properties such as unique 2-D structure [36], extreme mechanical strength [16, 65], controllable electrical conductivity (depending on specific materials) [39, 42] , etc. Being solution processable and mass producible [143, 179], graphene oxide

(GO) is particularly promising in achieving large-scale applications. Indeed, a few theoretical and experimental studies have reported the potential of GO in developing highly efficient membranes for water purification [44, 45, 61, 92, 93].

The concept of graphene-based water separation membranes was first examined by molecular simulations and other theoretical tools [77-80]. Generally, graphene sheets are impermeable [81], and thus pores ranging from sub-nanometer to nanometer size were designed on the graphene sheets, and passivated with functionalities. Molecular transport was then simulated through such nanoporous graphene membranes. Results suggest that while pore size and chemical functionalization may determine the selectivity of the porous graphene, ultrafast water transport can be achieved which is orders of magnitude than the conventional counterparts [77-80]. While these theoretical findings are encouraging, creating such pores is challenging in large scale [45, 79].

Alternatively, GO membranes are obtained in the form of stacked GO sheets by simply filtering or spray-/spin-coating GO suspensions. As a proof of concept study for water separation membranes, Nair et al. demonstrated that micrometer thick GO laminates allow unimpeded permeation of water yet block other liquids, vapors, and gases, including helium [44]. Their molecular simulations attributed the anomalous water transport to the capillaries formed between graphene sheets, which provide a capillary-like pressure to maintain wetting on the external GO surface and low-friction flow pathways for monolayer water. This evaporation-limiting transport excludes the passage of other molecules due to reversible narrowing of the capillaries so that water cannot fill in low humidity, and/or to the clogging in the functional groups/spacers region by water molecules [44]. The high capillary-like pressure also acts on ions that fit in the formed

nanocapillary, making GO films precise molecular sieves with a sharp diameter cutoff at 9 Å [92]. For solutes of hydrated radii greater than 4.5 Å, no permeation occur through the GO laminates, yet smaller species, disregarding the charge, travel through the film at a similar rate that is three orders of magnitude higher than diffusion. Han et al. later conducted more detailed experiments to showcase the potential of the stacked graphene sheets for nanofiltration (NF) [93]. They used reduced GO to make the ultrathin laminates (22–53 nm thick, controlled by GO loading) via filtration, and found the flux to double that of GO films made in the same manner due to the disappearance of the functional groups. Pure water flux reached ~22 $Lm^{-2}h^{-1}bar^{-1}$, and such high flux cannot be accounted for by parallel plate Hagen–Poiseuille equation. Rather, it could be well explained by the slip flow theory that suggests enhanced water flux with water flow velocity on the graphene surface. Although moderate rejections (20-60%) were achieved against ion salts, the reduced GO membranes showed near complete retention (> 99%) of organic dyes in dead end filtration mode due to both size exclusion and Donnan exclusion.

The ultrafast water transport and precise sieving features inspired us to develop GO membranes for forward osmosis (FO) in practical applications (Chapter 4) [61]. The GO membrane was synthesized via a simple layer-by-layer (LbL) process, in which GO nanosheets were sequentially deposited onto a charged substrate along with poly(allylaime hydrochloride) (PAH). Water permeability of the GO membrane was found to be about one order of magnitude higher than that of a commercial FO membrane. In this chapter, water and solute transport mechanisms shall be explored to

decipher the observed favorable transport phenomenon. Moreover, the understanding transport mechanisms is crucial to tailor-designing and optimizing GO membranes.

5.3 Theory

5.3.1 Water Transport in GO Membrane

The 10-bilayer GO membrane was used as an example to estimate the velocity of water transport in a GO membrane. The velocity of water transport in the GO channel under a transmembrane pressure (ΔP) of 1 atm is estimated in

$$v_{GO} = \tau J \Delta P / \varepsilon \tag{5-1}$$

where τ is the tortuosity of the GO membrane, J is the water permeability of the GO membrane, and ε is the porosity of the GO membrane. The tortuosity of the GO membrane is calculated as

$$\tau = (L \times N)/(N \times \delta_1) \tag{5-2}$$

where L is the nominal dimension of a GO nanosheets, N is the total number of GO-PAH bilayers, and δ_1 is the average thickness of one GO-PAH bilayer. The average number of water flow channels within one GO-PAH bilayer is calculated as

$$Nc = \delta_1/(h+d_0) \tag{5-3}$$

where h is the inter-GO-layer spacing (i.e., water flow channel), and d_0 is the average thickness of a GO nanosheets. The average number of water flow channels can be used to compute the porosity of the GO membrane in

$$\varepsilon = N_c(4L \times h)/(L^2) \tag{5-4}$$

All parameters needed for the calculations are obtained from previous studies (Chapters 3&4), and listed in Table 5.1. Note that the inter-GO-layer spacing (i.e., water flow

channel) is taken as 1 nm, based on the rejection of sucrose and TSC (with a hydrated radius between 0.5 and 0.6 nm) by the present GO membrane.

In order to compare the estimated water flow velocity with that expected from a Poiseuille flow, the average velocity is determined of a laminar water flow between two parallel plates by using the following the plate-Poiseuille flow equation:

$$v_P = \left(h^2/12\mu\right)\left(\Delta P/NL\right) \tag{5-5}$$

where v_P is the flow velocity between two parallel plates, μ is the dynamic viscosity of water (0.001 Pa-s at 25 ºC), and $\Delta P/L$ is the rate of pressure drop along the flow channel.

Table 5.1 Parameters for calculating the velocity of water transport in the GO membrane.

Parameters	**Symbols**	**Values**
Water permeability	J	5.8 LMH/atm[a]
Total number of GO-PAH bilayers	N	20
Average thickness of a GO-PAH bilayer, per QCM-D	δ_1	16.5 nm
Inter-GO-layer spacing	h	1 nm
Average thickness of a GO nanosheet	d_0	0.3 nm
Average number of GO channels in a bilayer	N_c	12.7
Nominal dimensions of a GO nanosheets [45]	$L \times L$	500 nm × 500 nm
Porosity of the GO membrane	ε	0.10
Channel tortuosity of the GO membrane	τ	30

[a] LMH/atm = l/m^2/h/atm

5.3.2 Diffusion in GO Membrane

The diffusion coefficients of $MgCl_2$ and TSC ($Na_3C_6H_5O_7$) were estimated based on the coupled diffusion of ions by using the following equation derived from the Nernst-Planck equation:

$$D_{A_aB_b} = \frac{abD_AD_B}{ab^2D_A + a^2bD_B} \tag{5-6}$$

where $D_{A_aB_b}$ is the diffusion coefficient of a neutral species with formula A_aB_b, and D_A and D_B are the diffusion coefficients of the dissociated ions *A* and *B*, respectively. The diffusion coefficients of dissociated ions and coupled ions are listed in Table 5.2.

Table 5.2. Diffusion coefficients of different ionic species.

Ionic Species	Mg^{2+}	Cl^-	$MgCl_2$	Na^+	$C_6H_5O_7^{3-}$	$Na_3C_6H_5O_7$
Diffusion coefficient (cm^2/s) (Buffle et al. [180])	7.1×10^{-6}	2.0×10^{-5}	4.2×10^{-6}	1.3×10^{-5}	6.1×10^{-6}	2.6×10^{-6}

5.3.3 Solute Partitioning and Transport of GO Membrane

Note that there is no ICP in PRO mode and the external concentration polarization can be neglected due to the low permeate flux and high cross-flow rate. For this reason, the solute flux data measured in PRO mode was used to calculate the solute rejection *R* and permeation coefficient *B* of the GO membrane:

$$R = 1 - \left(J_s / J_w\right)/C_d \tag{5-7}$$

$$B = J_s/C_d \tag{5-8}$$

where J_s is the solute flux, J_w is the water flux, and C_d is the draw solution concentration.

The solute partitioning into the 10-bilayer GO membrane was measured using QCM-D at a concentration the same as that of draw solution. The solute concentration in the GO-PAH film is obtained by dividing the adsorbed solute mass (Figure 5.1) by the volume (i.e., sensor area times film thickness) of the film. As shown in Figure 5.1, the solute adsorption for the uncoated and coated sensors were quite similar, indicating membrane support had little effect on solute partitioning. The partition coefficient K can then be calculated as

$$K = C_m / C_s \tag{5-9}$$

where C_m and C_s are solute concentrations in the GO-PAH film and in the solution, respectively.

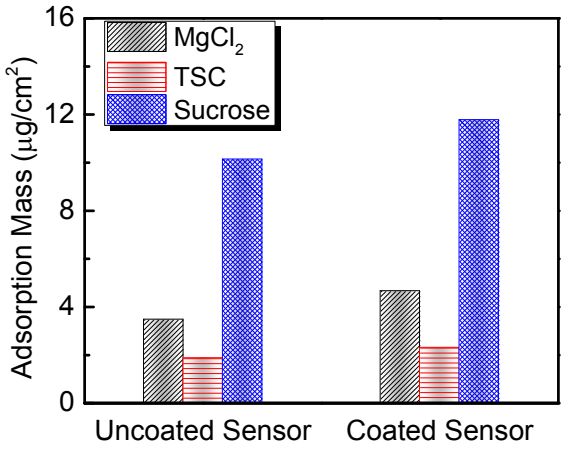

Figure 5.1 Mass of solutes adsorbed on the uncoated and hPAN-coated sensors, respectively.

The solute diffusion coefficient for the GO-PAH film can be calculated as

$$D_m = B\delta_m / K \tag{5-10}$$

where D_m is the hindered diffusion coefficient of solute in the GO membrane, and δ_m is the total thickness of the GO-PAH film and is estimated to be 330 nm, with each side of the hPAN support coated with ten ~16.5-nm-thick GO-PAH bilayers [61].

5.4 Results and Discussions

5.4.1 Water Transport in GO Membrane

The water flux of the GO membrane was measured in a hydraulically pressurized membrane system. As shown in Figure 5.2, the water permeability (i.e., water flux normalized by transmembrane pressure) of the GO membranes ranged from 2.0 to 5.8 LMH/atm and was much lower than that of the PAN (88.4 LMH/atm) and hPAN support (14.6 LMH/atm), indicating that the existence of GO-PAH bilayers led to significant hydraulic resistance and hence lowered the water flux.

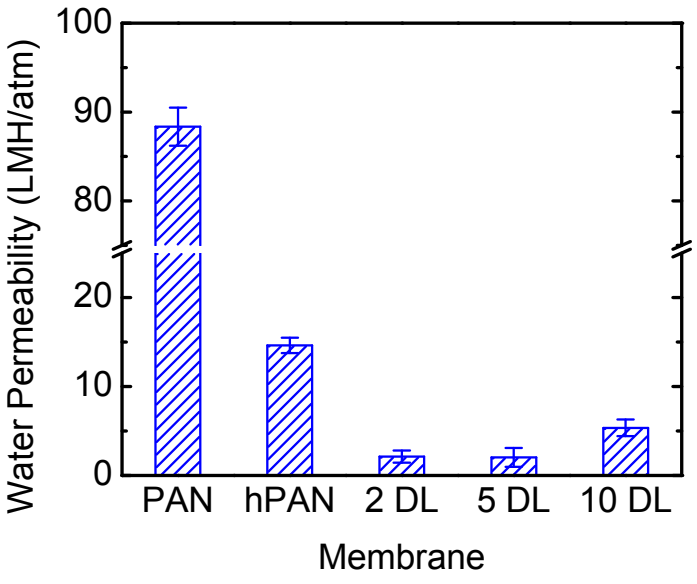

Figure 5.2 Pure water permeability of polyacrylonitrile (PAN) membrane, hydrolyzed PAN (hPAN) membrane, and GO membranes with 2-10 double layers of poly(allylamine hydrochloride) and GO.

As an example, the 10-bilayer GO membrane is used to estimate the velocity of water transport within a GO membrane. Assuming on average a GO lateral dimension of 500 nm [45], clear inter-GO-layer spacing of 1 nm, and single GO-PAH bilayer thickness of 16.5 nm [61], the water permeability (5.8 LMH/atm) of the GO membrane can be converted to a water transport velocity of 4.8×10^{-4} m/s under a 1-atm transmembrane pressure. This estimated velocity turns out to be two orders of magnitude higher than the velocity (8.4×10^{-7} m/s) of water flowing between two hypothetical parallel plates, as predicted by the plate-Poiseuille equation. Note that such a fast water transport has been experimentally demonstrated in a previous study but only for membranes made of pure GO nanosheets [44]. The functional groups on the basal planes act as spacers between neighboring GO sheets, which enables the frictionless flow on the graphene surface [44]. Hence, our study provides for the first time the experimental verification of a fast water transport through GO channels in an electrostatically assembled GO membrane. Similarly, the majority of the graphene area is likely to remain largely intact in this case, as PAH molecules further intercalate the GO sheets while not retarding water transport. Upon knowing that the sandwiching of certain polymers (e.g., PAH) between GO layers may not necessarily reduce water transport velocity in a layered GO membrane, researchers are much encouraged to explore the synthesis of highly tunable GO membranes by using carefully selected polymeric spacers that have exceptional properties.

5.4.2 Mechanisms of Solute Transport in GO Membrane

To understand solute transport in the GO membrane, we measured the solute flux in FO as well as in PRO mode. Figure 4.8 in Chapter 4 shows that the sucrose flux of a GO

membrane was more than 7 times that of an HTI membrane. However, there seems no conclusive correlation between the number of bilayers and the solute flux of a GO membrane. Note that the sucrose flux of a GO membrane in FO mode was consistently lower than that in PRO mode. This is because typically the ICP in FO mode caused the dilution of draw solution in the membrane support, thereby minimizing the passage of solutes through the membrane.

Table 5.3 Water and solute transport parameters for the 10-bilayer GO membrane.

Parameters	**Symbol**	**Unit**	**$MgCl_2$**	**TSC**	**Sucrose**
Mass adsorption		$\mu g/cm^2$	3.5	1.9	10
Concentration in membrane	C_m	mol/L	3.0	0.6	2.5
Concentration in solution	C_s	mol/L	1.0	0.25	1.0
Partition coefficient	K	-	3.0	2.4	2.5
Water flux	J	$L/m^2/h$	19.9	9.6	26.5
Solute flux	J_s	$mol/m^2/h$	1.1	0.94	0.15
Solute rejection	R	--	78%	90%	99%
Solute permeation coefficient	B	m/s	3.0×10^{-7}	1.0×10^{-6}	4.2×10^{-8}
Diffusion coefficient	D_m	cm^2/s	2.3×10^{-10}	1.0×10^{-9}	4.1×10^{-11}

Information on solute rejection of the GO membrane can be used to estimate its pore cutoff size. As shown in Table 5.3, the 10-bilayer GO membrane exhibited much higher rejection of sucrose (99%) than that of $MgCl_2$ (78%) and TSC (90%), indicating that the channel cutoff size (i.e., the inter-GO-layer spacing) of the GO membrane was close to the hydrated diameter of sucrose (~1 nm). The relatively low rejection of ionic

species can be most likely attributed to the hydration effect of the GO-PAH film under high ionic strength. Therefore, the GO membrane at the current stage may not be directly applicable for desalination, because without covalent cross-linking, the GO membrane would probably swell under high ionic strength and thus considerably lose its solute rejection capability. Nevertheless, the present GO membrane can be well suited for many important applications such as FO-based emergency water supply systems that use sugary draw solutions as well as water purification and wastewater reuse that do not mandate high ionic strength conditions.

In order to determine the mechanisms controlling the solute transport in the GO membrane, the partition coefficients and diffusion coefficients were characterized for the three draw solutes (Table 5.3). As given in Table 5.3, partition coefficients of the three solutes are between 2.4 and 3.0 (so they do not differ significantly), indicating that partitioning of these solutes into the GO membrane was neither affected by the size or charge of the specific solute nor a governing factor for the huge difference in the permeation of these solutes.

As plotted in Figure 5.3, the diffusion coefficients of $MgCl_2$ (4.2×10^{-6} cm^2/s), TSC (2.6×10^{-6} cm^2/s), and sucrose (4.3 to 5.2×10^{-6} cm^2/s) are similar in bulk water [180, 181]. Their diffusion coefficients for the GO membrane, however, are 3 to 5 orders of magnitude lower. The hindering effect is the most pronounced for sucrose, with the lowest diffusion coefficient of 4.1×10^{-11} cm^2/s. It is hypothesized that the ring structure in sucrose may have strong interactions with the carbon rings in GO (e.g., hydrophobic interactions and π-π interactions), thereby increasing the hindrance by friction and decreasing the diffusion of sucrose. The much lower hindering effects for the two ionic

species ($MgCl_2$ and TSC) again can be attributed to the hydration of GO-PAH films under high ionic strength.

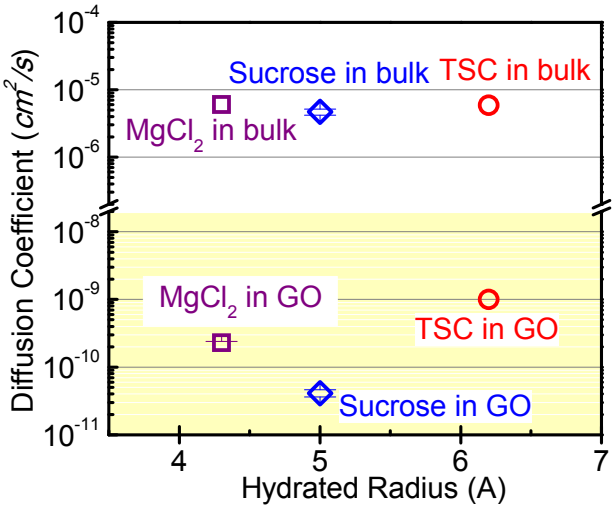

Figure 5.3 Diffusion coefficients of draw solutes for the 10-bilayer GO membrane, compared with those in bulk water. Since $MgCl_2$ and TSC dissociate into counter ions in water, the hydraulic radius of the relatively larger ion for each species (i.e., Mg^{2+} for $MgCl_2$ and $C_6H_5O_7^{3-}$ for TSC) is used in the plot.

A closer comparison of the two ionic species ($MgCl_2$ and TSC) helps us identify the most possible solute transport path in the GO membrane. Since TSC is composed of one $C_6H_5O_7^{3-}$ and three Na^+, the diffusion of $C_6H_5O_7^{3-}$ should be faster than TSC [180] and thus more than 25 times that of sucrose, although the hydrated radius of $C_6H_5O_7^{3-}$ is even slightly higher than that of sucrose (Figure 5.3). The increase in the transport rate of negative ions (Table 5.3) indicates that the dominant path for solute transport was negatively charged, since a positively charged path would tend to adsorb negative ions onto its surface and thereby increase the ion-surface friction and consequently decrease the diffusion rate. This indication is further reinforced by the fact that the diffusion coefficient of $MgCl_2$ (controlled by Mg^{2+}) is only one fourth that of TSC, although

$MgCl_2$ diffuses faster than TSC in bulk water. Therefore, the dominant transport path in the GO membrane should be that formed by the negatively charged GO nanosheets instead of positively charged PAH polymers. This conclusion is consistent with the foregoing observation that the existence of PAH did not interfere with the fast water transport in GO channels, indicating that most likely PAH connected GO nanosheets only at their edges while leaving their surface areas largely untouched.

5.5 Conclusions

Transport mechanisms were explored for the GO membranes synthesized via electrostatic interactions in this chapter. Using a 10 DL GO membrane (10 bilayers of PAH and GO) as an example, water transport velocity (4.8×10^{-4} m/s at 1 atm) through the GO membrane was estimated to be two orders of magnitude higher than that (8.4×10^{-7} m/s at 1 atm) flowing between two hypothetical parallel plates, as predicted by the plate-Poiseuille equation. This ultrafast water transport is attributed to the frictionless flow pathways created by the graphene surfaces of neighboring GO sheets, which was not covered by the partnering cationic polymer, i.e., PAH. Solute diffusion and partitioning were characterized for the GO membrane. It was found that the GO layers significantly impeded the diffusion of the solutes tested ($MgCl_2$, TSC, and sucrose), with the most pronounced effect on sucrose (diffusion coefficient of 4.1×10^{-11} cm^2/s). The hindering effect was a result of the strong interactions between the solutes and the GO nanosheets. These observations draw a picture of the dominant transport mechanisms in the GO membrane: PAH most likely connected GO nanosheets only at their edges, which left the graphene surface areas largely intact for ultrafast water flow, and formed negatively

charged pathways for impeded solute transport. Understanding the transport mechanisms is crucial to designing GO membranes to achieve the full potential of GO. For example, given that the intercalation by PAH did not affect the water transport in the GO membrane, it is possible that highly tunable membranes can be synthesized by carefully selecting spacers with exceptional properties.

Chapter 6: Organic Fouling of Graphene Oxide Membranes and Implications for Fouling Control in Pressure Retarded Osmosis

6.1 Abstract

Pressure retarded osmosis (PRO) has been gaining wider popularity due to the pressing energy crisis. However, membrane fouling lowers the water permeability and thus the power density generated from the PRO process. Herein we demonstrate a novel and simple strategy to control membrane fouling for PRO by introducing an anti-fouling GO layer at the back the support layer. This physical barrier was effective at preventing the foulants from fouling the support interior and from causing severe flux decline. Our experiments show that the control membrane (without such a GO layer) saw flux decreases of ~30% after BSA fouling in PRO mode, whereas the GO membrane (with the GO layer) only reported negligible (less than 10%) flux reduction. With the worse alginate fouling, the flux dropped by ~50% for the control membrane in comparison to 0% (without Ca^{2+}) or 30% (with Ca^{2+}) for the GO membrane. Moreover, physical cleaning by increasing the cross-flow velocity almost fully restored the flux for the GO membrane in both fouling cases, yet had minimal impact on recovering the flux for the control membrane. We further conducted QCM-D experiments to study the interactions between the organic foulants and the membranes at the molecular level. It was found that the GO membrane presented a higher affinity (4~5 times) towards the organic foulants than from the control membrane. This is likely due to the large surface area of GO contributing to the adsorption capacity of the GO membrane. The results indicate that the low fouling propensity of the GO membrane was due to (1) the role of GO nanosheets as a barrier layer that prevented fouling of the support interior, and (2) the diminished

possibility of bridging with foulants because of the low density of available carboxylate functional groups. These findings settle the competing effects between the hydrophilicity and the adsorptive property when considering GO for fouling control applications, and open up a new avenue to improving membrane anti-fouling performance.

6.2 Introduction

Graphene oxide (GO), being a single-layer carbon sheet with unique 2-dimensional (2D) shape, carrying abundant oxygenated functional groups [44, 182], holds great promise as an emerging antifouling material for membrane surface modification due to high hydrophilicity and charge properties [183-185]. For example, GO was blended into the polymer matrix of polyvinylidene fluoride (PVDF) microfiltration (MF) [184], PVDF ultrafiltation (UF) [183, 185], and polyether sulfone (PES) nanofiltration (NF) membranes [186] to reduce organic fouling. In another study, GO and amine-functionalized GO were stacked onto polyamide (PA) membranes via electrostatic interactions, and the resulted membranes showed enhanced fouling resistance to bovine serum albumin (BSA) [104]. The superior fouling performance was attributed to GO-enhanced hydrophilicity, which led to weaker adhesion forces between foulants and membrane surfaces [187, 188]. Another study synthesized a GO-doped polysulfone membrane for wastewater treatment, and found that the negative charge introduced by GO creates electrostatic repulsion against microorganisms and inhibit membrane biofouling [189].

Another interesting property of GO that is potentially useful in membrane fouling control is its antimicrobial properties [69-71]. GO exhibits promising antibacterial

properties against different bacterial species (e.g., *E. coli, B. Subtilis)* [71, 190-193]. Possible antibacterial mechanisms include (i) the oxidative stress generated by the production of reactive oxygen species, (ii) the membrane stress caused by the direct contact with sharp nanosheets during the initial cell deposition on GO, and (iii) cell wrapping that reduces the metabolic activities and eventually causes the death of bacterial cells [71, 191]. Such antibacterial properties of GO have been used to control membrane biofouling by grafting GO onto polyamide membranes, which resulted in 65% bacterial inactivation upon direct contact with bacteria [194].

Although previous research show some evidence of GO as a promising candidate material to reduce membrane fouling, these studies have overlooked some other properties of GO, such as strong adsorption capability towards organic molecules [195, 196] and large surface area (around 2630 m^2/g) [197], which may adversely deteriorate membrane fouling. Therefore, more comprehensive and thorough studies are needed to evaluate and explain the antifouling properties of GO. For example, we need to understand how the hydrophilicity and adsorption properties of GO nanosheets possibly interact with one another to contribute to the antifouling properties of a membrane. Additionally, most of the previous research embedded GO into membrane polymer matrix that obviously reduced the chance of GO being exposed to foulants and thus weakened the any potential effects of GO. Therefore, it is necessary to conduct research with GO fully exposed on the membrane surface so that the effects of GO can be maximized and comprehensively characterized.

None of the previous study, to our best knowledge, has discussed the potential benefit of the unique 2D shape of GO in membrane fouling control. The 2D shape of GO

makes it extremely convenient to assemble a thin film on any surfaces, including the porous and rough surface on the back side of an asymmetric membrane. This unique property is especially useful in preventing membrane fouling that occurs in the back side of a membrane in pressure retarded osmosis (PRO) membrane processes. PRO is a membrane process that utilizes the osmotic pressure difference between two streams to create water flow from the low concentration stream to the high concentration stream through a semipermeable membrane, and the water flow can power a mechanical turbine to generate electricity [198-201]. PRO has been proposed to harvest the natural salinity energy from mixing river water and high-salinity water [202-204], which is believed to add a green and renewable energy source to meet the grand energy challenges for the present and the future [205-207].

However, membrane fouling in PRO has become one of the major limiting factors to inhibit the advancement of this technology, mainly because foulants enter the porous support layer of a semipermeable membrane from the backside and accumulate inside the porous structure of the membrane [202, 206]. Such fouling is extremely challenging to prevent because all the state-of-the-art semipermeable membranes we used nowadays have a relatively open structure (i.e., large pores and rough surfaces) on the back side so that foulants can easily penetrate. The ultimate negative consequence of PRO membrane fouling is decreased power generation due to the increased transport resistance (i.e., reduced water flux) and fouling enhanced concentration polarization [202, 208-213]. Yip and Elimelech found that membrane fouling in PRO by natural organic matter (NOM) caused water permeability to drop by ~39%, which was equivalent to a 26% decline in

projected power density [202]. Similar observations are also reported in other studies [209, 211, 212, 214], proving the negative effect on the PRO process.

PRO fouling is not only hard to prevent, but also extremely challenging to clean as it occurs inside the support layer [202]. For example, Mi and Elimelech compared membrane fouling behavior in PRO and in forward osmosis (FO), where fouling occurs only on membrane surfaces [27]. They found that a simple physical cleaning (by increasing cross-flow velocity) could almost completely remove the fouling layer and restore water flux in FO, but such cleaning (or even chemical cleaning) is significantly less effective in PRO due to the shielding effects of support layer, i.e., any changes in hydrodynamic conditions cannot reach the fouling layer inside the pores [202]. Even an osmotic backwash (achieved by switching the feed and draw solutions) could only recover ~60% water flux or ~44% project power density [202]. Researcher also tried to modify the membrane support to alleviate fouling in PRO. For instance, Li et al. grafted hyperbranched polyglycerol on dopamine coated poly(ether sulfone) (PES) hollow fiber support layers [215]. The resulting TFC membranes showed higher flux when fouled by bovine serum albumin (BSA), and ~94% flux recovery after DI water cleaning [215]. However, grafting with soft polymers still cannot prevent the accumulation of foulants inside the membrane support thus presenting long-term fouling concerns.

Intuitively, PRO membrane fouling can be addressed by creating an antifouling "barrier" that totally blocks the entrance of the foulants into the support layer [215, 216]. However, the traditional membrane synthesis approaches, such as phase inversion or interfacial polymerization, pose significant technical challenges to create such a dense layer on the back side. Additionally, the often large pores (with sizes ranged between

hundreds of nm to a few micronmeter) on the back side of the membrane cannot be fully covered by any surface modification techniques using soft polymers. GO nanosheets, in the contrary, has a unique 2D shape with lateral dimensions often up to a few micronmeters, thus providing great opportunities to create an effective dense barrier on the back side of a porous support.

Therefore, the objective of the study is to thoroughly evaluate the antifouling behavior of a GO membrane and demonstrate its advantageous potential to effectively control PRO membrane fouling. The GO membrane was prepared by the layer-by-layer (LbL) assembly of GO nanosheet and cationic polyelectrolyte on both the top and back sides of a membrane support. The fouling performance of the GO membrane was thoroughly evaluated in comparison with that of a benchmark polyamide membrane in both FO and PRO modes. Quartz crystal microbalance with dissipation was used to characterize the membrane-foulant interactions in order to explain the fouling mechanisms.

6.3 Materials and Methods

6.3.1 Chemicals and Materials

All chemicals were used as received from Sigma-Aldrich (St. Louis, MO) unless listed otherwise. The following chemicals were used for membrane synthesis: polyacrylonitril (PAN) (Mw ≈ 150,000), *N,N*-Dimethylformamide (DMF), sodium hydroxide (NaOH), poly(allylamine hydrochloride) (PAH), polysulfone (PSf) pellets (Udel P3500, Solvay Specialty Polymers USA, Douglasville, GA), 1-methyl-2pyrrolidinone (NMP), 1,3,5-benzenetricarbonyl trichloride (TMC), 1,3-phenylenediamine (MPD), and isopar-G

(Univar, Redmond, WA). Sodium chloride (NaCl) and sucrose were used as draw solutes in the fouling experiments. Sodium alginate (Mw 12–80 kDa) and bovine serum albumin (BSA, lyophilized powder, Mw ~ 66 kDa) (Sigma Aldrich, St. Louis, MO) were selected as model organic foulants in the study. Stock solutions were prepared by dissolving 10 g/L of each foulant in deionized (DI), and were stored in sterilized bottles at 4 °C.

6.3.2 Preparation of GO and PA Membranes

GO was prepared by the modified Hummer's method as described in our previous studies [45, 61]. The GO membrane was synthesized by LbL assembly of GO and PAH [61]. Briefly, a hand-cast PAN membrane was hydrolyzed in 1.5 M NaOH solution for 90 min to get a hydrolyzed PAN (hPAN) support. Then, the hPAN support was alternately soaked in 1 g/L PAH and 0.5 g/L GO solutions (both at pH~4) for five times to assemble a five-double layer (DL) GO-PAH film on both sides of the hPAN support. The polyamide (PA) membranes were prepared by interfacial polymerization [172, 217]. First, a PSf membrane support was prepared by casting 125-μm thick PSf film (12 wt% dissolved in NMP) onto a polyester nonwoven fabric (PET, grade 3249, Ahlstrom, Helsinki, Finland), which was then immediately transferred into a 3 wt% NMP/DI coagulation bath and submerged for 10 min to allow complete phase separation. The thus formed PSf membrane was stored in DI water for several days with frequent DI replacement to remove residual NMP in the support. To form PA layer on the support, the PSf membrane was mounted in a 6-inch frame with the top side forming a reservoir to hold 15 mL MPD solution (3.4 wt% in DI) for 2 min; then the support was dried with a filter paper and 15 mL TMC solution (0.15 wt% in Isopar-G) was poured onto the membrane to allow interfacial polymerization; after 1-min reaction time, the frame was

held vertically for 2 min to drain the TMC solution; and finally the membrane was released from the frame and underwent a series of post-treatment by soaking in 95 °C water for 2 min, in 200 ppm NaOCl aqueous solution for 2 min, in 1000 ppm $NaHSO_3$ aqueous solution for 0.5 min, and eventually in 95 °C water for 2 min. The synthesized GO and PA membranes were thoroughly rinsed with DI water and stored in 4 °C before tests.

6.3.3 Membrane Performance Tests

The membrane performance was tested in a custom built FO membrane crossflow system as described in previous study. [218] The system consists of a membrane cell with an effective membrane area of 20.02 cm^2, two magnetic pumps (75211-30, Cole-Parmer, Vernon Hills, IL) that circulate the feed and draw solutions through the membrane cell from their reservoirs, a water bath (NESLAB RTE 10, Thermo Scientific, Newington, NH) to keep the system temperature at 25 °C throughout each experiment, a digital balance that sends the weight of the draw solution to a personal computer for recording every 5 min, a stir plate to mix the feed solution constantly.

The water permeability coefficient (A) and solute permeability coefficient (B) of the membrane selective layer and the structural parameter (S) of the membrane support layer were characterized using the protocols developed by Tiraferri et al.[219]. Each characterization experiment consists of four stages, in which the concentration of the draw solution was raised incrementally. The weight change of the draw solution was monitored to calculate the water flux, J_w, and the concentration of the feed solution to calculate the solute flux, J_s, using the following equations:

$$J_w = \frac{\Delta m}{\rho A_m \Delta t} \tag{6-1}$$

$$J_s = \frac{C(V_0 - J_w A_m \Delta t) - C_0 V_0}{A_m \Delta t} \quad (6\text{-}2)$$

where Δm is the weight change for the draw solution in a given time, Δt, ρ is the density of water, A_m is the effective membrane area, C_0 and C are the respective concentration before and after time Δt, V_0 and V are the respective volume of feed tank before and after time Δt.

In order to characterize the fouling behavior of the membranes, 40 mL foulant stock solution was added to the feed solution (50 mM NaCl) after achieving equilibrium in the system, and the initial foulant concentration in the feed was 200 mg/L. All the fouling experiments were performed with the same initial water flux at ~4 μm/s, which was achieved by adjusting the concentration of the draw solution. The feed and draw solutions flowed concurrently at a crossflow velocity of 10.7 cm/s. The fouling experiment was stopped when the accumulated volume in the draw solution reached ~400 mL (16~20 hours depending on membranes). Physical cleaning was immediately performed by flushing DI through the system concurrently at a crossflow velocity of 21.5 cm/s for 15 min, after which the water flux was measured again (using the initial feed and draw solution compositions used in the fouling experiments) to determine the flux recovery rate.

6.3.4 QCM-D Experiments

Quartz crystal micro-balance with dissipation (QCM-D) (E-4, Biolin Scientific, Linthicum Heights, MD) was used to quantify the charge density of membranes and adsorption of foulants onto the membrane. In order to perform the QCM-D measurements, GO and PA membranes were coated onto a gold sensor (Biolin Scientific, Linthicum Heights, MD) using the same procedure as used in membrane synthesis. Both

the GO- and PA-coated sensors were then exposed to a series of 1 mM CsCl solutions at pHs in the sequence of 10, 7, and 4 to quantify the charge density [173]. The pH of the CsCl solutions was adjusted with 1 mM CsOH solution. After thoroughly rinsing both of the layers with DI water, both the BSA and alginate foulant solutions (200 mg/L in 50 mM NaCl solution, as used in the membrane fouling experiments) were pumped through the chambers to determine the adsorption of foulants on the membrane surface, and to study the interactions between the foulants and the membrane surfaces. The changes in frequency (*f*) and dissipation (*D*) were recorded upon the introduction of the foulants, and were modeled in the viscoelastic model for the mass of foulants adsorbed onto the GO- and PA-coated sensors.

6.4 Results and Discussion

6.4.1 Permeation properties of GO membranes compared with PA membrane

We characterized the transport (*A* and *B*) and structural (*S*) parameters for both the GO and PA membranes according to reference [219]. The results are summarized in Table 1. The GO membrane had similar *B* values as the PA membrane when sucrose was used as the draw solute. Yet a much higher A was observed with the GO membrane, indicating a significantly lower intrinsic permeation resistance. The structural parameter kept relatively constant for the PA membrane using either solute, which implies that the PA support was not affected (swollen or plasticized) by the solutes. It should be noted that the GO membrane had a higher *S* than that of the PA membrane, as the diffusion distance was elongated by the PAH/GO coating on the support layer. Although this extra "layer" is likely to enhance internal concentration polarization by shielding the solutes from

external hydrodynamic conditions, it is expected to block the foulants from entering the support layer and causing flux deterioration as shown in the following section.[220]

Table 6.1 Transport and structural parameters for the PA and GO membranes.

Membrane	Draw Solute	A (LMH/bar)	B (LMH)	S (μm)
PA	NaCl	0.686 ± 0.144	1.55 ± 0.08	256 ± 27
	Sucrose	0.818	2.84	218
GO	Sucrose	5.36 ± 4.72	2.10 ± 1.24	354 ± 151

Note: LMH = l/m^2-h

6.4.2 The fouling behavior of GO membrane compared with PA membrane

BSA fouling. Minimal fouling was observed with either the PA or the GO membranes when BSA was present under FO mode (Figure 6.1(a&b)). This is likely due to the low flux (initially ~ 4 μm/s) at which the series of experiments were performed. It is well known that physical conditions, such as initial permeation flux, affect membrane fouling.[221] As foulants are brought and deposited onto the membrane surface, a higher initial flux generates a greater permeation drag force and thus faster foulant deposition, which leads to elevated flux decline. The presence of Ca^{2+} (0.5 mM) in the feed slightly enhanced BSA fouling in FO mode for the PA membrane. Ca^{2+} ions are reported to interact with carboxylate groups of organic molecules to form complexes, and also with the carboxylate groups of the membrane surface to bridge the organic foulants and the membrane.[221, 222] Due to this effect, the flux dropped to 83% for the PA membranes after the fouling run with Ca^{2+}, while only 3% flux decline was observed without Ca^{2+}. For the GO membrane, there appeared to be negligible fouling as the flux kept constant

during the fouling experiments after baseline correction, presumably due to the lower affinity between the GO layer and BSA (Section 3.3).

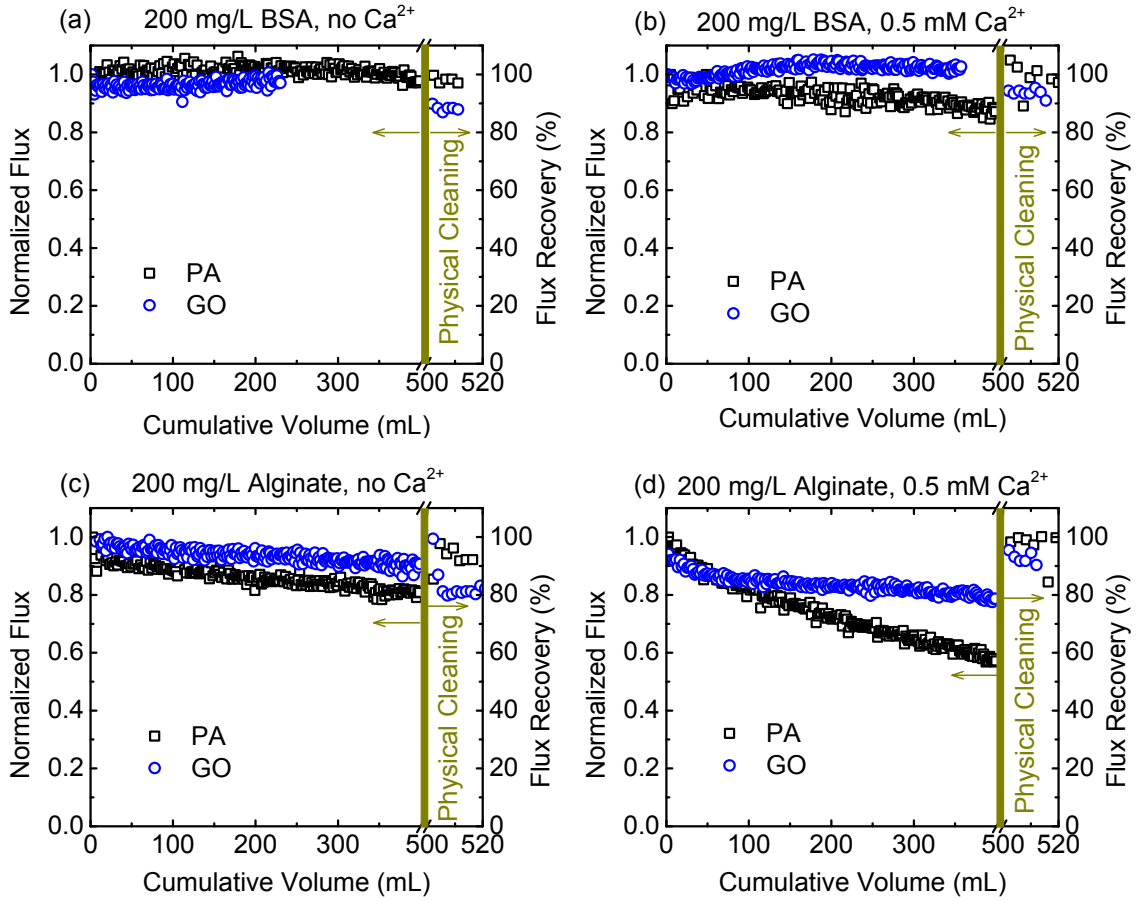

Figure 6.1 Comparison of the fouling behavior of GO and PA membranes in FO mode. (a) BSA fouling without Ca^{2+}, and (b) BSA fouling with 0.5 mM Ca^{2+}, (c) alginate fouling without Ca^{2+}, and (d) alginate fouling with 0.5 mM Ca^{2+}. The initial flux was ~ 4 µm/s for all experiments, which were stopped when the cumulative volume reached ~400 mL. The system (with the fouled membrane) was then flushed with DI for 15 min at a crossflow velocity of 21.4 cm/s.

Immediately after fouling, the membranes were physically cleaned by flushing the system at a crossflow rate of 21.5 cm/s with DI water for 15 min. This cleaning approach has shown to be effective to remove loose fouling layer on the active surface of

FO membranes.[27] After cleaning, the flux of the tested membranes all restored their full capacity, even for the PA membrane fouled by BSA with Ca^{2+}. Surprisingly for the GO membrane, the flux did not seem to fully recover after cleaning (80~90%), even though no fouling was observed. We attribute this lower observed recovery to the re-arrangement of the PAH/GO layers upon environmental changes as reported for self-assembled polymeric multi-layers [61]. To verify this assumption, an additional series of experiments were conducted, which consisted of the following tasks: (1) a baseline was first obtained for a GO membrane, (2) the cleaning protocols were applied, and the recovery was determined, and (3) the GO membrane was subject to BSA fouling, physical cleaning, and flux recovery. The flux recovery was 89.42% after obtaining the baseline, and remained practically constant at 90.55% after fouling (see Supporting Info). This result confirms that the PAH/GO layers underwent arrangements during and re-stabilized after the first physical cleaning. Thus, the lower than unit flux recovery is not indicative of membrane fouling.

Alginate fouling. Compared to BSA fouling, membrane fouling by alginate was more severe, irrespective of the presence of Ca^{2+} in the feed solution (Figure 6.1(c&d)). The flux decreased to ~90% (without Ca^{2+}) and ~80% (with Ca^{2+}) after fouling with alginate for the GO membranes, in comparison to ~100% (without or with Ca^{2+}) for BSA fouling. It is more pronounced with the PA membranes, with ~80% (without Ca^{2+}) and a staggering ~60% (with Ca^{2+}) after alginate fouling. The presence of Ca^{2+} is observed to exacerbate alginate fouling, as Ca^{2+} ions were found to bridge alginate molecules by the carboxylate groups and form gel-like fouling layers [221, 222]. This elevated fouling is likely due to the higher intermolecular adhesion force between alginate molecules, which

led to aggravated membrane fouling than with BSA under similar hydrodynamic conditions [221]. However, the physical cleaning proved to be adequate to recover membrane permeability for both types of membranes despite the enhanced membrane fouling. Note again that the lower than full recovery was partially, if not completely, due to the re-arrangement of the PAH/GO layers upon physical cleaning.

6.4.3 Understanding the effects of charge and adsorption properties of GO on fouling

The GO layer has negligible carboxylate groups compared to the PA membrane (Figure 6.2(a)). The low carboxylate group density is due to (1) limited carboxylate groups in the GO sheets [44, 182] and (2) their participation in the electrostatic interactions to self-assemble the composite PAH/GO layers [61]. It has been demonstrated that membrane surfaces with lower carboxyl group density result in weakened foulant-surface interactions (lower adhesion force and rupture distance) in the presence of calcium ions.[223] Thus the likelihood is minimized for the intermolecular bridging between the carboxylate groups of the membranes and those of the foulants in the presence of divalent cations [221-223].

One limitation for the anti-fouling GO layers, however, is the high adsorption capacity of the GO nanosheets. Figure 6.2(b) depicts the amount of the two organic foulants (BSA and alginate) deposited on the PA and GO membranes determined from the QCM-D experiments. Compared to that adsorbed on the PA membrane, more foulants (nearly four times as much BSA and five times as much alginate) accumulated on the GO membrane despite the countering effect of reduced carboxylate groups. This finding again substantiates that foulant deposition in the support matrix has a more adverse impact on flux than that on the external layer in PRO mode, as will be discussed below.

While this study demonstrates that membrane fouling is substantially improved by relocating the foulants from the support layer to the GO-coated anti-fouling layer, the limitation of high adsorption for such layers may be addressed by functionalizing the GO nanosheets for even better fouling performance.

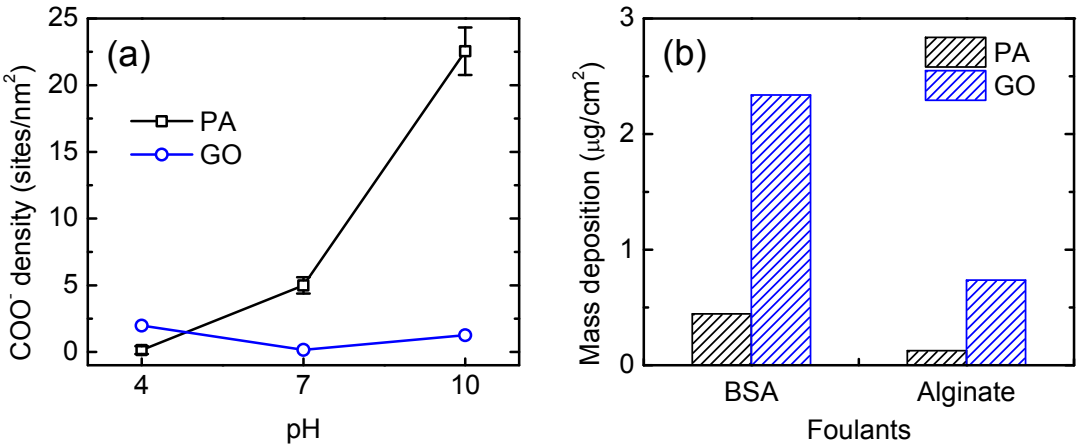

Figure 6.2 (a) Density of carboxylate groups on membrane surface at different pHs, and (b) deposition of foulants on the PA and the GO membranes as monitored by QCM-D. 1 mM CsCl at pHs 4, 7, and 10 were introduced to the GO- and PA-coated sensor for charge probing. After rinsing thoroughly with DI, both coated sensors were exposed to model foulant solutions (200 mg/L in 50 mM NaCl solution) to monitor the deposition of foulants on modeled membrane surfaces.

6.4.4 Effective control of PRO membrane fouling using double-sided GO membrane

BSA fouling. Compared to in FO mode, foulants deposit inside the porous support layer (and at the interface between the active and support layer) of an asymmetric membrane. Therefore, asymmetric membranes experience worse fouling in PRO mode, since the support layer shields the deposited foulants from being flushed away by the shear force originating from the cross-flow. The shielding effect not only favors foulant deposition at

a faster pace, it also renders the physical cleaning not as effective as in FO mode. Thus, it is critical to "intercept" the foulants at the entrance of the support layer by creating the GO barrier atop.

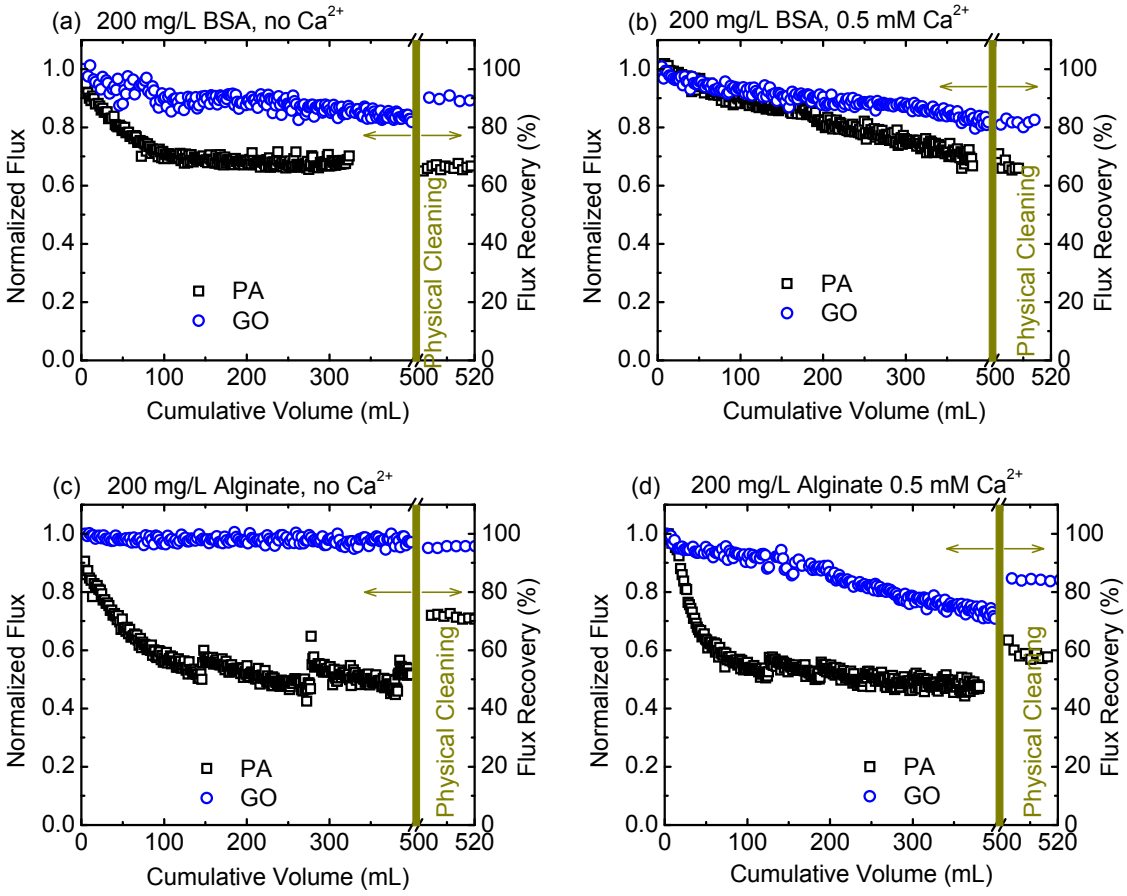

Figure 6.3 Comparison of the fouling behavior of GO and PA membranes in PRO mode. (a) BSA fouling without Ca^{2+}, and (b) BSA fouling with 0.5 mM Ca^{2+}, (c) alginate fouling without Ca^{2+}, and (d) alginate fouling with 0.5 mM Ca^{2+}. The initial flux was ~ 4 µm/s for all experiments, which were stopped when the cumulative volume reached ~400 mL. The system (with the fouled membrane) was then flushed with DI for 15 min at a crossflow velocity of 21.4 cm/s, after which the flux recovery was measured.

Figures 6.3 demonstrate the impact of the GO layer on the fouling performance. The GO membranes showed negligible BSA fouling in the absence or presence of Ca^{2+}, as reflected in the flux (80~90%) after fouling. On the contrary, the PA membrane, without the GO barrier at the support, suffered higher flux decline to 60~70% (Figure 6.3 (a&b)). The difference is presumably due to the fact that BSA accumulated within the support of the PA membranes, while the GO layer blocked the BSA and retained the foulants outside the support of the GO membranes. This hypothesis is reinforced by the discrepancy of cleaning efficiency for the two membranes. Physical cleaning had little impact on the flux recovery on the PA membrane, which is attributed to the deposition of foulants in the support so that the shear force could not reach. With the additional GO barrier, however, the foulants were expected to accumulate outside the support (on the GO layer). And the cleaning-related shear force could easily flush off the foulants and restore the permeability of the GO membrane, as shown in the high flux recovery for the GO membranes.

Alginate fouling. Similar to FO mode, PRO mode saw increased membrane fouling by alginate than by BSA for both the PA and GO membranes (Figure 6.3(c&d)). For example, the flux dropped by ~50% after alginate fouling on the PA membrane, compared to by ~30% after BSA fouling. Surprisingly, the addition of Ca^{2+} slightly worsened fouling on the PA membrane, yet it had a clear impact on the GO membrane. This comparison again implies that the alginate molecules accumulated inside the PA support, but deposited on the GO layer outside the support of the GO membrane. Ca^{2+} can bridge alginate molecules to form gel-like fouling layers on membrane surfaces, as seen in the steady and sharper flux decline for both the PA and GO membranes in FO

mode. A similar trend of flux decline was observed for the GO membrane in PRO mode, but disappeared for the PA membrane. In analogy, alginate fouling occurred mostly outside the GO membrane yet inside the PA membrane in PRO mode. Because the cleaning-induced shear force could only act upon the foulants on the membrane surface, the effect of physical cleaning was different on the flux recovery for the two types of membranes. When the foulants deposited on the membrane surface as for the GO membrane, cleaning by increasing the cross-flow velocity was adequate to restore membrane flux close to its original level. On the other hand, when the PA membrane was fouled on the inside of the support, the same cleaning method had limited effect on flux recovery (only recovered to 60~70% of the initial flux).

6.4.5 Anti-Fouling mechanisms for GO membrane

As discussed above, the major anti-fouling mechanism is to prevent the foulants from clogging the support layer in PRO operations. As demonstrated by the surface image of front and back sides of the GO membrane in Figure 6.4(a), continuous GO membrane was created on both sides of the membrane [61]. This coverage creates a selective layer on the active side of the hPAN support as well as the "anti-fouling barrier" for PRO. In our previous study, the thickness of each bilayer of GO and PAH was estimated to be 16.5 nm, and the equivalent molecular weight cutoff was around 1 nm [61]. The roughness of the GO membrane active layer is comparable to the PA selective layer with the ridge-and-valley surface.

By physically setting a barrier layer at the entrance, foulants are retained outside the support layer rather than deposit inside to cause severe irreversible fouling (Figure 6.4(b)). As displayed in Figures 6.3, the GO barrier was successful in preventing the

foulants from moving into the support layer, which was the case for the PA membrane without such a layer. Accumulation of foulants within the porous support drastically increases transport resistance, thus reduces membrane permeability, and ultimately causes severe irreversible membrane fouling [202]. The negative effect was in full display for the PA membranes, which only registered 60~70% of the initial flux upon physical cleaning after fouling in PRO mode. The relocation of the foulants onto the membrane surface, however, lessened membrane fouling significantly. For the GO membrane, PRO mode fouling (by both BSA and alginate) had similar flux patterns to FO mode fouling. Because the GO layers were coated on both sides of the support, both coated layers acted as selective layers. One GO layer serves as the tight selective layer, whereas the other is relatively loose residing on the porous support. So the deposition of foulants on the tight GO layer in FO mode was expected to behave similarly to that on the other loose GO layer in PRO mode, as long as both GO layers maintain high rejection against the foulants. The *B* parameter for the GO membrane was on the same magnitude as that for the tight PA membrane when using sucrose as the draw solute, indicating the "integrity" of both the GO layers. Therefore, fouling in PRO mode was essentially converted to fouling in FO mode, which has been extensively studied and reported to be affected by various chemical (e.g., pH, ionic strength) and physical (e.g., shear and permeation drag forces) aspects.

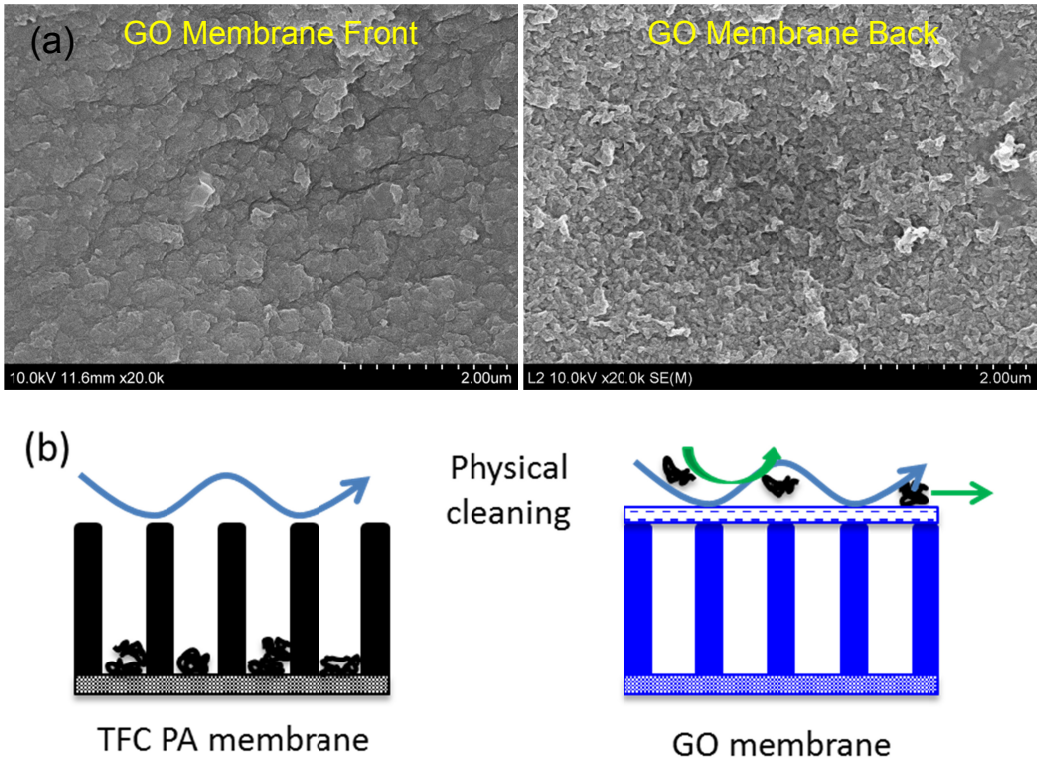

Figure 6.4 (a) SEM images of the front and back side surfaces of the GO membrane, and (b). mechanisms of physical cleaning for the PA and GO membranes

6.4.6 Effect of draw solute on fouling

As pointed out in our previous study, the electrostatic interactions between the PAH and GO make the GO layers subject to swelling in environments of high ionic strength [61]. In such a case, the PAH/GO layers become loose and the active layer not as tight. Foulants may accordingly reach the membrane support through and/or be trapped in the relaxed PAH/GO layer, in addition to depositing atop the GO layer. As a result, the GO barrier may not be as effective in controlling membrane fouling in PRO mode. This effect is manifested in Figure 6.5, which compares the flux decline behaviors of the GO membranes with BSA fouling in PRO mode using $MgCl_2$ (an ionic species) and sucrose (neutral species) as the draw solutes. It is apparent that the flux decreased to a greater

extent (by ~60%) after fouling when $MgCl_2$ was used as the draw solute. Physical cleaning recovered the water flux from ~40% to ~60%, in comparison to the near full recovery when sucrose was the draw solute. The low recovery hints that the loose GO layer at high ionic strength was not sufficient to block the foulants from traversing into the support. The accumulated foulants then caused the major fouling (irreversible flux decline), since the physical cleaning was proved to be adequate to restore the membrane flux close to the original level when a neutral solute (i.e., sucrose) was used as the draw solute. The drawback may be circumvented by chemically cross-linking the GO/PAH layers such that the electrostatic interactions are replaced by covalent bonds, which are not influenced by ionic strength.

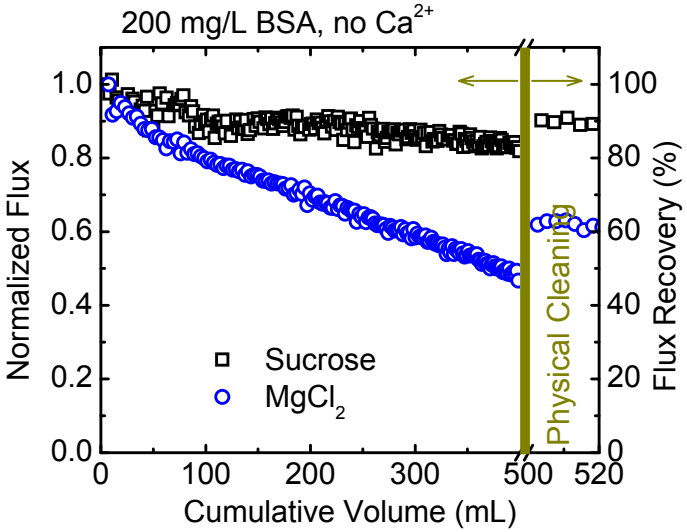

Figure 6.5 Effect of draw solutes on BSA fouling for the GO membrane. The initial flux was ~ 4 µm/s for all experiments, which were stopped when the cumulative volume reached ~400 mL. The system (with the fouled membrane) was then flushed with DI for 15 min at a crossflow velocity of 21.4 cm/s, after which the flux recovery was measured.

Chapter 7: Regenerable Forward Osmosis Membranes

7.1 Abstract

Membrane regeneration presents as a promising alternative to frequent membrane cleaning and replacement. Using the graphene oxide (GO) membranes based on the layer-by-layer (LbL) approach, this chapter demonstrates that the regeneration of the GO membrane can be easily accomplished by first soaking in a pH 13 solution and then repeating the LbL synthesis process. The regeneration procedures were capable of fully restoring the performance of the GO membrane. Upon close examining the membrane deconstruction mechanisms, it was found that the GO multilayers assembled along with a cationic polyelectrolyte (poly(allylamine hydrochloride), PAH) were exceptionally stable, likely due to the ring-opening reaction of the epoxide groups on the GO sheets. The covalent bond may impart the GO membranes with resistance to various harsh conditions that would decompose multilayers of regular polyelectrolytes built using the LbL method. With the strong GO-PAH layers, the membrane deconstruction was ascribed to the diminished electrostatic interactions between the carboxylate groups on the substrate and the neutral amine groups of PAH, leading to the peeling off of blocks of GO-PAH layer composite. Finally, membrane regeneration will be performed on fouled membranes, illustrating its applicability in practice.

7.2 Introduction

Forward osmosis (FO) has proven to be a sustainable alternative to pressure-driven processes such as reverse osmosis (RO), nanofiltration (NF), ultrafiltration (UF), etc. [166]. Rather than using hydraulic pressure as the driving force, FO eliminates such a

necessity as it utilizes the natural osmotic pressure between draw and feed solutions. This feature leads to significant reductions in energy input, and enables potential reclamation of low quality heat [224]. In addition, the FO process also offers an array of other advantages, such as higher water recovery and lower brine discharge [225]. Yet as with the traditional pressure-driven membrane processes, FO also faces a major challenge—membrane fouling, albeit less severe due to the absence of hydraulic pressure [27, 221]. Extensive research efforts have been devoted to understanding the fouling mechanisms for FO processes recently, which suggest that fouling is dependent on a multitude of factors including membrane surface chemistry, the nature of foulants, solution chemistry, hydrodynamic conditions, and so forth. Such research point to the inevitability of fouling in FO and the development of anti-fouling strategies.

Surface modification of FO membranes may be the most widely employed approach to improve fouling resistance. The strategy aims at altering membrane surface properties, e.g., hydrophilicity, charge, cyto-toxicity, etc., in order to minimize the interactions between foulant molecules and membranes and thus membrane fouling. For example, poly(dopamine) coating has been frequently adopted to enhance surface hydrophilicity [226, 227], which decreases membrane fouling propensity thanks to the hydration layer formed consequently [228-230]. In the same token, poly(ethylene glycol) (PEG) has also been grafted to membrane surface to control membrane fouling [231-233]. In addition to polymers, nanoparticles are promising as well in tuning membrane hydrophilicity to mitigate fouling [115, 230, 234-236]. Notably, Tiraferri *et al.* functionalized positively charged, super hydrophilic silica nanoparticles onto polyamide membrane surfaces that experienced significantly lower organic fouling level due to the

combined effect of higher hydrophilicity and shielding of fouling-prone carboxyl groups [230, 234]. Intrinsic anti-microbial properties of certain nanoparticles, such as silver and TiO_2, have also led to their role in preventing biofouling [115, 235]. One potential disadvantage of nanoparticle functionalization is the positive charge the nanoparticles may impart on membrane surfaces [230]. The positive charge promotes deposition of negatively charged foulants, counteracting the goal of such modification. The drawback can be addressed by introducing zwitterionic moieties to the membrane surface. Modification with zwitterionic polymers results in enhanced hydrophilicity, lowered surface roughness, shielded foulant-binding sites, and steric repulsion against foulants, all of which contribute to increased fouling resistance [237-239]. Despite the effectiveness, the aforementioned modification approaches seem to be cumbersome to implement in practice, particularly when dealing with delicate and complex procedures. Moreover, the modified membranes are likely to lose their functions after prolonged operation, at which point membrane cleaning and/or replacement is necessary. The overall consequence is increased operational costs.

The concept of regenerating membranes is thus conceived: after membrane performance severely deteriorates due to either fouling or frequent cleaning, the old selective layer is removed and a new selective layer is then re-constructed. For this idea to be feasible, it should be relatively easy to fabricate and remove the selective layer. The pursuit of such a "regenerable" membrane has been gaining momentum recently, especially with the surging layer-by-layer (LbL) technique. The LbL process involves only dipping of a substrate sequentially in solutions containing polyelectrolytes of opposite charges, which forms thin films via electrostatic and/or interactions [110]. This

simple yet facile method makes possible the formation and the decomposition of a selective layer that is suitable for membrane applications [116-118, 240].

Our previous studies report a new type of FO membranes based on graphene oxide (GO), a two dimensional carbon sheet decorated with oxygenated groups [61]. GO was used as an anionic polyelectrolyte, and the LbL method was used to assemble multilayer films. The GO membranes showed high performance and antifouling potential. Herein we demonstrate the regenerability of the GO membranes that, together with the above advantages, constitute one prototype of next generation membranes.

7.3 Materials and Methods

7.3.1 Preparation of membrane support and GO membrane

The details of membrane support and GO membrane synthesis have been delineated in Chapter 4. Briefly, a polyacrylonitrile (PAN) film was cast at 125 μm on a glass plate from a 18% *N,N*-dimethylformamide (DMF) solution. After phase separation in DI water for 10 min, the PAN membrane formed and stored in DI water before partial hydrolysis in 1.5 M NaOH for 1.5 h at 45 °C. Upon rinsing the hydrolyzed PAN (hPAN) thoroughly, the membrane support for making GO membranes was obtained.

The GO membrane was prepared via the LbL assembly by sequentially soaking the hPAN support in poly(allylamine hydrochloride) (PAH) solution (1 g/L, pH 4) and GO solution (1 g/L, pH 4) for 30 min each. The hPAN was rinsed thoroughly with DI before soaking in the next solution. Each cycle of the mentioned process added a double layer (DL) of PAH-GO on the hPAN support, and was repeated to a prescribed number

(e.g., 2 DLs and 5 DLs). Note that the soaking cycle always ended with GO solution unless stated otherwise.

7.3.2 Probing the stability of PAH/GO multilayers in QCM-D

Quartz crystal microbalance with dissipation (QCM-D) (E-4, Biolin Scientific, Linthicum Heights, MD) was used to monitor the process of assembling and decomposing GO–PAH multilayers. A gold crystal sensor was mounted into the QCM-D chamber, and was successively exposed to the PAH and GO solutions used above with DI rinsing. After reaching the prescribed number of DLs, the assembled PAH-GO multilayers were equilibrated in DI for several hours, as reflected in the stable frequency curve. The PAH-GO layers were then subjected to various conditions (e.g., pH 2-13, high ionic strength, etc.) to explore their stability. Decrease in frequency indicates the deposition/swelling of the multilayers, whereas increase the decomposition.

7.3.3 Membrane deconstruction and regeneration

Regeneration of the GO membrane consisted of two steps: the first was to remove the PAH-GO multilayers (i.e., membrane deconstruction) that served as the selective layer, and the second was to re-coat the PAH-GO selective layer (membrane regeneration) on the hPAN support. To decompose the PAH-GO multilayers, the GO membranes were soaked in 0.1 M NaOH solution (pH 13) with mild mixing induced by a stir bar. After thoroughly rinsing with DI, the treated GO membrane was tested in a FO system and a reverse osmosis (RO) system as per our previous studies (see Chapter 4 for details). The performance was compared to that before the alkaline treatment to assess the removal efficiency of the PAH-GO layers. Membrane regeneration was achieved by repeating the synthesis process where the treated GO membrane was alternately dipped into the PAH

and GO solutions. Again, the performance of the regenerated GO membrane was characterized in both the FO and RO system.

7.4 Results and Discussions

7.4.1 Stability of PAH-GO multilayers

As a screening tool, QCM-D was used to probe the stability of the PAH-GO multilayers in order to probe the possibility of the layer model. Figure 7.1(a) shows a typical 2DL assembly on an Au sensor in QCM-D. Similar results have been reported in our previous study [61]. The frequency decreased to ~-70 Hz for the two double layers of GO and PAH, implying the deposition of the films. The layers were then exposed to various harsh conditions with the purpose of removing the adsorbed layers.

Effect of pH. pH is known to impact the stability of multilayer films by altering charges of weak polyelectrolytes. Since the assembly of multilayers is driven by the pairing of charged/ionized polyelectrolytes, the degree of ionization directly affects the charge density of the polyelectrolytes and thus film properties. For weak polyelectrolytes, the ionization degree can be controlled by simply adjusting solution pH. Once the polyelectrolytes are neutralized in the film, the electrostatic interactions, that previously hold the multilayers together, may be too minute to keep the film intact. As a result, the multilayers collapse. For example, many have reported the decomposition of films containing poly(acrylic acid) (PAA) as the anionic polyelectrolyte in highly acidic solutions [175, 241]. This is because at pH conditions much lower than its pKa, the carboxylate groups protonate and thus the electrostatic interactions are interrupted, which leads to the disintegration of the film.

The pKa of PAH used in the study is ~ 9 [242], whereas GO has multiple pKa's at 4.3, 6.6, and 9 [243]. Hence we covered a wide pH range of 2-13 in assessing the stability of the PAH/GO layers in response to pH. As shown in Figure 7.1(b), except for at pH 13, other pH solutions had negligible effect on the film. This is indicative of the fact that GO may be considered a strong polyelectrolyte, along with our previous study that reported negative charge for GO in the pH range of 2 ~ 10 [61]. The abrupt frequency and dissipation changes imply that the pKa of PAH shifted from ~9 in solution to between 10 and 13 in the multilayer. Yet no mass loss was observed after pH 13 treatment, which was expected to neutralize PAH and weaken the electrostatic interactions between GO and PAH. The results demonstrate the pH resistance of the GO/PAH films in the range 2 to 13, and further suggest that there may exist stronger bonding between GO and PAH than ionic interactions previously reported. It points to the necessity of future research on the nature of the interactions when GO is employed as a polyelectrolyte.

Effect of ionic strength. Subsequently, the film was subjected to solutions of extremely high ionic strengths (up to 5 M NaCl). It is well established that immersion of polyelectrolyte multilayers in salt solutions can lead to swelling and subsequent dissolution of the multilayers upon high concentrations [244-246]. This occurs as excessive salt ions increase the mobility of the polyelectrolyte chains and weaken the interactions between the polyelectrolyte pairs[244]. Due to this property, solutions with high ionic strengths have been used to "etch" polyelectrolyte films. For example, Heuvingh *et al*. observed swelling and mass loss for films made of PAH and poly(styrenesulfonate) in NaCl solutions above 3 M [245].

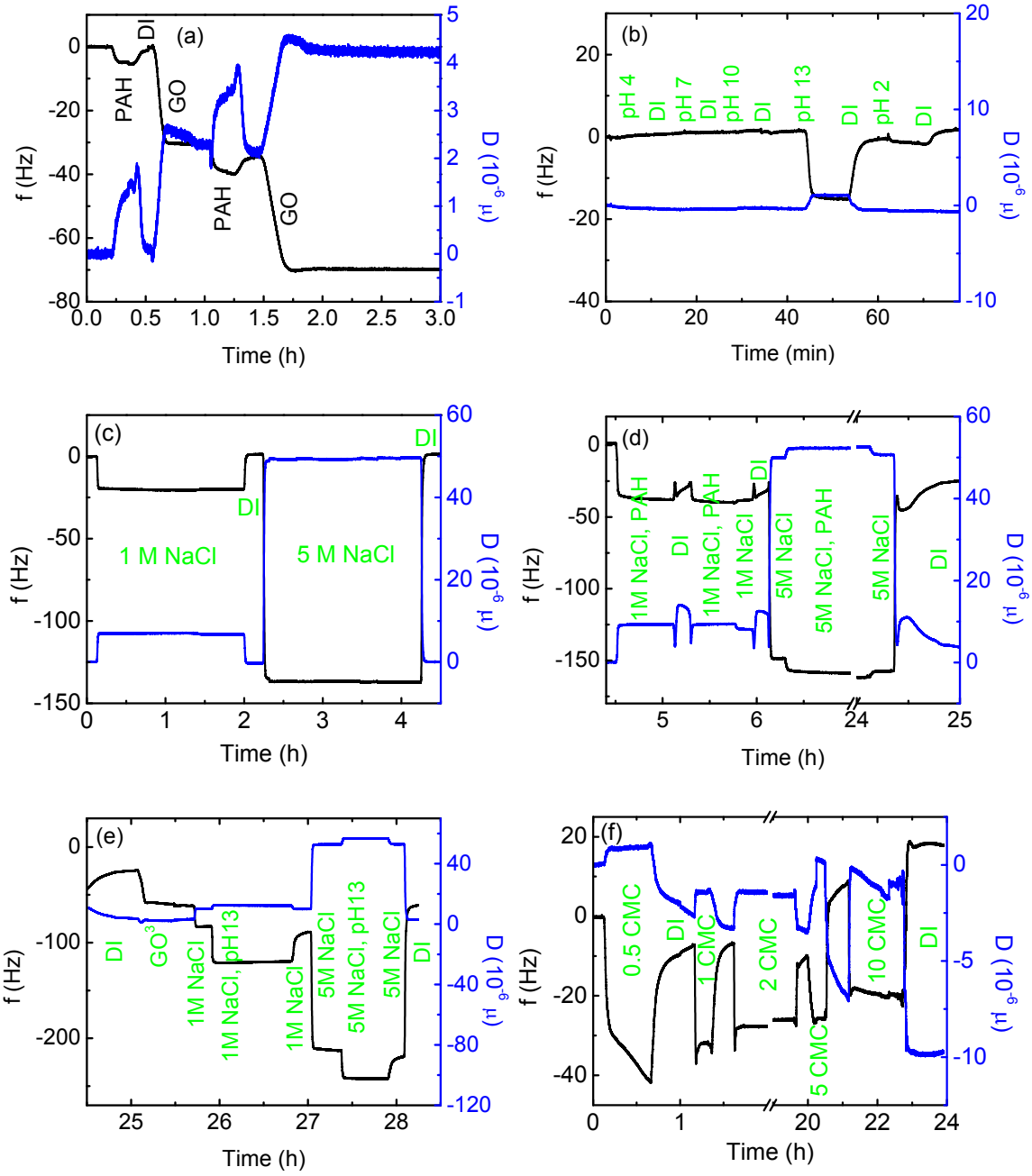

Figure 7.1 (a) 2DL of PAH and GO on a Au sensor, (b-e) treatment of the 2DL with pH, ionic strength, polyion (PAH)+salt, pH + ionic strength, and surfactant (SDS).

In our case, we used 1 M and 5 M NaCl solutions to "attack" the pre-formed PAH/GO layers. Significant swelling occurred when the films were in contact with the solutions, as indicated by the sharp frequency drops and dissipation spikes in Figure 7.1(c). Upon DI rinsing, however, the film returned to its original state with no mass loss (i.e., no frequency change) and no change in viscoelastic properties (i.e., no dissipation change). It was surprising to find out that the PAH/GO films could withstand such high ionic strengths, especially considering that charge of GO nanosheets were significantly screened at NaCl concentrations of even mM level [176]. It was due to this very reason that no salt was added to the GO solution during synthesis of the multilayers. As such, the charges of one component (PAH or GO) in the film were predominantly compensated intrinsically by the other (GO or PAH), rather than extrinsically by salts. The film prepared in such a fashion is susceptible to swelling and decomposition, when salt ions permeate into the film to expand and plasticize the multilayers [244]. While it is attempting to attribute the failure to remove the film to possibilities of either a higher concentration or a stronger salt plasticizer, our experience of testing the films with different solutions may disagree [61]. In an opposite perspective, the result reflects the stability of the GO membranes in solutions of high ionic strengths up to 5 M NaCl.

Effect of salt and polyion. Based on the discussion above, we come to the conclusion that using salt alone may not be enough to dissolve the GO films. We then turn our attention to free polyelectrolyte in the presence of salt. By adjusting the concentrations of salt and polyelectrolyte in the solutions, Kovacevic *et al*. turned regular growth of multilayers to an adsorption/dissolution process [247]. While salt ions still serve to plasticize and mobilize the films above a critical concentration, excessive free

polyelectrolytes then penetrate through the film and form soluble complexes with oppositely charged polyelectrolytes in the films [247]. Both of these factors contribute to the stripping of the multilayers [247, 248].

Figure 7.1(d) shows the impact of the combination of NaCl and PAH on the GO film. 1 g/L PAH in 1 M NaCl solution was first introduced onto the GO layer, and an irreversible frequency decrease was observed even after DI rinsing. As described previously, it was anticipated that PAH would not only bind to the top GO layer, but it would also stretch into the entire multilayer and form soluble complexes with GO with the presence of NaCl. Instead, PAH in the coming solution only adsorbed to the GO layer as a cationic polyelectrolyte via electrostatic interactions, since the overall frequency change was negative after DI rinsing. Note that the frequency decrease was markedly greater than the previous two PAH steps, because more PAH were adsorbed as the polymer chains adopted a more coiled structure under high ionic strength. The PAH solution with 1 M NaCl was applied again, yet no disintegration of the film occurred. Similar observations were made when the concentration of the NaCl solution increased to 5 M, with the difference of even more pronounced swelling. The frequency finally stabilized at the level after the adsorption of PAH in this series of experiment, which proved the ineffectiveness of this strategy in decomposing the multilayers.

Effect of extreme pH and high ionic strength. The synergistic effect of pH and ionic strength has been demonstrated on the stability of multilayer films [249]. As discussed above, pH modulates the ionization degree of polyelectrolytes, whereas salt ions mobilize the polymer segments and weaken the ionic association. Although each factor exerts different impact on the decomposition of multilayers, the synergistic effect

of both is the dissociation in the films. Indeed, such a combination has been used to remove fouled polyelectrolyte multilayers for a nanofiltration membrane [250].

We probed the combining effect after the free PAH solution in the presence of concentrated salts failed to dissemble the pre-formed layers, so an additional GO layer was deposited before treatment with pH 13 at high ionic strengths. As Figure 7.1(e) suggests, the film was not affected by the combination of high pH and ionic strength.

At this point, it is speculated that covalent bonding might have formed between PAH and GO, which results in the robustness of the GO membrane. We previously reported that epoxy functional groups exist on the basal plane of the GO nanosheets produced. The reactive epoxy groups are susceptible to nucleophilic attack by the amine groups from PAH, leading to the opening of the three-membered epoxide ring to relieve the ring strain [251]. The ring-opening reaction is accompanied by the nucleophilic substitution with an amine group on one C atom and the formation of a hydroxyl group on the other. In the perspective of membrane deconstruction and regeneration, the newly formed covalent bond (C—N) between PAH and GO is undesirable. Yet it enhances the stability of the GO-PAH layers, as evidenced by the full restoration after exposing to various harsh conditions (Figure 7.1). Different from the common amide bond seen in TFC membranes, the C—N bond may be immune to chlorine attack, which may improve the chlorine resistance of the GO membrane.

7.4.2 Membrane deconstruction and regeneration: experimental observations

Let us continue the discussion with the observation that the performance of the 2 DL GO membrane deteriorated significantly after soaking in 0.1 M NaOH solution (pH 13). The water flux for the as-prepared 2DL was 25.9 l/m^2-h (LMH) in FO mode and 25.0 LMH

PRO mode, tested under conditions delineated above. After immersing in the pH 13 solution with mild mixing for 1 hour, the water flux decreased to 15.6 LMH (FO) and 5.7 LMH (PRO), respectively (Figure 7.2). The decreases were accompanied with considerable increases of solute flux, indicating that the selective layer, the GO-PAH layers, was compromised—either being peeled off in a layer-by-layer fashion or being removed block by block (as will be proved by permeability tests in RO). The performance deterioration worsened after further soaking the treated membrane overnight. The water decreased to 6.2 (FO) and 11.6 (PRO) LMH, whereas the solute flux increased to 12.0 (FO) and 9.2 (PRO) mol/m^2-h (MMH). This rough trend suggests that the removal of the GO selective layer proceeded in a relatively slow manner (kinetics at the scale of hours).

The synthesis process was repeated on the treated membrane to regenerate another 2 bilayers of PAH and GO at this point. After testing with the same conditions, the regenerated membrane recovered its water flux and solute flux to the original levels (Figure 7.2). The high recovery implies that two bilayers of PAH and GO were successfully re-assembled on the treated GO membrane. Despite the favorable outcome for regeneration, the membrane "decomposition" mechanism is still at large. It is possible that, upon pH 13 treatment, (1) the interactions between the hPAN support and the GO-PAH layers weaken so that the selective layer comes off in blocks of GO-PAH (block model); or (2) the interactions between each GO and PAH layers weaken so that the selective layer comes off in single layers of GO or PAH gradually (layer model). As demonstrated previously, the GO-PAH layers were stable after the treatment at pH 13, and thus the layer model was ruled out. To confirm that the decomposition was due to the

complete removal of the GO-PAH layer as an entirety, further experiments were conducted and are discussed below.

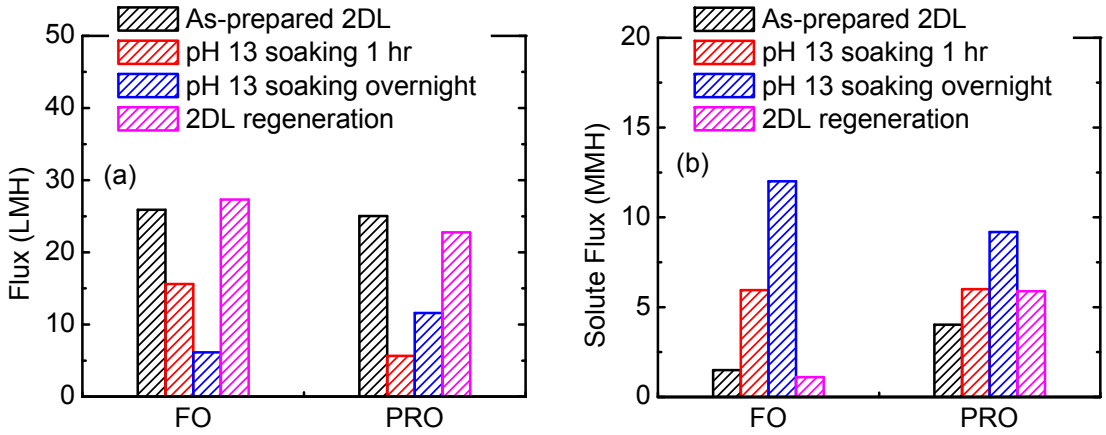

Figure 7.1 Membrane flux (a) and solute flux (b) of a 2 DL GO membrane in the sequence of after synthesis, after soaking in a pH 13 solution (0.1 M NaOH) for 1 hour and overnight (~15 hours), after repeating the synthesis process for the regeneration of 2 DLs of PAH and GO, respectively. The performance was measured in a FO system under both FO and PRO modes using 1 M $MgCl_2$ as the draw solution and DI as the feed solution.

Chapter 8: Conclusions and Future Work

8.1 Conclusions

This Ph.D. study focused on the application of graphene oxide (GO) to develop high performance membranes for water purification. The GO nanosheets contain an unoxidized graphene surface, which allows water to flow with no friction. Other properties of GO, such as hydrophilicity and functionality, are also intriguing particularly for membrane applications. The goal of the dissertation, therefore, was to translate the unique and promising characteristics of GO to next generation membranes for sustainable water purification.

Two layer-by-layer (LbL) approaches were introduced based on the properties of GO for the synthesis of the GO membranes. One method involves the chemical reactively of the functional groups of GO, which were cross-linked for the buildup of the GO layers. The other was based on the charge of the functional groups of GO, which enabled the deposition of GO layers via electrostatic interactions along with a partnering cationic polyelectrolyte. Both types of GO membranes were tested and compared against commercial membranes, and characterized with various techniques to understand the transport mechanisms. As an integral part of any membrane process, membrane fouling was investigated for the GO membranes in order to assess the possibility of using GO to control membrane fouling. Two model foulants, namely bovine serum albumin and alginate, were used in the fouling studies to unveil the fouling mechanisms for the GO membranes. Finally, a strategy was developed for the regeneration of the GO membranes upon severe fouling or dramatic performance loss.

Major findings from the dissertation are listed below:

(1) The characterizations herein confirm that GO is a single layer carbon lattice with various oxygenation functional groups. The GO used in this study was prepared using the modified Hummers' method, and the heights of GO nanosheets were in the range of 1–2 nm, indicating the GO nanosheets contained either single or double layers of carbon lattice. The XPS data show that about 60% of carbon was not oxidized, 32% had C–O bond (representing hydroxyl and epoxide groups), and 7% had COOH bond.

(2) Exploiting the reactivity of the functional groups, GO nanosheets were deposited alternately with the crosslinking by *1,3,5*-benzenetricarbonyl trichloride. These procedures led to a new type of nanofiltration (NF) membrane for using GO nanosheets such that water can flow through the nanochannels between GO layers while unwanted solutes are rejected by size exclusion and charge effects. As such, the GO membrane presented a high rejection (93–95%) of Rhodamine-WT (MW 567 Da), although it exhibited a relatively low rejection (6–46%) of monovalent and divalent salts and a moderate rejection (46–66%) of Methylene blue (MW 320 Da). More importantly, the GO membrane outperformed commercial NF membranes by a factor of 4—10 times.

(3) GO nanosheets become negatively charged upon ionization, which makes possible the layer-by-layer (LbL) assembly with a cationic polyelectrolyte. Thus, a GO-based forward osmosis (FO) was synthesized by the LbL assembly of GO and poly(allylamine hydrochloride) (PAH) as the partnering polyelectrolyte via electrostatic interactions. Quartz crystal microbalance-dissipation (QCM-D) results showed that each GO–PAH bilayer in the membrane is around 16.5 nm

thick and dominated by GO (mass of GO is 2–5 times higher than that of PAH), indicating multiple layers of GO nanosheets exist in each bilayer. Water permeability of the GO membrane was found to be about one order of magnitude higher than that of a commercial FO membrane. The solute flux of the GO membrane for sucrose (as a representative uncharged species) was much lower than that for an ionic species, most likely due to the swelling of the GO-PAH bilayers in ionic solutions. The GO membrane can be well suited for applications such as FO-based emergency water purification using sugary draw solutions and water treatment not requiring high ionic strength.

(4) By characterizing the transport rates of both water and solutes through the GO membrane assembled via electrostatic interactions, it was found that water traveled at a velocity of 4.8×10^{-4} m/s under a 1-atm transmembrane pressure, while solute diffusion was impeded by up to 5 orders of magnitude. The water transport speed was two orders of magnitude higher than the velocity (8.4×10^{-7} m/s) of water flowing between two hypothetical parallel plates, owing to the frictionless graphene surface on GO. It implies that the PAH molecules most likely to have connected GO on their edges, leaving the graphene surface largely uncovered. This edge-connection also created negative charge-dominant transport paths that imposed a hindering effect on solute transport.

(5) GO was employed to control fouling in pressure retarded osmosis (PRO) processes. By introducing an anti-fouling GO layer at the back the support layer, foulants were blocked on the surface and easily removed to restore membrane performance by physical cleaning. The experiments show that the control

membrane (without such a GO layer) saw flux decreases of ~30% after BSA fouling in PRO mode, whereas the GO membrane (with the GO layer) only reported negligible (less than 10%) flux reduction. With the worse alginate fouling, the flux dropped by ~50% for the control membrane in comparison to 0% (without Ca^{2+}) or 30% (with Ca^{2+}) for the GO membrane. Moreover, physical cleaning by increasing the cross-flow velocity almost fully restored the flux for the GO membrane in both fouling cases, yet had minimal impact on recovering the flux for the control membrane. Despite the higher affinity of the GO layer, the barrier strategy proved to be effective at controlling PRO fouling due to the relocation of foulants and diminished possibility of bridging between membranes and foulants.

(6) The regeneration of the GO membrane was accomplished by first soaking in a pH 13 solution and then repeating the LbL synthesis process. The regeneration procedures were capable of fully restoring the performance of the GO membrane. Upon close examining the membrane deconstruction mechanisms, it was found that the GO-PAH multilayers were exceptionally stable, likely due to the ring-opening reaction of the epoxide groups on the GO sheets. The covalent bond may impart the GO membranes with resistance to various harsh conditions that would decompose multilayers of regular polyelectrolytes built using the LbL method. With the strong GO-PAH layers, the membrane deconstruction was ascribed to the diminished electrostatic interactions between the carboxylate groups on the substrate and the neutral amine groups of PAH, leading to the peeling off of blocks of GO-PAH layer composite.

To summarize, the dissertation research provided first-ever experimental proof that GO can be used to develop high performance membranes for water purification. The LbL method may prove facile and sustainable for large-scale employment of the GO membranes. The high water flow velocity and hindered solute transport were found to be unique of GO due in large to the graphene surface, implying that highly tunable GO membranes could be designed by maintaining the graphene surface in the transport pathways while narrowing the inter-layer spacing. In addition, GO was successfully used to control fouling for PRO, thanks to its ability to block foulants from fouling the support interior and its diminished interactions with the foulants. Finally, the addition of membrane regeneration makes the GO membrane a prototype for the next generation membrane for water purification.

8.2 Future Work

While the study serves as a tip-of-the-iceberg effort in developing high performance GO membranes for water purification, much more work needs to be done to unleash the full potential of GO in this regard. Listed below are some follow-up research in the immediate future.

(1) Chlorine resistance of the GO membrane. As discussed in the dissertation, a ring-opening reaction may have occurred between PAH and the epoxide groups of GO during membrane synthesis, besides the electrostatic interactions between PAH and GO. The covalent C—N bond may be immune to chlorine attack, thus impart the GO membrane with chlorine resistance. This property is highly sought after, since traditional thin-film composite (e.g., polyamide) membranes are prone to

degradation by active chlorine species produced from agents used to deter and remove biofouling [10]. The task can be completed with a new support, such as sulfonated polysulfone, for the GO-PAH multilayers.

(2) Improving GO membrane performance by tuning inter-layer spacing. This can be achieved by using smaller partnering polyelectrolytes or crosslinkers to synthesize GO layers. For example, diamine may connect GO nanosheets based on the nucleophilic substitution reaction. Alternatively, GO nanosheets can be functionalized with positively charged functional groups (Figure 8.1(b)), e.g., with $–NH_2$ groups [104], before the LbL process of negatively and positively charged GO.

(3) Creating nanotube-like GO membranes. Based on the findings from Chapter 5, the existence of the graphene surface on GO not only exhibits ultrafast water flow but also impedes solute transport. Thus it is desirable to expose only the graphene surface for the flow pathways, creating nanotube-like GO membranes. Three strategies may be employed for this purpose. The most ambitious one is to vertically align GO nanosheets, the other two are to alter the shape of GO (e.g., from 2-D sheet to 3-D spheres [176] exposing the hydrophobic graphene surface) and to increase the porosity of GO sheets (e.g., by controlling oxidation degree during GO preparation) (Figure 8.1(c)). For the ultimate membrane performance, a continuous single-layer GO membrane may be obtained by Langmuir-Blodgett assembly [252] or interfacial reaction [253]. Note that Lockheed Martin Corporation has been investigating nanoporous graphene fabricated by chemical

vapor deposition for desalination. Yet it remains an obstacle to scale-up due to the restrictions of the synthesis method.

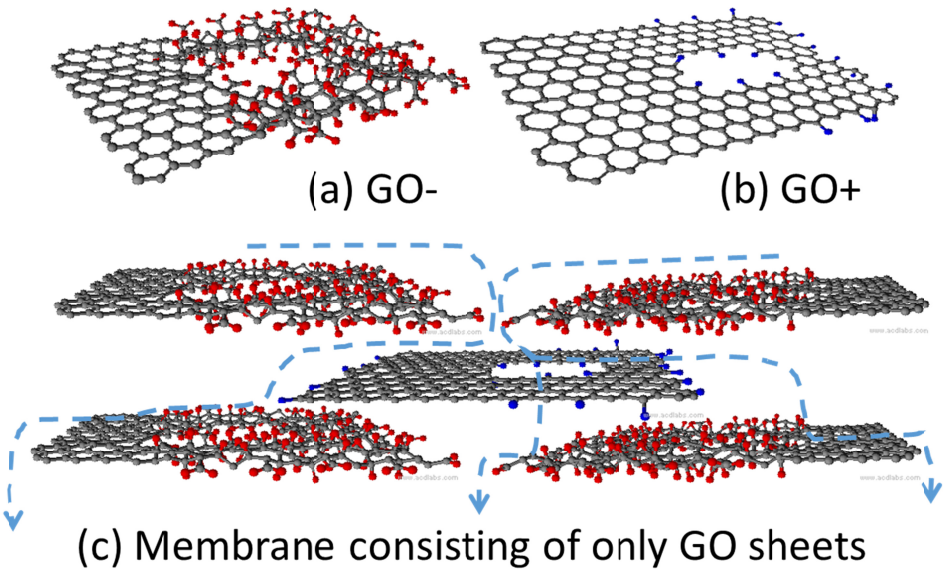

Figure 8.1 (a) Original GO sheet, (b) positively charged GO sheet via functionalization, and (c) GO membrane made of GO sheets only, the porosity of which can be manipulated, for example, by controlling oxidation degree during GO synthesis process.

(4) Adsorptive and catalytic GO membranes. Due to the unique properties of GO, GO membranes may be rendered highly adsorptive and catalytic for specific applications. For example, our lab has initiated research on the removal of emerging contaminants by adsorption onto the GO membranes. Moreover, it has been recently reported that suspended GO may undergo photodegradation and decompose in water [254]. It would be interesting to find out how the anchoring by PAH may affect the (in)stability of the GO membrane and impact its adsorptive and catalytic performance.

References

[1] Elimelech, M.; Phillip, W. A. The Future of Seawater Desalination: Energy, Technology, and the Environment. *Science* **2011,** *333* (6043), 712-717.

[2] Shannon, M. A.; Bohn, P. W.; Elimelech, M.; Georgiadis, J. G.; Marinas, B. J.; Mayes, A. M. Science and technology for water purification in the coming decades. *Nature* **2008,** *452* (7185), 301-310.

[3] Basile, T.; Petrella, A.; Petrella, M.; Boghetich, G.; Petruzzelli, V.; Colasuonno, S.; Petruzzelli, D. Review of Endocrine-Disrupting-Compound Removal Technologies in Water and Wastewater Treatment Plants: An EU Perspective. *Ind Eng Chem Res* **2011,** *50* (14), 8389-8401.

[4] Comerton, A. M.; Andrews, R. C.; Bagley, D. M.; Hao, C. Y. The rejection of endocrine disrupting and pharmaceutically active compounds by NF and RO membranes as a function of compound a water matrix properties. *Journal of Membrane Science* **2008,** *313* (1-2), 323-335.

[5] Kimura, K.; Toshima, S.; Amy, G.; Watanabe, Y. Rejection of neutral endocrine disrupting compounds (EDCs) and pharmaceutical active compounds (PhACs) by RO membranes. *Journal of Membrane Science* **2004,** *245* (1-2), 71-78.

[6] Larson, R. E.; Cadotte, J. E.; Petersen, R. J. The Ft-30 Sea-Water Reverse-Osmosis Membrane - Element Test-Results. *Desalination* **1981,** *38* (1-3), 473-483.

[7] Petersen, R. J. Composite reverse osmosis and nanofiltration membranes. *Journal of Membrane Science* **1993,** *83* (1), 81-150.

[8] Yip, N. Y.; Tiraferri, A.; Phillip, W. A.; Schiffman, J. D.; Elimelech, M. High Performance Thin-Film Composite Forward Osmosis Membrane. *Environmental science & technology* **2010,** *44* (10), 3812-3818.

[9] Gu, J. E.; Jun, B. M.; Kwon, Y. N. Effect of chlorination condition and permeability of chlorine species on the chlorination of a polyamide membrane. *Water research* **2012,** *46* (16), 5389-5400.

[10] Shin, D. H.; Kim, N.; Lee, Y. T. Modification to the polyamide TFC RO membranes for improvement of chlorine-resistance. *Journal of Membrane Science* **2011,** *376* (1-2), 302-311.

[11] Mi, B. X.; Elimelech, M. Gypsum Scaling and Cleaning in Forward Osmosis: Measurements and Mechanisms. *Environmental science & technology* **2010,** *44* (6), 2022-2028.

[12] Mi, B. X.; Elimelech, M. Organic fouling of forward osmosis membranes: Fouling reversibility and cleaning without chemical reagents. *Journal of Membrane Science* **2010,** *348* (1-2), 337-345.

[13] Shaffer, D. L.; Yip, N. Y.; Gilron, J.; Elimelech, M. Seawater desalination for agriculture by integrated forward and reverse osmosis: Improved product water quality for potentially less energy. *Journal of Membrane Science* **2012,** *415*, 1-8.

[14] Liu, C.; Rainwater, K.; Song, L. F. Energy analysis and efficiency assessment of reverse osmosis desalination process. *Desalination* **2011,** *276* (1-3), 352-358.

[15] McCutcheon, J. R.; Elimelech, M. Modeling water flux in forward osmosis: Implications for improved membrane design. *AIChE Journal* **2007,** *53* (7), 1736-1744.

[16] Dikin, D. A.; Stankovich, S.; Zimney, E. J.; Piner, R. D.; Dommett, G. H. B.; Evmenenko, G.; Nguyen, S. T.; Ruoff, R. S. Preparation and characterization of graphene oxide paper. *Nature* **2007,** *448* (7152), 457-460.

[17] Dreyer, D. R.; Park, S.; Bielawski, C. W.; Ruoff, R. S. The chemistry of graphene oxide. *Chem Soc Rev* **2010,** *39* (1), 228-240.

[18] Suk, M. E.; Aluru, N. R. Water Transport through Ultrathin Graphene. *J Phys Chem Lett* **2010,** *1* (10), 1590-1594.

[19] Cohen-Tanugi, D.; Grossman, J. C. Water Desalination across Nanoporous Graphene. *Nano letters* **2012**.

[20] Koenig, S. P.; Wang, L. D.; Pellegrino, J.; Bunch, J. S. Selective molecular sieving through porous graphene. *Nature nanotechnology* **2012,** *7* (11), 728-732.

[21] Zhu, A. Z.; Christofides, P. D.; Cohen, Y. Effect of Thermodynamic Restriction on Energy Cost Optimization of RO Membrane Water Desalination. *Ind Eng Chem Res* **2009,** *48* (13), 6010-6021.

[22] Li, M. H. Minimization of Energy in Reverse Osmosis Water Desalination Using Constrained Nonlinear Optimization. *Ind Eng Chem Res* **2010,** *49* (4), 1822-1831.

[23] Wilf, M. Design consequences of recent improvements in membrane performance. *Desalination* **1997,** *113* (2-3), 157-163.

[24] Nemeth, J. E. Innovative system designs to optimize performance of ultra-low pressure reverse osmosis membranes. *Desalination* **1998,** *118* (1-3), 63-71.

[25] Fethi, K. Optimization of energy consumption in the 3300 m(3)/d RO Kerkennah plant. *Desalination* **2003,** *157* (1-3), 145-149.

[26] Mi, B. X.; Elimelech, M. Gypsum Scaling and Cleaning in Forward Osmosis: Measurements and Mechanisms. *Environmental Science & Technology* **2010,** *44* (6), 2022-2028.

[27] Mi, B.; Elimelech, M. Organic fouling of forward osmosis membranes: Fouling reversibility and cleaning without chemical reagents. *Journal of Membrane Science* **2010,** *348* (1–2), 337-345.

[28] Liu, Y. L.; Mi, B. X. Combined fouling of forward osmosis membranes: Synergistic foulant interaction and direct observation of fouling layer formation. *Journal of Membrane Science* **2012,** *407*, 136-144.

[29] Mi, B. X.; Elimelech, M. Silica scaling and scaling reversibility in forward osmosis. *Desalination* **2013,** *312*, 75-81.

[30] Wang, L.; Wang, X. D.; Fukushi, K. I. Effects of operational conditions on ultrafiltration membrane fouling. *Desalination* **2008,** *229* (1-3), 181-191.

[31] Lee, E. K.; Chen, V.; Fane, A. G. Natural organic matter (NOM) fouling in low pressure membrane filtration - effect of membranes and operation modes. *Desalination* **2008,** *218* (1-3), 257-270.

[32] Gu, J. E.; Jun, B. M.; Kwon, Y. N. Effect of chlorination condition and permeability of chlorine species on the chlorination of a polyamide membrane. *Water Research* **2012,** *46* (16), 5389-5400.

[33] Do, V. T.; Tang, C. Y. Y.; Reinhard, M.; Leckie, J. O. Degradation of Polyamide Nanofiltration and Reverse Osmosis Membranes by Hypochlorite. *Environmental Science & Technology* **2012,** *46* (2), 852-859.

[34] Kearney, L. T.; Howarter, J. A. QCM-Based Measurement of Chlorine-Induced Polymer Degradation Kinetics. *Langmuir* **2014,** *30* (29), 8923-8930.

[35] Powell, J.; Luh, J.; Coronell, O. Bulk Chlorine Uptake by Polyamide Active Layers of Thin-Film Composite Membranes upon Exposure to Free Chlorine-Kinetics, Mechanisms, and Modeling. *Environmental Science & Technology* **2014,** *48* (5), 2741-2749.

[36] Novoselov, K. S.; Geim, A. K.; Morozov, S. V.; Jiang, D.; Zhang, Y.; Dubonos, S. V.; Grigorieva, I. V.; Firsov, A. A. Electric field effect in atomically thin carbon films. *Science* **2004,** *306* (5696), 666-669.

[37] Brodie, B. Sur le poids atomique du graphite. *Ann. Chim. Phys* **1860,** *59* (466), e472.

[38] Park, S.; Ruoff, R. S. Chemical methods for the production of graphenes. *Nature nanotechnology* **2009,** *4* (4), 217-224.

[39] Eda, G.; Chhowalla, M. Chemically Derived Graphene Oxide: Towards Large-Area Thin-Film Electronics and Optoelectronics. *Advanced Materials* **2010,** *22* (22), 2392-2415.

[40] Chabot, V.; Higgins, D.; Yu, A. P.; Xiao, X. C.; Chen, Z. W.; Zhang, J. J. A review of graphene and graphene oxide sponge: material synthesis and applications to energy and the environment. *Energ Environ Sci* **2014,** *7* (5), 1564-1596.

[41] Robinson, J. T.; Perkins, F. K.; Snow, E. S.; Wei, Z. Q.; Sheehan, P. E. Reduced Graphene Oxide Molecular Sensors. *Nano letters* **2008,** *8* (10), 3137-3140.

[42] Loh, K. P.; Bao, Q. L.; Eda, G.; Chhowalla, M. Graphene oxide as a chemically tunable platform for optical applications. *Nat Chem* **2010,** *2* (12), 1015-1024.

[43] Kemp, K. C.; Seema, H.; Saleh, M.; Le, N. H.; Mahesh, K.; Chandra, V.; Kim, K. S. Environmental applications using graphene composites: water remediation and gas adsorption. *Nanoscale* **2013,** *5* (8), 3149-3171.

[44] Nair, R. R.; Wu, H. A.; Jayaram, P. N.; Grigorieva, I. V.; Geim, A. K. Unimpeded Permeation of Water Through Helium-Leak–Tight Graphene-Based Membranes. *Science* **2012,** *335* (6067), 442-444.

[45] Hu, M.; Mi, B. Enabling Graphene Oxide Nanosheets as Water Separation Membranes. *Environmental science & technology* **2013,** *47* (8), 3715-3723.

[46] Staudenmaier, L. Verfahren zur Darstellung der Graphitsäure. *Berichte der deutschen chemischen Gesellschaft* **1898,** *31* (2), 1481-1487.

[47] Hummers, W. S.; Offeman, R. E. Preparation of Graphitic Oxide. *J. Am. Chem. Soc.* **1958,** *80*, 1339–1339.

[48] Marcano, D. C.; Kosynkin, D. V.; Berlin, J. M.; Sinitskii, A.; Sun, Z.; Slesarev, A.; Alemany, L. B.; Lu, W.; Tour, J. M. Improved Synthesis of Graphene Oxide. *ACS Nano* **2010,** *4* (8), 4806-4814.

[49] Boehm, H. P.; Eckel, M.; Scholz, W. Untersuchungen am Graphitoxid V. Über den Bildungsmechanismus des Graphitoxids. *Zeitschrift für anorganische und allgemeine Chemie* **1967,** *353* (5-6), 236-242.

[50] Luo, Z. T.; Lu, Y.; Somers, L. A.; Johnson, A. T. C. High Yield Preparation of Macroscopic Graphene Oxide Membranes. *Journal of the American Chemical Society* **2009,** *131* (3), 898-+.

[51] Hofmann, U.; Holst, R. Über die Säurenatur und die Methylierung von Graphitoxyd. *Berichte der deutschen chemischen Gesellschaft (A and B Series)* **1939,** *72* (4), 754-771.

[52] Lerf, A.; He, H. Y.; Forster, M.; Klinowski, J. Structure of graphite oxide revisited. *J Phys Chem B* **1998,** *102* (23), 4477-4482.

[53] Meyer, J. C.; Kisielowski, C.; Erni, R.; Rossell, M. D.; Crommie, M. F.; Zettl, A. Direct Imaging of Lattice Atoms and Topological Defects in Graphene Membranes. *Nano Letters* **2008,** *8* (11), 3582-3586.

[54] Wilson, N. R.; Pandey, P. A.; Beanland, R.; Young, R. J.; Kinloch, I. A.; Gong, L.; Liu, Z.; Suenaga, K.; Rourke, J. P.; York, S. J.; Sloan, J. Graphene Oxide: Structural Analysis and Application as a Highly Transparent Support for Electron Microscopy. *ACS Nano* **2009,** *3* (9), 2547-2556.

[55] Gomez-Navarro, C.; Meyer, J. C.; Sundaram, R. S.; Chuvilin, A.; Kurasch, S.; Burghard, M.; Kern, K.; Kaiser, U. Atomic Structure of Reduced Graphene Oxide. *Nano Letters* **2010,** *10* (4), 1144-1148.

[56] Erickson, K.; Erni, R.; Lee, Z.; Alem, N.; Gannett, W.; Zettl, A. Determination of the Local Chemical Structure of Graphene Oxide and Reduced Graphene Oxide. *Advanced Materials* **2010,** *22* (40), 4467-4472.

[57] Pacile, D.; Meyer, J. C.; Rodriguez, A. F.; Papagno, M.; Gomez-Navarro, C.; Sundaram, R. S.; Burghard, M.; Kern, K.; Carbone, C.; Kaiser, U. Electronic properties and atomic structure of graphene oxide membranes. *Carbon* **2011,** *49* (3), 966-972.

[58] Majumder, M.; Chopra, N.; Andrews, R.; Hinds, B. J. Nanoscale hydrodynamics - Enhanced flow in carbon nanotubes. *Nature* **2005,** *438* (7064), 44-44.

[59] Wei, N.; Peng, X. S.; Xu, Z. P. Breakdown of fast water transport in graphene oxides. *Phys Rev E* **2014,** *89* (1).

[60] Wei, N.; Peng, X. S.; Xu, Z. P. Understanding Water Permeation in Graphene Oxide Membranes. *Acs Appl Mater Inter* **2014,** *6* (8), 5877-5883.

[61] Hu, M.; Mi, B. Layer-by-layer assembly of graphene oxide membranes via electrostatic interaction. *Journal of Membrane Science* **2014,** *469* (0), 80-87.

[62] Roh, I. J.; Kim, J. J.; Park, S. Y. Mechanical properties and reverse osmosis performance of interfacially polymerized polyamide thin films. *Journal of Membrane Science* **2002,** *197* (1-2), 199-210.

[63] Chung, J. Y.; Lee, J. H.; Beers, K. L.; Stafford, C. M. Stiffness, Strength, and Ductility of Nanoscale Thin Films and Membranes: A Combined Wrinkling-Cracking Methodology. *Nano Letters* **2011,** *11* (8), 3361-3365.

[64] Lee, C.; Wei, X. D.; Kysar, J. W.; Hone, J. Measurement of the elastic properties and intrinsic strength of monolayer graphene. *Science* **2008,** *321* (5887), 385-388.

[65] Gomez-Navarro, C.; Burghard, M.; Kern, K. Elastic properties of chemically derived single graphene sheets. *Nano Letters* **2008,** *8* (7), 2045-2049.

[66] Paci, J. T.; Belytschko, T.; Schatz, G. C. Computational studies of the structure, behavior upon heating, and mechanical properties of graphite oxide. *J Phys Chem C* **2007,** *111* (49), 18099-18111.

[67] Suk, J. W.; Piner, R. D.; An, J.; Ruoff, R. S. Mechanical Properties of Monolayer Graphene Oxide. *ACS Nano* **2010,** *4* (11), 6557-6564.

[68] Cohen-Tanugi, D.; Grossman, J. C. Mechanical Strength of Nanoporous Graphene as a Desalination Membrane. *Nano Letters* **2014,** *14* (11), 6171-6178.

[69] Hu, W. B.; Peng, C.; Luo, W. J.; Lv, M.; Li, X. M.; Li, D.; Huang, Q.; Fan, C. H. Graphene-Based Antibacterial Paper. *ACS Nano* **2010,** *4* (7), 4317-4323.

[70] Akhavan, O.; Ghaderi, E. Toxicity of Graphene and Graphene Oxide Nanowalls Against Bacteria. *ACS Nano* **2010,** *4* (10), 5731-5736.

[71] Liu, S. B.; Zeng, T. H.; Hofmann, M.; Burcombe, E.; Wei, J.; Jiang, R. R.; Kong, J.; Chen, Y. Antibacterial Activity of Graphite, Graphite Oxide, Graphene Oxide, and Reduced Graphene Oxide: Membrane and Oxidative Stress. *ACS Nano* **2011,** *5* (9), 6971-6980.

[72] Kang, S.; Pinault, M.; Pfefferle, L. D.; Elimelech, M. Single-walled carbon nanotubes exhibit strong antimicrobial activity. *Langmuir* **2007,** *23* (17), 8670-8673.

[73] Vecitis, C. D.; Zodrow, K. R.; Kang, S.; Elimelech, M. Electronic-Structure-Dependent Bacterial Cytotoxicity of Single-Walled Carbon Nanotubes. *ACS Nano* **2010,** *4* (9), 5471-5479.

[74] Tu, Y. S.; Lv, M.; Xiu, P.; Huynh, T.; Zhang, M.; Castelli, M.; Liu, Z. R.; Huang, Q.; Fan, C. H.; Fang, H. P.; Zhou, R. H. Destructive extraction of phospholipids from Escherichia coli membranes by graphene nanosheets. *Nature nanotechnology* **2013,** *8* (8), 594-601.

[75] Li, Y. F.; Yuan, H. Y.; von dem Bussche, A.; Creighton, M.; Hurt, R. H.; Kane, A. B.; Gao, H. J. Graphene microsheets enter cells through spontaneous membrane penetration at edge asperities and corner sites. *P Natl Acad Sci USA* **2013,** *110* (30), 12295-12300.

[76] Romero-Vargas Castrillón, S.; Perreault, F.; de Faria, A. F.; Elimelech, M. Interaction of Graphene Oxide with Bacterial Cell Membranes: Insights from Force Spectroscopy. *Environ Sci Tech Let* **2015,** *2* (4), 112-117.

[77] Jiang, D. E.; Cooper, V. R.; Dai, S. Porous Graphene as the Ultimate Membrane for Gas Separation. *Nano Letters* **2009,** *9* (12), 4019-4024.

[78] Suk, M. E.; Aluru, N. R. Water Transport through Ultrathin Graphene. *The Journal of Physical Chemistry Letters* **2010,** *1* (10), 1590-1594.

[79] Cohen-Tanugi, D.; Grossman, J. C. Water Desalination across Nanoporous Graphene. *Nano Letters* **2012,** *12* (7), 3602-3608.

[80] Cohen-Tanugi, D.; McGovern, R. K.; Dave, S. H.; Lienhard, J. H.; Grossman, J. C. Quantifying the potential of ultra-permeable membranes for water desalination. *Energ Environ Sci* **2014,** *7* (3), 1134-1141.

[81] Bunch, J. S.; Verbridge, S. S.; Alden, J. S.; van der Zande, A. M.; Parpia, J. M.; Craighead, H. G.; McEuen, P. L. Impermeable atomic membranes from graphene sheets. *Nano Letters* **2008,** *8* (8), 2458-2462.

[82] Suk, M. E.; Aluru, N. R. Molecular and continuum hydrodynamics in graphene nanopores. *Rsc Adv* **2013,** *3* (24), 9365-9372.

[83] Zhu, C. Q.; Li, H.; Meng, S. Transport behavior of water molecules through two-dimensional nanopores. *J Chem Phys* **2014,** *141* (18).

[84] Sint, K.; Wang, B.; Kral, P. Selective Ion Passage through Functionalized Graphene Nanopores. *Journal of the American Chemical Society* **2008,** *130* (49), 16448-+.

[85] Konatham, D.; Yu, J.; Ho, T. A.; Striolo, A. Simulation Insights for Graphene-Based Water Desalination Membranes. *Langmuir* **2013,** *29* (38), 11884-11897.

[86] Boukhvalov, D. W.; Katsnelson, M. I.; Son, Y. W. Origin of Anomalous Water Permeation through Graphene Oxide Membrane. *Nano Letters* **2013,** *13* (8), 3930-3935.

[87] Shan, Y. P.; Tiwari, P. B.; Krishnakumar, P.; Vlassiouk, I.; Li, W. Z.; Wang, X. W.; Darici, Y.; Lindsay, S. M.; Wang, H. D.; Smirnov, S.; He, J. Surface modification of graphene nanopores for protein translocation. *Nanotechnology* **2013,** *24* (49).

[88] O'Hern, S. C.; Boutilier, M. S. H.; Idrobo, J. C.; Song, Y.; Kong, J.; Laoui, T.; Atieh, M.; Karnik, R. Selective Ionic Transport through Tunable Subnanometer Pores in Single-Layer Graphene Membranes. *Nano Letters* **2014,** *14* (3), 1234-1241.

[89] O'Hern, S. C.; Stewart, C. A.; Boutilier, M. S. H.; Idrobo, J. C.; Bhaviripudi, S.; Das, S. K.; Kong, J.; Laoui, T.; Atieh, M.; Karnik, R. Selective Molecular Transport through Intrinsic Defects in a Single Layer of CVD Graphene. *ACS Nano* **2012,** *6* (11), 10130-10138.

[90] Celebi, K.; Buchheim, J.; Wyss, R. M.; Droudian, A.; Gasser, P.; Shorubalko, I.; Kye, J. I.; Lee, C.; Park, H. G. Ultimate Permeation Across Atomically Thin Porous Graphene. *Science* **2014,** *344* (6181), 289-292.

[91] Surwade, S. P.; Smirnov, S. N.; Vlassiouk, I. V.; Unocic, R. R.; Veith, G. M.; Dai, S.; Mahurin, S. M. Water desalination using nanoporous single-layer graphene. *Nat Nano* **2015,** *advance online publication*.

[92] Joshi, R. K.; Carbone, P.; Wang, F. C.; Kravets, V. G.; Su, Y.; Grigorieva, I. V.; Wu, H. A.; Geim, A. K.; Nair, R. R. Precise and Ultrafast Molecular Sieving Through Graphene Oxide Membranes. *Science* **2014,** *343* (6172), 752-754.

[93] Han, Y.; Xu, Z.; Gao, C. Ultrathin Graphene Nanofiltration Membrane for Water Purification. *Advanced Functional Materials* **2013,** *23* (29), 3693-3700.

[94] Qiu, L.; Zhang, X.; Yang, W.; Wang, Y.; Simon, G. P.; Li, D. Controllable corrugation of chemically converted graphene sheets in water and potential application for nanofiltration. *Chemical Communications* **2011,** *47* (20), 5810-5812.

[95] Stankovich, S.; Dikin, D. A.; Compton, O. C.; Dommett, G. H. B.; Ruoff, R. S.; Nguyen, S. T. Systematic Post-assembly Modification of Graphene Oxide Paper with Primary Alkylamines. *Chemistry of Materials* **2010,** *22* (14), 4153-4157.

[96] Huang, H. B.; Song, Z. G.; Wei, N.; Shi, L.; Mao, Y. Y.; Ying, Y. L.; Sun, L. W.; Xu, Z. P.; Peng, X. S. Ultrafast viscous water flow through nanostrand-channelled graphene oxide membranes. *Nat Commun* **2013,** *4*.

[97] Han, Y.; Jiang, Y.; Gao, C. High-Flux Graphene Oxide Nanofiltration Membrane Intercalated by Carbon Nanotubes. *Acs Appl Mater Inter* **2015,** *7* (15), 8147-8155.

[98] Burress, J. W.; Gadipelli, S.; Ford, J.; Simmons, J. M.; Zhou, W.; Yildirim, T. Graphene Oxide Framework Materials: Theoretical Predictions and Experimental Results. *Angew Chem Int Edit* **2010,** *49* (47), 8902-8904.

[99] Zhu, J. M.; Zhu, L. W.; Lu, Z. F.; Gu, L.; Cao, S. L.; Cao, X. B. Selectively Expanding Graphene Oxide Paper for Creating Multifunctional Carbon Materials. *J Phys Chem C* **2012,** *116* (43), 23075-23082.

[100] Hung, W. S.; Tsou, C. H.; De Guzman, M.; An, Q. F.; Liu, Y. L.; Zhang, Y. M.; Hu, C. C.; Lee, K. R.; Lai, J. Y. Cross-Linking with Diamine Monomers To Prepare Composite Graphene Oxide-Framework Membranes with Varying d-Spacing. *Chemistry of Materials* **2014,** *26* (9), 2983-2990.

[101] Goh, K.; Setiawan, L.; Wei, L.; Si, R.; Fane, A. G.; Wang, R.; Chen, Y. Graphene oxide as effective selective barriers on a hollow fiber membrane for water treatment process. *Journal of Membrane Science* **2015,** *474* (0), 244-253.

[102] Ganesh, B. M.; Isloor, A. M.; Ismail, A. F. Enhanced hydrophilicity and salt rejection study of graphene oxide-polysulfone mixed matrix membrane. *Desalination* **2013,** *313*, 199-207.

[103] Zhao, H. Y.; Wu, L. G.; Zhou, Z. J.; Zhang, L.; Chen, H. L. Improving the antifouling property of polysulfone ultrafiltration membrane by incorporation of isocyanate-treated graphene oxide. *Phys Chem Chem Phys* **2013,** *15* (23), 9084-9092.

[104] Choi, W.; Choi, J.; Bang, J.; Lee, J. H. Layer-by-Layer Assembly of Graphene Oxide Nanosheets on Polyamide Membranes for Durable Reverse-Osmosis Applications. *Acs Appl Mater Inter* **2013,** *5* (23), 12510-12519.

[105] Perreault, F.; Tousley, M. E.; Elimelech, M. Thin-Film Composite Polyamide Membranes Functionalized with Biocidal Graphene Oxide Nanosheets. *Environ Sci Tech Let* **2014,** *1* (1), 71-76.

[106] Bano, S.; Mahmood, A.; Kim, S. J.; Lee, K. H. Graphene oxide modified polyamide nanofiltration membrane with improved flux and antifouling properties. *J Mater Chem A* **2015,** *3* (5), 2065-2071.

[107] He, L.; Dumée, L. F.; Feng, C.; Velleman, L.; Reis, R.; She, F.; Gao, W.; Kong, L. Promoted water transport across graphene oxide–poly(amide) thin film composite membranes and their antibacterial activity. *Desalination* **2015,** *365* (0), 126-135.

[108] Zhang, Z. B.; Wu, J. J.; Su, Y.; Zhou, J.; Gao, Y.; Yu, H. Y.; Gu, J. S. Layer-by-layer assembly of graphene oxide on polypropylene macroporous membranes via click

chemistry to improve antibacterial and antifouling performance. *Appl Surf Sci* **2015,** *332*, 300-307.

[109] Hegab, H. M.; Wimalasiri, Y.; Ginic-Markovic, M.; Zou, L. Improving the fouling resistance of brackish water membranes via surface modification with graphene oxide functionalized chitosan. *Desalination* **2015,** *365* (0), 99-107.

[110] Decher, G. Fuzzy Nanoassemblies: Toward Layered Polymeric Multicomposites. *Science* **1997,** *277* (5330), 1232-1237.

[111] Krasemann, L.; Tieke, B. Ultrathin self-assembled polyelectrolyte membranes for pervaporation. *Journal of Membrane Science* **1998,** *150* (1), 23-30.

[112] Krasemann, L.; Toutianoush, A.; Tieke, B. Self-assembled polyelectrolyte multilayer membranes with highly improved pervaporation separation of ethanol/water mixtures. *Journal of Membrane Science* **2001,** *181* (2), 221-228.

[113] Zhang, G.; Yan, H.; Ji, S.; Liu, Z. Self-assembly of polyelectrolyte multilayer pervaporation membranes by a dynamic layer-by-layer technique on a hydrolyzed polyacrylonitrile ultrafiltration membrane. *Journal of Membrane Science* **2007,** *292* (1–2), 1-8.

[114] Jin, W.; Toutianoush, A.; Tieke, B. Use of Polyelectrolyte Layer-by-Layer Assemblies as Nanofiltration and Reverse Osmosis Membranes. *Langmuir* **2003,** *19* (7), 2550-2553.

[115] Liu, X.; Qi, S.; Li, Y.; Yang, L.; Cao, B.; Tang, C. Y. Synthesis and characterization of novel antibacterial silver nanocomposite nanofiltration and forward osmosis membranes based on layer-by-layer assembly. *Water Research* **2013,** *47* (9), 3081-3092.

[116] Malaisamy, R.; Bruening, M. L. High-Flux Nanofiltration Membranes Prepared by Adsorption of Multilayer Polyelectrolyte Membranes on Polymeric Supports. *Langmuir* **2005,** *21* (23), 10587-10592.

[117] Ouyang, L.; Malaisamy, R.; Bruening, M. L. Multilayer polyelectrolyte films as nanofiltration membranes for separating monovalent and divalent cations. *Journal of Membrane Science* **2008,** *310* (1–2), 76-84.

[118] Stanton, B. W.; Harris, J. J.; Miller, M. D.; Bruening, M. L. Ultrathin, Multilayered Polyelectrolyte Films as Nanofiltration Membranes. *Langmuir* **2003,** *19* (17), 7038-7042.

[119] Zhou, Y.; Yu, S.; Gao, C.; Feng, X. Surface modification of thin film composite polyamide membranes by electrostatic self deposition of polycations for improved fouling resistance. *Separation and Purification Technology* **2009,** *66* (2), 287-294.

[120] Qiu, C.; Qi, S.; Tang, C. Y. Synthesis of high flux forward osmosis membranes by chemically crosslinked layer-by-layer polyelectrolytes. *Journal of Membrane Science* **2011,** *381* (1–2), 74-80.

[121] Qiu, C.; Setiawan, L.; Wang, R.; Tang, C. Y.; Fane, A. G. High performance flat sheet forward osmosis membrane with an NF-like selective layer on a woven fabric embedded substrate. *Desalination* **2012,** *287*, 266-270.

[122] Saren, Q.; Qiu, C. Q.; Tang, C. Y. Synthesis and Characterization of Novel Forward Osmosis Membranes based on Layer-by-Layer Assembly. *Environmental Science & Technology* **2011,** *45* (12), 5201-5208.

[123] Hammond, P. T. Recent explorations in electrostatic multilayer thin film assembly. *Current Opinion in Colloid & Interface Science* **1999,** *4* (6), 430-442.

[124] Li, D.; Mueller, M. B.; Gilje, S.; Kaner, R. B.; Wallace, G. G. Processable aqueous dispersions of graphene nanosheets. *Nature nanotechnology* **2008,** *3* (2), 101-105.

[125] Szabó, T.; Berkesi, O.; Forgó, P.; Josepovits, K.; Sanakis, Y.; Petridis, D.; Dékány, I. Evolution of Surface Functional Groups in a Series of Progressively Oxidized Graphite Oxides. *Chemistry of Materials* **2006,** *18* (11), 2740-2749.

[126] Kotov, N. A.; Dékány, I.; Fendler, J. H. Ultrathin graphite oxide–polyelectrolyte composites prepared by self-assembly: Transition between conductive and non-conductive states. *Advanced Materials* **1996,** *8* (8), 637-641.

[127] Kovtyukhova, N. I.; Ollivier, P. J.; Martin, B. R.; Mallouk, T. E.; Chizhik, S. A.; Buzaneva, E. V.; Gorchinskiy, A. D. Layer-by-layer assembly of ultrathin composite films from micron-sized graphite oxide sheets and polycations. *Chemistry of Materials* **1999,** *11* (3), 771-778.

[128] Elimelech, M. The global challenge for adequate and safe water. *J Water Supply Res T* **2006,** *55* (1), 3-10.

[129] Mi, B.; Elimelech, M. Silica scaling and scaling reversibility in forward osmosis. *Desalination* **2013,** *312* (0), 75-81.

[130] Zhang, K.; Kemp, K. C.; Chandra, V. Homogeneous anchoring of TiO2 nanoparticles on graphene sheets for waste water treatment. *Mater Lett* **2012,** *81*, 127-130.

[131] Ji, L.; Rao, M.; Aloni, S.; Wang, L.; Cairns, E. J.; Zhang, Y. Porous carbon nanofiber–sulfur composite electrodes for lithium/sulfur cells. *Energy & Environmental Science* **2011,** *4* (12), 5053.

[132] Huang, Z. H.; Zheng, X. Y.; Lv, W.; Wang, M.; Yang, Q. H.; Kang, F. Y. Adsorption of Lead(II) Ions from Aqueous Solution on Low-Temperature Exfoliated Graphene Nanosheets. *Langmuir* **2011,** *27* (12), 7558-7562.

[133] Machida, M.; Mochimaru, T.; Tatsumoto, H. Lead(II) adsorption onto the graphene layer of carbonaceous materials in aqueous solution. *Carbon* **2006,** *44* (13), 2681-2688.

[134] Mishra, A. K.; Ramaprabhu, S. Functionalized graphene sheets for arsenic removal and desalination of sea water. *Desalination* **2011,** *282*, 39-45.

[135] Koinuma, M.; Ogata, C.; Kamei, Y.; Hatakeyama, K.; Tateishi, H.; Watanabe, Y.; Taniguchi, T.; Gezuhara, K.; Hayami, S.; Funatsu, A.; Sakata, M.; Kuwahara, Y.; Kurihara, S.; Matsumoto, Y. Photochemical Engineering of Graphene Oxide Nanosheets. *J Phys Chem C* **2012,** *116* (37), 19822-19827.

[136] Kannam, S. K.; Todd, B. D.; Hansen, J. S.; Daivis, P. J. Slip length of water on graphene: Limitations of non-equilibrium molecular dynamics simulations. *J Chem Phys* **2012,** *136* (2).

[137] Marti, J.; Sala, J.; Guardia, E. Molecular dynamics simulations of water confined in graphene nanochannels: From ambient to supercritical environments. *J Mol Liq* **2010,** *153* (1), 72-78.

[138] Xiong, W.; Liu, J. Z.; Ma, M.; Xu, Z. P.; Sheridan, J.; Zheng, Q. S. Strain engineering water transport in graphene nanochannels. *Phys Rev E* **2011,** *84* (5).

[139] Cicero, G.; Grossman, J. C.; Schwegler, E.; Gygi, F.; Galli, G. Water confined in nanotubes and between graphene sheets: A first principle study. *J Am Chem Soc* **2008,** *130* (6), 1871-1878.

[140] Dhiman, P.; Yavari, F.; Mi, X.; Gullapalli, H.; Shi, Y. F.; Ajayan, P. M.; Koratkar, N. Harvesting Energy from Water Flow over Graphene. *Nano Lett* **2011,** *11* (8), 3123-3127.

[141] Gordillo, M. C.; Marti, J. Structure of water adsorbed on a single graphene sheet. *Phys Rev B* **2008,** *78* (7).

[142] Gordillo, M. C.; Marti, J. Water on graphene surfaces. *J Phys-Condens Mat* **2010,** *22* (28).

[143] Hummers, W. S.; Offeman, R. E. Preparation of Graphitic Oxide. *Journal of the American Chemical Society* **1958,** *80* (6), 1339-1339.

[144] Lai, L. F.; Chen, L. W.; Zhan, D.; Sun, L.; Liu, J. P.; Lim, S. H.; Poh, C. K.; Shen, Z. X.; Lin, J. Y. One-step synthesis of NH2-graphene from in situ graphene-oxide reduction and its improved electrochemical properties. *Carbon* **2011,** *49* (10), 3250-3257.

[145] Marcano, D. C.; Kosynkin, D. V.; Berlin, J. M.; Sinitskii, A.; Sun, Z. Z.; Slesarev, A.; Alemany, L. B.; Lu, W.; Tour, J. M. Improved Synthesis of Graphene Oxide. *Acs Nano* **2010,** *4* (8), 4806-4814.

[146] Shen, J. F.; Shi, M.; Ma, H. W.; Yan, B.; Li, N.; Hu, Y. Z.; Ye, M. X. Synthesis of hydrophilic and organophilic chemically modified graphene oxide sheets. *J Colloid Interf Sci* **2010,** *352* (2), 366-370.

[147] Chen, G. F.; Zhai, S. Y.; Zhai, Y. L.; Zhang, K.; Yue, Q. L.; Wang, L.; Zhao, J. S.; Wang, H. S.; Liu, J. F.; Jia, J. B. Preparation of sulfonic-functionalized graphene oxide as ion-exchange material and its application into electrochemiluminescence analysis. *Biosens Bioelectron* **2011,** *26* (7), 3136-3141.

[148] Fernandez-Merino, M. J.; Paredes, J. I.; Villar-Rodil, S.; Guardia, L.; Solis-Fernandez, P.; Salinas-Torres, D.; Cazorla-Amoros, D.; Morallon, E.; Martinez-Alonso, A.; Tascon, J. M. D. Investigating the influence of surfactants on the stabilization of aqueous reduced graphene oxide dispersions and the characteristics of their composite films. *Carbon* **2012,** *50* (9), 3184-3194.

[149] Hong, J.; Kang, Y. S.; Kang, S. W. Nanoassembly of Block Copolymer Micelle and Graphene Oxide to Multilayer Coatings. *Ind Eng Chem Res* **2011,** *50* (6), 3095-3099.

[150] Whitby, R. L. D.; Korobeinyk, A.; Mikhalovsky, S. V.; Fukuda, T.; Maekawa, T. Morphological effects of single-layer graphene oxide in the formation of covalently bonded polypyrrole composites using intermediate diisocyanate chemistry. *J Nanopart Res* **2011,** *13* (10), 4829-4837.

[151] Salgado, S.; Pu, L.; Maheshwari, V. Targeting Chemical Morphology of Graphene Oxide for Self-Assembly and Subsequent Templating of Nanoparticles: A Composite Approaching Capacitance Limits in Graphene. *J Phys Chem C* **2012,** *116* (22), 12124-12130.

[152] Xu, L. Q.; Wang, L.; Zhang, B.; Lim, C. H.; Chen, Y.; Neoh, K. G.; Kang, E. T.; Fu, G. D. Functionalization of reduced graphene oxide nanosheets via stacking interactions with the fluorescent and water-soluble perylene bisimide-containing polymers. *Polymer* **2011,** *52* (11), 2376-2383.

[153] Nair, R. R.; Wu, H. A.; Jayaram, P. N.; Grigorieva, I. V.; Geim, A. K. Unimpeded Permeation of Water Through Helium-Leak-Tight Graphene-Based Membranes. *Science* **2012,** *335* (6067), 442-444.

[154] Han, Y.; Xu, Z.; Gao, C. Ultrathin Graphene Nanofiltration Membrane for Water Purification. *Advanced Functional Materials* **2013,** *doi: 10.1002/adfm.201202601*.

[155] Peeters, J. M. M.; Boom, J. P.; Mulder, M. H. V.; Strathmann, H. Retention measurements of nanofiltration membranes with electrolyte solutions. *Journal of Membrane Science* **1998,** *145* (2), 199-209.

[156] Arena, J. T.; McCloskey, B.; Freeman, B. D.; McCutcheon, J. R. Surface modification of thin film composite membrane support layers with polydopamine: Enabling use of reverse osmosis membranes in pressure retarded osmosis. *J Membrane Sci* **2011,** *375* (1-2), 55-62.

[157] Fornasiero, F.; Park, H.; Holt, J.; Stadermann, M.; Grigoropoulos, C.; Noy, A.; Bakajin, O. Ion exclusion by sub-2-nm carbon nanotube pores. *P NATL ACAD SCI USA* **2008,** *105* (45), 17250-17255.

[158] Qiu, L.; Zhang, X. H.; Yang, W. R.; Wang, Y. F.; Simon, G. P.; Li, D. Controllable corrugation of chemically converted graphene sheets in water and potential application for nanofiltration. *Chem Commun* **2011,** *47* (20), 5810-5812.

[159] Kannam, S. K.; Todd, B. D.; Hansen, J. S.; Daivis, P. J. Interfacial slip friction at a fluid-solid cylindrical boundary. *The Journal of Chemical Physics* **2012,** *136* (24), 244704.

[160] Huang, H.; Song, Z.; Wei, N.; Shi, L.; Mao, Y.; Ying, Y.; Sun, L.; Xu, Z.; Peng, X. Ultrafast viscous water flow through nanostrand-channelled graphene oxide membranes. *Nat Commun* **2013,** *4*.

[161] Mi, B. Graphene oxide membranes for ionic and molecular sieving. *Science* **2014,** *343* (6172), 740–742.

[162] Liu, S. Z.; Sun, H. Q.; Liu, S. M.; Wang, S. B. Graphene facilitated visible light photodegradation of methylene blue over titanium dioxide photocatalysts. *Chem Eng J* **2013,** *214*, 298-303.

[163] Ahmadiannamini, P.; Li, X.; Goyens, W.; Joseph, N.; Meesschaert, B.; Vankelecom, I. F. J. Multilayered polyelectrolyte complex based solvent resistant nanofiltration membranes prepared from weak polyacids. *Journal of Membrane Science* **2012,** *394-395*, 98-106.

[164] Joseph, N.; Ahmadiannamini, P.; Hoogenboom, R.; Vankelecom, I. F. J. Layer-by-layer preparation of polyelectrolyte multilayer membranes for separation. *Polymer Chemistry* **2014,** *5* (6), 1817-1831.

[165] Klaysom, C.; Cath, T. Y.; Depuydt, T.; Vankelecom, I. F. J. Forward and pressure retarded osmosis: potential solutions for global challenges in energy and water supply. *Chemical Society Reviews* **2013,** *42* (16), 6959-6989.

[166] Cath, T. Y.; Childress, A. E.; Elimelech, M. Forward osmosis: Principles, applications, and recent developments. *Journal of Membrane Science* **2006,** *281* (1–2), 70-87.

[167] Chung, T.-S.; Li, X.; Ong, R. C.; Ge, Q.; Wang, H.; Han, G. Emerging forward osmosis (FO) technologies and challenges ahead for clean water and clean energy applications. *Current Opinion in Chemical Engineering* **2012,** *1* (3), 246-257.

[168] Zhao, S.; Zou, L.; Tang, C. Y.; Mulcahy, D. Recent developments in forward osmosis: Opportunities and challenges. *Journal of Membrane Science* **2012,** *396* (0), 1-21.

[169] McGinnis, R. L.; Elimelech, M. Global Challenges in Energy and Water Supply: The Promise of Engineered Osmosis. *Environmental Science & Technology* **2008,** *42* (23), 8625-8629.

[170] Yip, N. Y.; Tiraferri, A.; Phillip, W. A.; Schiffman, J. D.; Hoover, L. A.; Kim, Y. C.; Elimelech, M. Thin-Film Composite Pressure Retarded Osmosis Membranes for Sustainable Power Generation from Salinity Gradients. *Environmental Science & Technology* **2011,** *45* (10), 4360-4369.

[171] Wang, R.; Shi, L.; Tang, C. Y.; Chou, S.; Qiu, C.; Fane, A. G. Characterization of novel forward osmosis hollow fiber membranes. *Journal of Membrane Science* **2010,** *355* (1), 158-167.

[172] Tiraferri, A.; Yip, N. Y.; Phillip, W. A.; Schiffman, J. D.; Elimelech, M. Relating performance of thin-film composite forward osmosis membranes to support layer formation and structure. *Journal of Membrane Science* **2011,** *367* (1–2), 340-352.

[173] Perry, L. A.; Coronell, O. Reliable, bench-top measurements of charge density in the active layers of thin-film composite and nanocomposite membranes using quartz crystal microbalance technology. *Journal of Membrane Science* **2013,** *429* (0), 23-33.

[174] Decher, G.; Schmitt, J., Fine-tuning of the film thickness of ultrathin multilayer films composed of consecutively alternating layers of anionic and cationic polyelectrolytes. In *Prog Coll Pol Sci S*, Springer: 1992; pp 160-164.

[175] Shiratori, S. S.; Rubner, M. F. pH-Dependent Thickness Behavior of Sequentially Adsorbed Layers of Weak Polyelectrolytes. *Macromolecules* **2000,** *33* (11), 4213-4219.

[176] Zangmeister, C. D.; Ma, X.; Zachariah, M. R. Restructuring of Graphene Oxide Sheets into Monodisperse Nanospheres. *Chemistry of Materials* **2012,** *24* (13), 2554-2557.

[177] Yip, N. Y.; Tiraferri, A.; Phillip, W. A.; Schiffman, J. D.; Elimelech, M. High Performance Thin-Film Composite Forward Osmosis Membrane. *Environmental Science & Technology* **2010,** *44* (10), 3812-3818.

[178] Dubas, S. T.; Schlenoff, J. B. Polyelectrolyte Multilayers Containing a Weak Polyacid: Construction and Deconstruction. *Macromolecules* **2001,** *34* (11), 3736-3740.

[179] Li, D.; Muller, M. B.; Gilje, S.; Kaner, R. B.; Wallace, G. G. Processable aqueous dispersions of graphene nanosheets. *Nature nanotechnology* **2008,** *3* (2), 101-105.

[180] Buffle, J.; Zhang, Z.; Startchev, K. Metal Flux and Dynamic Speciation at (Bio)interfaces. Part I: Critical Evaluation and Compilation of Physicochemical Parameters for Complexes with Simple Ligands and Fulvic/Humic Substances. *Environmental Science & Technology* **2007,** *41* (22), 7609-7620.

[181] Miller, D. G.; Rard, J. A.; Eppstein, L. B.; Albright, J. G. Mutual diffusion coefficients and ionic transport coefficients lij of magnesium chloride-water at 25.degree.C. *The Journal of Physical Chemistry* **1984,** *88* (23), 5739-5748.

[182] Hu, M.; Mi, B. Enabling Graphene Oxide Nanosheets as Water Separation Membranes. *Environ Sci Technol* **2013,** *47* (8), 3715-3723.

[183] Wang, Z.; Yu, H.; Xia, J.; Zhang, F.; Li, F.; Xia, Y.; Li, Y. Novel GO-blended PVDF ultrafiltration membranes. *Desalination* **2012,** *299*, 50-54.

[184] Zhao, C.; Xu, X.; Chen, J.; Wang, G.; Yang, F. Highly effective antifouling performance of PVDF/graphene oxide composite membrane in membrane bioreactor (MBR) system. *Desalination* **2014,** *340*, 59-66.

[185] Xu, Z.; Zhang, J.; Shan, M.; Li, Y.; Li, B.; Niu, J.; Zhou, B.; Qian, X. Organosilane-functionalized graphene oxide for enhanced antifouling and mechanical properties of polyvinylidene fluoride ultrafiltration membranes. *Journal of Membrane Science* **2014,** *458*, 1-13.

[186] Zinadini, S.; Zinatizadeh, A. A.; Rahimi, M.; Vatanpour, V.; Zangeneh, H. Preparation of a novel antifouling mixed matrix PES membrane by embedding graphene oxide nanoplates. *Journal of Membrane Science* **2014,** *453*, 292-301.

[187] Zhang, J.; Xu, Z.; Shan, M.; Zhou, B.; Li, Y.; Li, B.; Niu, J.; Qian, X. Synergetic effects of oxidized carbon nanotubes and graphene oxide on fouling control and anti-fouling mechanism of polyvinylidene fluoride ultrafiltration membranes (vol 448, pg 81, 2013). *Journal of Membrane Science* **2014,** *451*, 319-319.

[188] Zhang, J.; Xu, Z.; Shan, M.; Zhou, B.; Li, Y.; Li, B.; Niu, J.; Qian, X. Synergetic effects of oxidized carbon nanotubes and graphene oxide on fouling control and anti-fouling mechanism of polyvinylidene fluoride ultrafiltration membranes. *Journal of Membrane Science* **2013,** *448*, 81-92.

[189] Lee, J.; Chae, H.-R.; Won, Y. J.; Lee, K.; Lee, C.-H.; Lee, H. H.; Kim, I.-C.; Lee, J.-m. Graphene oxide nanoplatelets composite membrane with hydrophilic and antifouling properties for wastewater treatment. *Journal of Membrane Science* **2013,** *448*, 223-230.

[190] Santos, C. M.; Mangadlao, J.; Ahmed, F.; Leon, A.; Advincula, R. C.; Rodrigues, D. F. Graphene nanocomposite for biomedical applications: fabrication, antimicrobial and cytotoxic investigations. *Nanotechnology* **2012,** *23* (39).

[191] Gurunathan, S.; Han, J. W.; Dayem, A. A.; Eppakayala, V.; Kim, J. H. Oxidative stress-mediated antibacterial activity of graphene oxide and reduced graphene oxide in Pseudomonas aeruginosa. *Int J Nanomed* **2012,** *7*, 5901-5914.

[192] Carpio, I. E. M.; Santos, C. M.; Wei, X.; Rodrigues, D. F. Toxicity of a polymer-graphene oxide composite against bacterial planktonic cells, biofilms, and mammalian cells. *Nanoscale* **2012,** *4* (15), 4746-4756.

[193] Santos, C. M.; Tria, M. C. R.; Vergara, R. A. M. V.; Ahmed, F.; Advincula, R. C.; Rodrigues, D. F. Antimicrobial graphene polymer (PVK-GO) nanocomposite films. *Chem Commun* **2011,** *47* (31), 8892-8894.

[194] Perreault, F.; Tousley, M. E.; Elimelech, M. Thin-Film Composite Polyamide Membranes Functionalized with Biocidal Graphene Oxide Nanosheets. **2013**.

[195] Zhao, G.; Jiang, L.; He, Y.; Li, J.; Dong, H.; Wang, X.; Hu, W. Sulfonated Graphene for Persistent Aromatic Pollutant Management. *Advanced Materials* **2011,** *23* (34), 3959-3963.

[196] Zhao, G.; Li, J.; Ren, X.; Chen, C.; Wang, X. Few-Layered Graphene Oxide Nanosheets As Superior Sorbents for Heavy Metal Ion Pollution Management. *Environmental Science & Technology* **2011,** *45* (24), 10454-10462.

[197] Lambert, T. N.; Chavez, C. A.; Hernandez-Sanchez, B.; Lu, P.; Bell, N. S.; Ambrosini, A.; Friedman, T.; Boyle, T. J.; Wheeler, D. R.; Huber, D. L. Synthesis and

Characterization of Titania-Graphene Nanocomposites. *J Phys Chem C* **2009,** *113* (46), 19812-19823.

[198] Achilli, A.; Childress, A. E. Pressure retarded osmosis: From the vision of Sidney Loeb to the first prototype installation - Review. *Desalination* **2010,** *261* (3), 205-211.

[199] Loeb, S. Production of energy from concentrated brines by pressure-retarded osmosis : I. Preliminary technical and economic correlations. *Journal of Membrane Science* **1976,** *1* (0), 49-63.

[200] Loeb, S. Osmotic Power-Plants. *Science* **1975,** *189* (4203), 654-655.

[201] Loeb, S.; Titelman, L.; Korngold, E.; Freiman, J. Effect of porous support fabric on osmosis through a Loeb-Sourirajan type asymmetric membrane. *Journal of Membrane Science* **1997,** *129* (2), 243-249.

[202] Yip, N. Y.; Elimelech, M. Influence of Natural Organic Matter Fouling and Osmotic Backwash on Pressure Retarded Osmosis Energy Production from Natural Salinity Gradients. *Environ Sci Technol* **2013,** *47* (21), 12607-12616.

[203] Yip, N. Y.; Elimelech, M. Thermodynamic and Energy Efficiency Analysis of Power Generation from Natural Salinity Gradients by Pressure Retarded Osmosis. *Environ Sci Technol* **2012,** *46* (9), 5230-5239.

[204] Lin, S.; Straub, A. P.; Elimelech, M. Thermodynamic limits of extractable energy by pressure retarded osmosis. *Energy & Environmental Science* **2014,** *7* (8), 2706-2714.

[205] Chu, S.; Majumdar, A. Opportunities and challenges for a sustainable energy future. *Nature* **2012,** *488* (7411), 294-303.

[206] Logan, B. E.; Elimelech, M. Membrane-based processes for sustainable power generation using water. *Nature* **2012,** *488* (7411), 313-319.

[207] Pattle, R. E. Production of Electric Power by Mixing Fresh and Salt Water in the Hydroelectric Pile. *Nature* **1954,** *174* (4431), 660-660.

[208] She, Q. H.; Jin, X.; Li, Q. H.; Tang, C. Y. Y. Relating reverse and forward solute diffusion to membrane fouling in osmotically driven membrane processes. *Water Res* **2012,** *46* (7), 2478-2486.

[209] She, Q. H.; Wong, Y. K. W.; Zhao, S. F.; Tang, C. Y. Y. Organic fouling in pressure retarded osmosis: Experiments, mechanisms and implications. *Journal of Membrane Science* **2013,** *428*, 181-189.

[210] Parida, V.; Ng, H. Y. Forward osmosis organic fouling: Effects of organic loading, calcium and membrane orientation. *Desalination* **2013,** *312*, 88-98.

[211] Thelin, W. R.; Sivertsen, E.; Holt, T.; Brekke, G. Natural organic matter fouling in pressure retarded osmosis. *Journal of Membrane Science* **2013,** *438*, 46-56.

[212] Zhang, M. M.; Hou, D. X.; She, Q. H.; Tang, C. Y. Y. Gypsum scaling in pressure retarded osmosis: Experiments, mechanisms and implications. *Water Res* **2014,** *48*, 387-395.

[213] Motsa, M. M.; Mamba, B. B.; D'Haese, A.; Hoek, E. M. V.; Verliefde, A. R. D. Organic fouling in forward osmosis membranes: The role of feed solution chemistry and membrane structural properties. *Journal of Membrane Science* **2014,** *460*, 99-109.

[214] Zhang, M. M.; Hou, D. X.; She, Q. H.; Tang, C. Y. Y. Gypsum scaling in pressure retarded osmosis: Experiments, mechanisms and implications. *Water Research* **2014,** *48*, 387-395.

[215] Li, X.; Cai, T.; Chung, T.-S. Anti-Fouling Behavior of Hyperbranched Polyglycerol-Grafted Poly(ether sulfone) Hollow Fiber Membranes for Osmotic Power Generation. *Environ Sci Technol* **2014**.

[216] Qi, S. R.; Qiu, C. Q.; Zhao, Y.; Tang, C. Y. Y. Double-skinned forward osmosis membranes based on layer-by-layer assembly-FO performance and fouling behavior. *Journal of Membrane Science* **2012,** *405*, 20-29.

[217] Yu, H. Y.; Kang, Y.; Liu, Y. L.; Mi, B. Grafting polyzwitterions onto polyamide by click chemistry and nucleophilic substitution on nitrogen: A novel approach to enhance membrane fouling resistance. *Journal of Membrane Science* **2014,** *449*, 50-57.

[218] Liu, Y.; Mi, B. Effects of organic macromolecular conditioning on gypsum scaling of forward osmosis membranes. *Journal of Membrane Science* **2014,** *450*, 153-161.

[219] Tiraferri, A.; Yip, N. Y.; Straub, A. P.; Castrillon, S. R. V.; Elimelech, M. A method for the simultaneous determination of transport and structural parameters of forward osmosis membranes. *Journal of Membrane Science* **2013,** *444*, 523-538.

[220] Duong, P. H. H.; Chung, T. S.; Wei, S.; Irish, L. Highly Permeable Double-Skinned Forward Osmosis Membranes for Anti-Fouling in the Emulsified Oil-Water Separation Process. *Environ Sci Technol* **2014,** *48* (8), 4537-4545.

[221] Mi, B.; Elimelech, M. Chemical and physical aspects of organic fouling of forward osmosis membranes. *Journal of Membrane Science* **2008,** *320* (1–2), 292-302.

[222] Li, Q.; Elimelech, M. Organic Fouling and Chemical Cleaning of Nanofiltration Membranes: Measurements and Mechanisms. *Environmental Science & Technology* **2004,** *38* (17), 4683-4693.

[223] Mo, Y. H.; Tiraferri, A.; Yip, N. Y.; Adout, A.; Huang, X.; Elimelech, M. Improved Antifouling Properties of Polyamide Nanofiltration Membranes by Reducing the Density of Surface Carboxyl Groups. *Environ Sci Technol* **2012,** *46* (24), 13253-13261.

[224] McGinnis, R. L.; Elimelech, M. Energy requirements of ammonia–carbon dioxide forward osmosis desalination. *Desalination* **2007,** *207* (1–3), 370-382.

[225] Cath, T. Y.; Gormly, S.; Beaudry, E. G.; Flynn, M. T.; Adams, V. D.; Childress, A. E. Membrane contactor processes for wastewater reclamation in space Part I. Direct osmotic concentration as pretreatment for reverse osmosis. *Journal of Membrane Science* **2005,** *257* (1-2), 85-98.

[226] McCloskey, B. D.; Park, H. B.; Ju, H.; Rowe, B. W.; Miller, D. J.; Chun, B. J.; Kin, K.; Freeman, B. D. Influence of polydopamine deposition conditions on pure water flux and foulant adhesion resistance of reverse osmosis, ultrafiltration, and microfiltration membranes. *Polymer* **2010,** *51* (15), 3472-3485.

[227] Nguyen, A.; Azari, S.; Zou, L. D. Coating zwitterionic amino acid L-DOPA to increase fouling resistance of forward osmosis membrane. *Desalination* **2013,** *312*, 82-87.

[228] Morra, M. On the molecular basis of fouling resistance. *J Biomat Sci-Polym E* **2000,** *11* (6), 547-569.

[229] Callow, J. A.; Callow, M. E. Trends in the development of environmentally friendly fouling-resistant marine coatings. *Nat Commun* **2011,** *2*.

[230] Tiraferri, A.; Kang, Y.; Giannelis, E. P.; Elimelech, M. Superhydrophilic Thin-Film Composite Forward Osmosis Membranes for Organic Fouling Control: Fouling Behavior

and Antifouling Mechanisms. *Environmental Science & Technology* **2012,** *46* (20), 11135-11144.

[231] Kang, G. D.; Liu, M.; Lin, B.; Cao, Y. M.; Yuan, Q. A novel method of surface modification on thin-film composite reverse osmosis membrane by grafting poly(ethylene glycol). *Polymer* **2007,** *48* (5), 1165-1170.

[232] Sagle, A. C.; Van Wagner, E. M.; Ju, H.; McCloskey, B. D.; Freeman, B. D.; Sharma, M. M. PEG-coated reverse osmosis membranes: Desalination properties and fouling resistance. *Journal of Membrane Science* **2009,** *340* (1-2), 92-108.

[233] Castrillon, S. R. V.; Lu, X. L.; Shaffer, D. L.; Elimelech, M. Amine enrichment and poly(ethylene glycol) (PEG) surface modification of thin-film composite forward osmosis membranes for organic fouling control. *Journal of Membrane Science* **2014,** *450*, 331-339.

[234] Tiraferri, A.; Kang, Y.; Giannelis, E. P.; Elimelech, M. Highly Hydrophilic Thin-Film Composite Forward Osmosis Membranes Functionalized with Surface-Tailored Nanoparticles. *Acs Appl Mater Inter* **2012,** *4* (9), 5044-5053.

[235] Kim, S. H.; Kwak, S. Y.; Sohn, B. H.; Park, T. H. Design of TiO2 nanoparticle self-assembled aromatic polyamide thin-film-composite (TFC) membrane as an approach to solve biofouling problem. *Journal of Membrane Science* **2003,** *211* (1), 157-165.

[236] Mo, J.; Son, S. H.; Jegal, J.; Kim, J.; Lee, Y. H. Preparation and characterization of polyamide nanofiltration composite membranes with TiO2 layers chemically connected to the membrane surface. *J Appl Polym Sci* **2007,** *105* (3), 1267-1274.

[237] Yang, R.; Xu, J. J.; Ozaydin-Ince, G.; Wong, S. Y.; Gleason, K. K. Surface-Tethered Zwitterionic Ultrathin Antifouling Coatings on Reverse Osmosis Membranes by Initiated Chemical Vapor Deposition. *Chemistry of Materials* **2011,** *23* (5), 1263-1272.

[238] Azari, S.; Zou, L. D. Fouling resistant zwitterionic surface modification of reverse osmosis membranes using amino acid L-cysteine. *Desalination* **2013,** *324*, 79-86.

[239] Yu, H. Y.; Kang, Y.; Liu, Y. L.; Mi, B. X. Grafting polyzwitterions onto polyamide by click chemistry and nucleophilic substitution on nitrogen: A novel approach to enhance membrane fouling resistance. *Journal of Membrane Science* **2014,** *449*, 50-57.

[240] Shan, W.; Bacchin, P.; Aimar, P.; Bruening, M. L.; Tarabara, V. V. Polyelectrolyte multilayer films as backflushable nanofiltration membranes with tunable hydrophilicity and surface charge. *Journal of Membrane Science* **2010,** *349* (1–2), 268-278.

[241] de Vos, W. M.; de Keizer, A.; Stuart, M. A. C.; Kleijn, J. M. Thin polymer films as sacrificial layers for easier cleaning. *Colloid Surface A* **2010,** *358* (1-3), 6-12.

[242] Choi, J.; Rubner, M. F. Influence of the degree of ionization on weak polyelectrolyte multilayer assembly. *Macromolecules* **2005,** *38* (1), 116-124.

[243] Konkena, B.; Vasudevan, S. Understanding Aqueous Dispersibility of Graphene Oxide and Reduced Graphene Oxide through pKa Measurements. *The Journal of Physical Chemistry Letters* **2012,** *3* (7), 867-872.

[244] Dubas, S. T.; Schlenoff, J. B. Swelling and smoothing of polyelectrolyte multilayers by salt. *Langmuir* **2001,** *17* (25), 7725-7727.

[245] Heuvingh, J.; Zappa, M.; Fery, A. Salt softening of polyelectrolyte multilayer capsules. *Langmuir* **2005,** *21* (7), 3165-3171.

[246] Han, L. L.; Mao, Z. W.; Wuliyasu, H.; Wu, J. D.; Gong, X.; Yang, Y. G.; Gao, C. Y. Modulating the Structure and Properties of Poly(sodium 4-styrenesulfonate)/Poly(diallyldimethylammonium chloride) Multilayers with Concentrated Salt Solutions. *Langmuir* **2012,** *28* (1), 193-199.

[247] Kovacevic, D.; van der Burgh, S.; de Keizer, A.; Stuart, M. A. C. Kinetics of formation and dissolution of weak polyelectrolyte multilayers: Role of salt and free polyions. *Langmuir* **2002,** *18* (14), 5607-5612.

[248] Sui, Z. J.; Salloum, D.; Schlenoff, J. B. Effect of molecular weight on the construction of polyelectrolyte multilayers: Stripping versus sticking. *Langmuir* **2003,** *19* (6), 2491-2495.

[249] Dubas, S. T.; Schlenoff, J. B. Polyelectrolyte multilayers containing a weak polyacid: Construction and deconstruction. *Macromolecules* **2001,** *34* (11), 3736-3740.

[250] Ilyas, S.; de Grooth, J.; Nijmeijer, K.; de Vos, W. M. Multifunctional polyelectrolyte multilayers as nanofiltration membranes and as sacrificial layers for easy membrane cleaning. *Journal of Colloid and Interface Science* **2015,** *446* (0), 386-393.

[251] Park, S.; Dikin, D. A.; Nguyen, S. T.; Ruoff, R. S. Graphene Oxide Sheets Chemically Cross-Linked by Polyallylamine. *J Phys Chem C* **2009,** *113* (36), 15801-15804.

[252] Shao, J. J.; Lv, W.; Yang, Q. H. Self-Assembly of Graphene Oxide at Interfaces. *Advanced Materials* **2014,** *26* (32), 5586-5612.

[253] Zou, J. L.; Kim, F. Self-Assembly of Two-Dimensional Nanosheets Induced by Interfacial Polyionic Complexation. *ACS Nano* **2012,** *6* (12), 10606-10613.

[254] Hou, W.-C.; Chowdhury, I.; Goodwin, D. G.; Henderson, W. M.; Fairbrother, D. H.; Bouchard, D.; Zepp, R. G. Photochemical Transformation of Graphene Oxide in Sunlight. *Environmental Science & Technology* **2015,** *49* (6), 3435-3443.